DESIGN, DEVELOPMENT, AND ANALYSIS OF LOW LOSS RECTANGULAR DIELECTRIC RESONATOR ANTENNA FOR WIRELESS APPLICATIONS

A Thesis Submitted

IN PARTIAL FULFILLMENT OF THE REQUIREMENTS

FOR THE DEGREE OF

DOCTOR OF PHILOSOPHY

IN

Electronics and Communication Engineering

By

Sovan Mohanty

Regd. No. – 1715302002

Under the supervision of

Dr. Baibaswata Mohapatra

GALGOTIAS UNIVERSITY
UTTAR PRADESH
2021

Approval Sheet

This thesis entitled "**Design, Development, and Analysis of Low Loss Rectangular Dielectric Resonator Antenna (RDRA) for Wireless Applications**" by **Sovan Mohanty** Regd. No. **1715302002** is approved for the degree of Doctor of Philosophy.

Examiners

_____

_____

Supervisor

_____

Chairman

_____

Date: _____

Place: _____

CANDIDATE'S DECLARATION

I hereby certify that the work which is being presented in the thesis, entitled **"Design, Development, and Analysis of Low Loss Rectangular Dielectric Resonator Antenna for Wireless Applications"** in fulfillment of the requirements for the award of the degree of Doctor of Philosophy in Electronics and communication Engineering and submitted in Galgotias University, Greater Noida is an authentic record of my own work carried out during a period from July 2017 under the supervision of Dr. Baibaswata Mohapatra (Supervisor).

The matter embodied in this thesis has not been submitted by me for the award of any other degree of this or any other University/Institute.

Sovan Mohanty

This is to certify that the above statement made by the candidate is correct to the best of our knowledge.

Dr. Baibaswata Mohapatra
Supervisor
Deptt. of ECE

The Ph.D. Viva-Voce examination of Sovan Mohanty, Research Scholar, has been held on ……..

Sign.of Supervisor Sign. of External Examiner

ABSTRACT

The world started to sense and realizes the acceleration of next-generation high speed, high reliable, and ultra-flexible wireless connectivity. The upcoming technology will create new possibilities while mitigating challenges in diverse fields such as data-intensive high bandwidth applications, wireless cognition, imaging, positioning, and sensing operations. With the advent of material engineering in developing magneto-dielectric material, isotropic material, and meta-material, it is possible to address challenging issues like dispersion, latency, coverage, power efficiency, scalability, diversity while enhancing the speed of communication.

RF and microwave technology have undergone rapid surge in the last decade in communication and navigational applications. The modern system demands ultra-wide bandwidth, polarization purity, consistent gain, and high radiation efficiency with temperature stability in the operating frequency intervals. The miniaturized design stimulates physically, electrically, and functionally small embeddable antenna as the front end device with considerable power handling capabilities. The operating bandwidth should be high for effective output radiation performance, input characteristics like impedance, and phase response while handling digital impulse signals. So far the traditional microstrip patch antenna is a dominating commercial technology, but its operation is restricted to narrowband due to its intrinsic reactive (capacitive) behavior.

To address these issues especially at microwave and mm-wave, DRA emerges. It provides minimum conductor and dielectric loss, ultra-wide bandwidth, miniaturized design, and stable output characteristics within the designed bandwidth. Dielectric will not allow the formation of any discrete pole and thus can effectively combat the surface wave. It will mitigate effect like back radiation and edge diffraction from the radiating structure. While calculating the loss it is required to estimate the tangential magnetic field. As DRA is not a capacitive structure, therefore it provides large bandwidth.

Resonance is said to be a condition in which the field exist without having any excitation. Resonant modes are field structure which can exist in the absence of

current source ‘J’.

In the proposed work concentration is more towards designing an electrically small, low loss, highly efficient rectangular and hybrid DRA. Signal transmission at microwave and millimeter-wave can incur propagation loss due to increased dispersion and can have absorption peaks at several frequencies. Therefore system-level simulation can help in the evaluation of system performance under various conditions to gain insight into the design requirements. With the invention of high-speed electronics, efforts are on in solving a practical, complex electromagnetic related problem.

The antenna structure is realized by using HFSS which uses numerical techniques like the FEM. The field assuming the source is a delta function source (Green function). The computational electromagnetic helps in finding the electric and magnetic field by replacing an object into equivalent electric and magnetic current sources. It reduces the domain of computation by reducing the dimensionality of the problem that is the 3D problem can be resolved by using the 2D approach. Therefore the cost of computation reduces drastically. Different choices of testing function and basis function give different accuracy. In FEM, Galerkin’s method is used where both the testing and basis functions are the same.

By exciting at higher-order mode or by integrating horn-like structure high gain can be achieved. By employing Hybrid DRA antenna impedance bandwidth can be controlled.

DRA is proved to be one of the best candidates at mm-wave frequency. DRA is suitable in those applications where there is a requirement of continuous change in frequency such as software-defined radio, military communication, etc. However, key challenges in the future front end technology will be interference of things, wireless standard pre-compliance, EMI/EMC pre-compliance, capturing complex and fast mode current waveform over time, narrow band IoT, massive MIMO, beam forming and beam steering technique.

ACKNOWLEDGEMENTS

Knowledge is the hidden beauty to uncover the truth and mind. If aspiration is attached with intense and spontaneous love then nothing stands in the way of victorious drive.

I take pleasure in expressing my appreciation to Prof. Baibaswata Mohapatra, Dean SEECE, for guiding me in this research work. His insightful guidance and profound response have encouraged me to raise the bar relentlessly. The scope of this thesis, the order of presentation of the material, research work arrangement, and testing were carried out jointly by us. He taught me how to look closer to a problem with peace of mind and dive deeper into it to discover solutions. Thank you sir for taking over the reins and ensured we got to the end on a high note.

I am thankful to the Vice Chancellor, members of the Doctorial Committee, and Deans of Galgotias University for providing me the opportunity and facilities to undertake my doctorial studies.

I am personally indebted to Prof. Bratin Ghosh, IIT Kharagpur, for shaping my mind to take up work on Rectangular Dielectric Resonator Antenna. The healthy discussions over different problems like Numerical Techniques laid a strong foundation in Antenna and Wave Propagation. Thank you sir to cut through the clutter and crystallize the central idea.

I wish to express my sincere gratitude to Mr. Dev Murti, Chairman SRMS Trust, for providing me the hardware and software platforms to undertake this research work.

My special thanks to Dr. Usha Chauhan, Associate Professor, SEECE, for her indomitable spirit and help. I am also thankful to all the faculties and staff members of SEECE, Galgotia University, and SRMS CET, Bareilly, for creating a healthy work environment for me. I am thankful to the Indian Air Force for embedding passion, hunger, and discipline within me.

I would like to express my emotional gratitude to my mother, father, uncle with my brothers (Satyakam, Sakti, Suman, Soumyakant, Avijeet) and sisters (Pragyan, Amruta), and my dearest students for their spiritual understanding and helping me to

improve my intellectual bandwidth to take up new challenges while stretching the self. I will be always grateful to my dearest wife who taught me how to climb the great wall of fear and how to be boundless while turning vision into reality.

Finally, I would like to thank and salute the dedication and determination of many generations of scientists, engineers, and practical minded philosophers, who have helped to enlighten the lost, to expand awareness and create a higher potential of survival for mankind in this universe.

Sovan Mohanty

TABLE OF CONTENTS

LIST OF FIGURES

LIST OF TABLES

LIST OF ACRONYMS

$\mathbf{Z_S}$	Source impedance
$\mathbf{Z_O}$	Characteristic impedance
$\mathbf{Z_L}$	Load Impedance
j	Complex part
G	Conductance
R	Resistance
L	Impedance
C	Capacitance
H	Magnetic field intensity
E	Electric field intensity
$\hat{\varepsilon}$	Complex permittivity
σ	Conductivity (material dependant parameter)
ε	Permittivity (medium dependant parameter)
μ	Permeability (medium dependant parameter)
J	Surface current density
ω	Angular frequency
$\mathbf{E_o}$	The magnitude of the tangential electric field component
η	The efficiency of the antenna
$\boldsymbol{\rho_v}$	Volume charge density
F	Operating frequency
$\mathbf{f_h}$	High cut off frequency
$\mathbf{f_l}$	Low cut off frequency
$\mathbf{f_c}$	Centre Frequency
Hz	Hertz
GHz	Gigahertz (in the frequency range of 10^9 Hz)
THz	Terahertz (in the frequency range of 10^{12} Hz)

LIST OF ABBREVIATIONS

BW	Bandwidth
CPW	Coplanar Waveguide
CDRA	Cylindrical Dielectric Resonator Antenna
CST	Computer Simulation Tool
DR	Dielectric Resonator
DRA	Dielectric Resonator Antenna
D2D	Device to Device
DWM	Dielectric Waveguide Model
EDC	Effective Dielectric Constant
EIRP	Effective Isotropic Radiated Power
ERP	Effective Radiated Power
EMI	Electromagnetic Interference
EMC	Electromagnetic Compatibility
FBW	Fractional Bandwidth
FDTD	Finite Difference Time Domain
FEM	Finite Element Method
FNBW	First Null Beam width
GHz	Giga Hertz
GNSS	Global Navigation Satellite System
GTD	Geometric Theory of Diffraction
HEM	Hybrid Electro-Magnetic Mode
HPBW	Half Power Beam width
IoT	Internet of Thing
LMDS	Local Multipoint Distributive System
LNA	Low Noise Amplifier
LSE	Longitudinal Section Electric
LSM	Longitudinal Section Magnetic
MDWM	Modified Dielectric Waveguide Model
MIC	Microwave Integrated Circuit

MIMO	Multiple Input and Multiple Output
MMIC	Monolithic Microwave Integrated Circuit
MU-MIMO	Multi-User Multiple Input and Multiple Output
MSA	Micro-strip Antenna
MoM	Method of Moments
NB-IoT	Narrow Band Internet of Thing
NFC	Near Field Communication
NRD	Non Radiating Dielectric
PCS	Personal Communication System
PEC	Perfect Electrical Conductor
PDA	Personal Digital Assistance
QED	Quantum Electro Dynamic
RDRA	Rectangular Dielectric Resonator Antenna
S11	Reflection Coefficient / S-parameter of same port input-output
SINR	Signal to Noise plus Interference Ratio
SLL	Side Lobe Level
TRP	Total Radiated Power
UWB	Ultra Wide Band
VHF	Very High Frequency
VNA	Vector Network Analyzer
VSWR	Voltage Standing Wave Ratio
Wi-Fi	Wireless Fidelity
WiMAX	Wireless Interoperability for Microwave Access Network
WLAN	Wireless Local Area Network
WLL	Wireless Local Loop
WSN	Wireless Sensor Network
X-Band	Fire Band

LIST OF PUBLICATIONS AND EVENTS ATTENDED

Following research papers are published/ communicated.

S.No.	Title of the Publication	Name of Journal/ Conference	Database	Impact Factor	Date of Publication/Research Paper
1	Leaky Wave-guide Based Dielectric Resonator Antenna for Millimeter-Wave Applications	Transaction on Electronic and Electrical Materials (2020), Springer	Emerging Sources Citation Index, SCImago, Semantic Scholar, SCOPUS	Impact Factor: 0.58, SJR: 0.192 h-index: =15	Volume 21, Issues 6, 15 Sep 2020 Online ISSN 2092-7592 Print ISSN 1229-7607 https://link.springer.com/article/10.1007/s42341-020-00240-w , https://doi.org/10.1007/s42341-020-00240-w
2	Multifunctional Integrated Hybrid Rectangular Dielectric Resonator Antenna for High-Speed Communication	Book titled "Microstrip Antenna Design for Wireless Application" 1st Edition, Chapter 14, CRC Press, Taylor and Francis Group.	Thomson Reuters Book Citation Index and SCOPUS		ISBN: 9780367554385,August 4, 2021
3	Narrowband Dielectric Resonator Antenna for Wireless Communication and Sensing Applications	Vigyan Prakash, Research Journal of Science and Technology	UGC CARE Listed Journal		ISSN: 1549-523-X, Volume-18, Issue:1-2,Page:30-40, Jan- June 2020 https://vigyanprakash.in/download/18.1.pdf
4	Micro-strip Fed Rectangular Dielectric Resonator Antenna for Broad Band Wireless Applications	Vigyan Garima Sindhu, Commission for Scientific & Technical Terminology	UGC CARE Listed Journal		ISSN 2320-7736, Vol.112, No.05, 2020, pp. 39-51

5	Analysis of Aperture Coupled Dual Band Rectangular Dielectric Resonator Antenna	Vigyan Prakash, Research Journal of Science and Technology	UGC CARE Listed Journal	ISSN: 1549-523-X, Volume-18, Issue:1-2,Page:16-23, Jan- June 2020 https://vigyanprakash.in/download/18.1.pdf
6	Analysis of Micro-strip Fed Cylindrical Dielectric Resonator Antenna	Vigyan Garima Sindhu, Commission for Scientific & Technical Terminology	UGC CARE Listed Journal	ISSN: 2320-7736, Vol.112, No.05, 2020, pp. 39-51,
7	Printed Slot Wideband Rectangular Dielectric Resonator Antenna	Springer's Innovations in Electrical and Electronic Engineering, Lecture Notes in Electrical Engineering 661.	Scopus	https://doi.org/10.1007/978-981-15-4692-1_44, Jan-2021.
8	Analysis of Cylindrical Dielectric Resonator Antenna with Modified Micro-strip Feed	International Conference on Contemporary Computing and Applications (IC3A), Feb 2020 (IEEE Xplore Digital Library)	Scopus	**DOI:** 10.1109/IC3A48958.2020.233271, 05-07 Feb 2020
9	Investigation of Rectangular Dielectric Resonator Antenna Excited by CPW Feed	Micro-electronics and Telecommunication Engineering, Springer Singapore	Scopus	Print ISBN: 978-981-15-2328-1, Electronic ISBN: 978-981-15-2329-8, Copy right Year: 2020, Sequence number:52 https://doi.org/10.1007/978-981-15-2329-8_52

10	Embedded Rectangular Dielectric Resonator Antenna for Ku-Band Application.	International Conference on Innovative Advancements in Engineering and Technology (IAET-2020), JNU, Jaipur	Elsevier SSRN Electronic Journal	ISSN:2214-7583 DOI: 2139/ssrn.3549250 January 2020
11	Comparative Analysis of Stacked Rectangular Dielectric Resonator Antennas Based on Finite Defected Ground Plane.	International Conference on Innovative Advancements in Engineering and Technology (IAET-2020), JNU, Jaipur	Elsevier SSRN Electronic Journal	ISSN:2214-7583 DOI: 10.2139/ssrn.3551000 January 2020
12	Modified Filleted Dual Band Dielectric Resonator Antenna for High	International Conference on Intelligent Control and Computation for Smart Energy and Mechatronic Systems		25-26 Sep 2020, JSSATE Noida, India
13	Low Profile Cylindrical Dielectric Resonator Antenna for Modern Wireless Communication.	International Conference on Engineering, Management, and Science (OCEMS-2019)		ISBN: 978-93-5351-211-8. 15 &16 Feb 2019, RIMT, Bareilly.
14	Wideband Cylindrical Dielectric Resonator Antenna	National Conference on Contemporar		ISBN: 978-93-5267-876-1), Vol. 05, 09 Mar 2019, SRMS CETR, Bareilly

	for High Speed Communication.	y Research in Green Computing NATCOM [CRGC-2019]		
15	Stacked Rectangular Dielectric Resonator Antenna for Biomedical Electromagnetic Application.	National Conference on Biomedical Engineering NCBE-2020, NITTR, Chandigarh		22, 23 &24 Jan 2020.
16	Dual Band Rectangular Dielectric Resonator Antenna for Portable Wireless Cellular Applications	Journal of Progress in Electromagn etic Research M (PIER-M)	Scopus	Communicated Date of communication: 18 Feb 2021 ISSN: 1937-8726
17	The Effect of Finite Ground Plane on Wideband Slim Rectangular Dielectric Resonator Antenna	International Conference On VLSI & Microwave and Wireless Technologies	Scopus	Communicated. Date of communication: 15 Feb 2021
18	Modified Micro-strip Fed Rectangular Dielectric Resonator Antenna for Ultra Wide Band Wireless Spectrum Sensing Applications	Australian Journal of Electrical & Electronics Engineering	Scopus	ISSN:1448-837-X, ISSN(e):2205-362X, Communicated. Date of communication: Nov 2019
19	Dual Band Dielectric Resonator Antenna for Wide Band Applications	International Journal of Energy Technology and Policy	Scopus	ISSN online 1741-508X ISSN print 1472-8923 Communicated. Date of communication: Oct 2020

20	Design of Micro-Strip Fed Aperture Coupled Broadside Cylindrical Dielectric Resonator Antenna Array	Engineering and Applied Science and Research	Scopus	**ISSN** 2539-6161 (Print) **ISSN** 2539-6218 (Online) Communicated. Date of communication:
21	Design and Analysis of Low Loss Rectangular Dielectric Resonator Antennas for Wireless Applications	International Journal of Microwave and Optical Technology (IJMOT)	Scopus	ISSN: 15530396 Communicated Date of communication: 20 Feb 2021
22	Aperture Coupled Modified Rectangular Dielectric Resonator Antenna Arrays for X-Band Applications	Transaction on Electronic and Electrical Materials, Springer	Scopus	Online ISSN 2092-7592 Print ISSN 1229-7607 Communicated. Date of communication:21 Feb 2021
23	Modeling of Aperture Coupled Stacked Rectangular Dielectric Resonator Antenna		Scopus	Communicated.

CHAPTER 1
INTRODUCTION

1.1 BACKGROUND

The last few decades have seen exponential growth in electronics devices for wireless communication, navigation, and sensing applications. The near field, short-range, high-speed communication technologies include the Narrow Band Internet of Things (NB- IoT), Blue tooth 5.0, Wireless Local Loop (WLL), Wireless Fidelity (Wi-Fi), Local Multipoint Distributive System (LMDS), Near Field Communication (NFC), etc. The performance of these techniques is deeply affected by the channel's response to noise, the medium for wave propagation, various sources of interferences, and its compatibility with the EMI/EMC environment [1, 2]. The major challenge is to develop a wideband front-end device such as an antenna in arrays, stacked, conformal, and reconfigurable configurations. These techniques concentrate on the wideband frequency range, covering the upper part of the VHF to the X-band range [3-5].

According to Shannon's first theorem for error-free high-speed communication, the data transmission rate (R) should be smaller than the channel capacity(C). The channel capacity is a system-level metric, and it needs to be optimized to achieve the maximum possible data throughput to the user terminal. [6, 7].

$$C = BW\ log_2\left[\det\left(I_R + \frac{\rho}{N_T} HH^T\right)\right] \tag{1.1}$$

where, BW = operating bandwidth, $N_R \times N_R$ matrix = arrangements of the receiver antenna, I_R= number of receiver antennas, ρ = signal to noise ratio, N_T = number of transmitting antennas, and HH^T= channel matrix.

By minimizing, the port isolation and field correlation channel paths become independent to achieve high channel capacity. The field correlations depend on impedance matching and S-parameter measurements. It is necessary to upscale microstrip patch antenna as the radiator or absorber/sensing device into microwave and mm-wave band. Eqn. 1 indicates the correlation channel capacity and the channel bandwidth, and they are related to the frequency of operation. Higher frequencies translate to higher electrical height, faster performance, wider bandwidth, and miniaturized design. It leads to better resolution for radars due to smaller wavelength,

lower interference due to lower signal crowding, and less crowded frequency spectrum. There is a higher antenna gain in a smaller space. Therefore, to achieve high-speed communication, the targeted technology will be microwave, millimeter-wave, and terahertz wave technologies [8-11]. But the random non-linearity, non-homogeneous, non-isotropic behavior, and attenuation due to skin effect increase the severity of the overall design challenges. When the wavelength is comparable to the physical dimension of the device, effects like phase reversal and transit time effect dominates, and circuit analysis will be on the distributive transmission line techniques [12-14].

A high-frequency quantum effect like tunneling can also cause a problem. At the high frequency of operation, the inductive properties of the metal begin to change, and even most dielectric material becomes lossy. Even dielectric such as water and glass becomes opaque in the portion of the infrared. As the frequency of operation enters into the visible domain, many dielectrics become lossless and transparent again. Therefore, except for the phenomenon of Quantum Electro-Dynamic, the solution will be obtained by Maxwell's equation and Wave equation. The field will encounter discontinuities like boundaries, scatterers, and other objects. The resultant EM field is the transmission and reflection coefficient. These transmission and reflection coefficients are complex quantities, and it depends upon the constitutive parameters. Electronics will have the flavor of optics called Quasi-optics. However, the major problem is due to the variation in phase velocity w.r.t the wavelength. It resulted in broadening of the pulse, called dispersion [15, 16].

The distribution of static charge elements induces vector potential at a far-away location. The vector potential due to the charges is the weighted sum. of the phase factor. [17-20].

In the patch antenna, the quality factor 'Q' is very high. DRA is a wideband radiator. In patch antenna, capacitive effect dominates, which results in the creations of non-spectral wave or GHOST wave. By eliminating these field patterns, we can optimize radiation efficiency [21, 22]. The patch antenna is highly affected by a surface wave and fringing field, whereas the performance of DRA is unaffected by the impact of the surface wave. The mode coupling in the patch antenna resulted in the creation of a degenerative mode. It is the formation of two similar types of lower-order modes that

reduce the radiation efficiency. But in DRA, there is no degenerative mode, and DRA is excited by the Hybrid LSE and LSM mode.

DRA is one of the best candidates at microwave and mm-wave frequency due to the flow of displacement current and ohmic losses. However, the 'Resonator Principle' governs both MSA and DRA [23, 24]. The lossy resonant cavity intentionally leaks the power to constitute radiation. MSA provides a high edge impedance of approximately 100Ω, and a quarter-wave transformer is used for impedance matching. Therefore, as substrate thickness increases, radiation efficiency increases [25]. For a thin substrate, the quality factor of a conductor (Qc) and quality factor of a dielectric (Qd) dominate. The total quality factor (Q) leads to low $\frac{}{}$ and low input impedance at resonance. Fig. 1.1

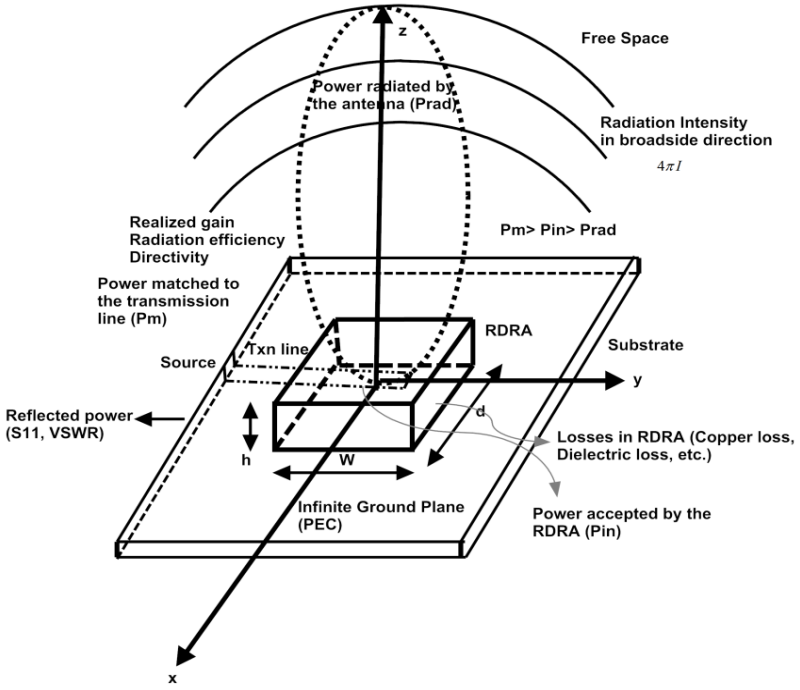

Fig.1.1: RDRA's radiation parameters

shows the radiation parameters of a simple rectangular DRA placed over a perfectly electrical conductor (PEC).

Brief history of DRA:

The electromagnetic field can exist within a source-free or loss-free region, enclosed by a perfect conductor. These fields can exist within the metallic cavity only at a

specified frequency called resonant frequency. The radiated field patterns were analyzed by Okaya and Barash [26-28]. Immediately after 1960, there was a surge in ceramic technology. Shielded dielectric material with high-quality factors acts as a source of the energy storage element used as a resonator in-circuit elements such as filters, oscillators, etc. It became an appropriate alternative to the waveguide cavity resonator and became compatible with printed circuit integration. With the removal of shielding, maintaining the aspect ratio, reducing dielectric constant, and adopting proper excitation mechanism, the dielectric resonator can become an efficient radiator. Research on dielectric resonator antenna began around 1980, and initial experiments were carried out with basic fundamental shapes like cylindrical, rectangular, hemispherical, spherical, Triangular, spherical cap, and cylindrical ring structure by Long, McAllister, and Shen. Initial emphasis was on analyzing input impedance, Q-factor, resonant modes, radiation patterns, linear polarization, and method of excitations of the unit cell of various structures of DRA. Under the influence of lower-order fundamental modes, DRA radiates like a magnetic dipole. The first linear and planar DRA array were designed and investigated by Birand, Gelsthrope, and Haneishi, Takizawa, respectively. Later it was extended from simple two elements to complex multi-elements phase arrays with beamforming and beam steering techniques. Characterization, modeling the nomenclature, formulation, and numerical analysis of DRA were credited to two research teams, one led by Kishk, Gilsson, and Junker and the other one led by Luk and Leung. Later around the mid-1990, DRA was amalgamated with ferrite material to form a ferrite resonator antenna. DRA designs have been reported as low as 1.32 GHz to as high as 40 GHz with nearly 40% of impedance bandwidth and very high efficiency [29-35]. Concentration was mainly on hybrid DRA for modern ultra-wideband systems. Fig. 1.2 shows the radiation model of RDRA indicating equivalent

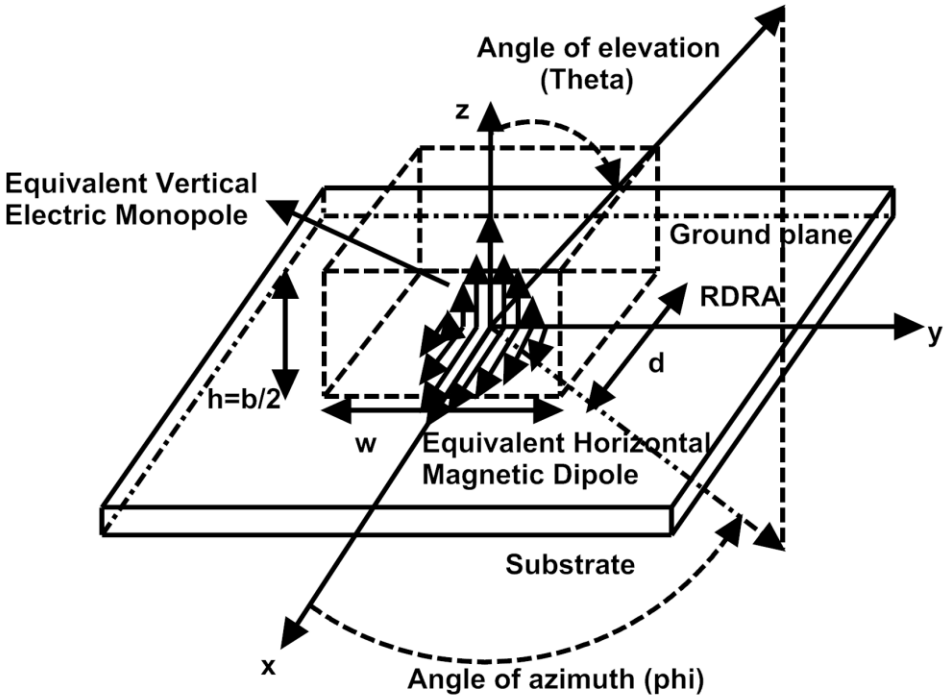

Fig.1.2: Radiation model of RDRA over infinite ground plane

vertical electric monopole and equivalent horizontal magnetic dipole over an infinite ground plane.

1.2 PROBLEM STATEMENT:

Future technology may complement or revamp the existing technology or completely discard the current wireless technology to surge ahead with speed, data integrity, and efficiency. An antenna as a front-end subsystem will play a significant role in building modern communication platforms.

Thesis aims to design, develop, and analyze highly efficient, low loss, miniaturized novel dielectric resonator antennas for emerging portable microwave and mm-wave wireless technologies such as PDAs, PCS, WSNs, etc. The goal is to develop robust techniques for DRA and RF sensors that can smartly facilitate new applications in emerging wireless technologies.

The thesis points out the methods of design, simple and complex structure, the general problem associated with them, and their corresponding solutions. The discussion is towards RDRA, leaky-wave, rectilinear, cylindrical, low loss, and

efficient DRA arrays operating in the microwave L-band to Ku-band for different wireless applications. The points emphasized are efficiency, bandwidth, and characterization of the ground plane, parametric variation, current distribution, directivity, and gain.

1.3 OBJECTIVE AND MOTIVATION:

The objective of this thesis work is:

(i) To design low profile, miniaturized narrow band, dual-band, multi-band, and wideband [36] rectangular DRA.

(ii) To study the radiation characteristics (Far-field radiation behavior) and to calculate radiation Q-factor and resonant frequency.

(iii) To study numerical and computational field behavior of RDRA (Approximate distribution of field patterns or modes within the RDRA under unloaded and loaded conditions) by using Finite Element Method.

(iv) To analyze excitation with different feeding mechanisms, its matching profile with normalized impedance, and the coupling coefficient.

(v) To understand the frequency response of the impedance with the infinite and finite ground plane.

(vi) To investigate with various techniques to enhance gain and bandwidth with circular polarization.

(vii) To implement array structure with different array feeds and mutual coupling.

(viii) To improve antenna efficiency, directivity, front to back ratio, co-polarization, etc. Radiation efficiency counts losses occur in the antenna that is conducted or dielectric losses.

(ix) To design a non-radiating dielectric-based Narrow Band Leaky Wave Resonator Antenna to radiate in the end-fire or off broadside direction to that of broadside direction for beamforming and beam steering technique.

(x) To address challenges like latency, beam coverage, cost, scalability, and diversity.

(xi) To integrate DR antenna technology to electronics and algorithm.

Design and Test Challenges:

When, the material with a high dielectric constant is chosen then the dimension of DRA reduces but the quality factor increases. The increase in quality factor reduces the impedance bandwidth. Further with an increase in the quality factor coupling coefficient reduces and resonance becomes sensitive to the change in temperature [37, 38]. When, $\varepsilon_r < 30$, the geometry of the 4G wireless devices operating at less than 3 GHz will become too big to unfit for the wireless handset. The potential challenges while designing, analyzing, and developing Rectangular Dielectric Resonator Antenna considering modern communication technologies are:

(i) Optimizing statistical peak to average signal characteristics by reducing noise, increasing signal by addressing unnecessary losses, linear and non-linear impairment, and selecting the right bandwidth and rejecting others. The noise contribution can be significant for wideband applications as noise power is an integral part of the wide bandwidth of the spectrum.

(ii) Improved radiation efficiency, gain, directivity, bandwidth stability over a wide range of frequencies, and variations in temperature.

(iii) Miniaturized design which leads to an increase in the reactive (capacitive) impedance, decrease in radiation resistance, difficulty in matching due to reduction in bandwidth, and challenges in the positioning of the source.

(iv) Controlling surface wave, back radiation, and edge diffraction by an antiphase electric field and uniplanar configuration Hybrid configuration.

(v) Active integration and development of miniaturized active antenna with on-chip/ on package/ in package hybrid antenna array solution. Testing and characterization of in package array, embedded antenna solution, surrounding effect, etc.

(vi) Conformal design with the realization of multi-band structure.

(vii) Investigation on new limits and open the door to 5G/6G beyond 100 GHz for short data limits.

(viii) The new era of health is zooming into technology. The current antenna technology is facing enormous problems like absorption of RF/Microwave power from the antenna into the head of the users. DRA technology will respond to this problem by decreasing the near field in the exposed area of the human body.

Motivation:

DRA provides many fascinating features which are instrumental in bridging the gap between microwave and optical communication.

(i) Radiation mechanism of DRA is different and depends upon the property of dielectric hysteresis.

(ii) DRA shows multi-functional characteristics similar to that of smart antenna technology. Therefore, its characteristics can be customized conveniently to solve practical problems without changing the physical dimension.

(iii) DRA array configuration for gain enhancement, directivity, beam steering, and switching techniques.

(iv) Optimization at microwave and millimeter-wave application.

(v) DRA has the un-matured numerical technique for the performance analysis. A mature numerical technique method solution can always track the requirement to estimate the solution.

(vi) To design conformal DRA structure.

(vii) To fulfill the modern requirements in Massive MIMO, 5G Sub GHz, and mm-Wave, capturing complex and fast transmission mode current waveform over time while speeding through wireless standards.

1.4 RESEARCH CONTRIBUTION

The fundamental concepts are based on the physical laws and their implications on governing the electromagnetic phenomenon. The field patterns within the DRA articulates the design equations. It is the front runner and one of the most viable alternatives to replace the most successful conventional microstrip patch antenna. It is mainly due to its capacitive nature, where the quality factor is on the higher side. These limitations are addressed effectively by the DRA, and it provides a high degree of versatility and flexibility to the design. The three fundamental aspects of DRA are the characteristics equation, radiation pattern, and excitation methodology. The transcendental and characteristics equation determines the propagation constant, radiation quality factor, and resonant frequency. The mode theory of RDRA provides a practical and orthogonal basis function. Further, detailed current distributions can be accomplished by applying the boundary value problem in terms of eigenvalues and eigenvectors [39-41]. The dielectric interface and boundary are crucial as reflection and refraction dominate to alter the inherent mode orientation. The initial focus is designing the fundamental structures such as hemispherical, cylindrical, and rectangular DRA (RDRA) with various feeding, excitation, and energy coupling techniques to operate on the fundamental and hybrid modes. The concentration is towards the designing of a rectangular dielectric resonator antenna.

The second objective is to direct the specialized data to achieve experimental, analytical, and numerical results to determine electric and magnetic field patterns or modes within the structure and external to it at the Fresnel and Fraunhofer zones. Based on the demand specifications, the wave equation will be resolved numerically and analytically followed by the fabrication of the prototype. The experimental technique is expensive, time-consuming, and usually does not allow flexibilities in the parameters setting. There are some continuous variables associated with it. The computational electromagnetic problem can be addressed in various ways. This work uses the Finite Element Method (FEM) as a computational technique for field calculations and High frequency structured simulator as a 3D electromagnetic tool. The FEM is a frequency domain differential technique, where the entire structure is chopping off in terms of space and time into some discrete variables [42, 43].

The third objective is to design some rectangular dielectric resonator antennas for

various wireless applications. Analysis of RDRAs is carried out by applying the waveguide theory model, such as Dielectric waveguide and modified dielectric waveguide model [44, 45]. The priority is designing a broadband antenna. Parameters like feeding techniques, impedance matching, and coupling techniques reduce the reflection and leakage of energy. It leads to the excitation of different modes within the structure. It leads to constructive interference with high gain, directivity, and front-to-back ratio. The mode control techniques result in the activation of hybrid modes. It leads to azimuthal field variation and altercation of operating frequency, output characteristics like beam pattern, beamwidth, co, and cross-polarization, etc. Various methods and geometries are described to enhance the frequency limit.

1.5 THESIS OUTLINES

This thesis is organized in coherent order with six chapters. The thesis focuses on the fundamental steps of designing, such as analytical, numerical modeling, experimental implementation, fabrication, and measurement of rectangular DRA in the ❍-wave band of operation. The outlines of the thesis are as follows:

Chapter one is devoted to an introduction to DRA as an efficient radiating element. It explains the characteristics of simple shaped and modified hybrid shaped DRA. Its research motivation, and objective of the research, scope, and contribution of the project.

Chapter two summarizes the literature survey, the design equations of the simple shaped DRA to calculate resonant frequency and radiation Q-factor, coupling and feeding mechanisms, impedance matching network, dielectric materials for the DRA and its substrate, finite element methods as computational technique, and introduction to a 3D electromagnetic simulation tools based high frequency structured simulator (HFSS).

Chapter three introduces the design and development of planar and non-planar dielectric resonator antenna. This chapter focuses on the design, analysis of embedded rectangular DRA, narrowband rectangular DRA, and leaky-wave guide-based DRA for mm-wave applications. It highlights various practical fabrication and implementation challenges and the ways to deal with them.

Chapter four discusses the simulations and designs of multi-functional hybrid

DRA. This chapter presents three novel designs: dual-band rectangular DRA for portable wireless cellular applications, filleted dual-band DRA for high-speed application, and dual-band hybrid rectangular DRA. The process of fabrication and measurements are illustrated.

Chapter five is devoted to the design and analysis of wideband DRA. This chapter describes three fundamental designs: the design of microstrip fed aperture coupled broadside cylindrical DRA array, the design of multi-functional hybrid DRA for high-speed communication, and microstrip inset fed rectangular DRA.

Chapter six presents the conclusion from the research carried out, their implications, critical analysis, and its impact on the next generation's future communication network.

CHAPTER 2
LITERATURE REVIEW: A SURVEY OF DRA

2.1 INTRODUCTION

DRA is a low-profile functional radiator. It operates in hybrid and some higher-order modes. The mode theory of RDRA provides a practical and orthogonal basis function. At the dielectric interface, reflection and refraction dominate to alter the inherent mode orientation. Eigenvalues and eigenvectors determine the current distribution in the dielectric. When the DRA is excited, then total current is the superposition of various modes initiated eigen current at a particular instant of time [46, 47]. The mode control results transformation of operating frequency, output characteristics like beam pattern, beamwidth, polarization, gain, etc. Technically, the modes are modeled by R, L, C networks. The critical aspects of DRA are the (i) characteristics equation, (ii) radiation pattern, and (iii) excitation methodology. The transcendental characteristics equation determines the propagation constant and the resonant frequency. Estimation of the f_r and the Q_{rad} is from a combined solution of time-averaged electric energy and time-averaged magnetic energy.

DRA is said to be a lossy resonator. For a perfect resonator, quality factor (Q) approaches infinity. Resonance is said to be a condition where the field exists without excitation. There are two types of resonance: (i) Source free resonance (ii) Loaded resonance. The source-free resonance gives the picture of the formation of the modes and the field pattern of the source-free radiation mode. Due to the presence of discontinuities, the transmission and reflection coefficient determines the loaded resonance. The resonant frequency is never a complex number if the antenna is radiating, and if the resonant frequency is a real number, then the antenna is not radiating. Wavenumber is the phase shift per unit length. The continuous wave number implies radiation, whereas the discrete wavenumber indicates no radiation.

Dielectric slab, rod, and film can guide and radiate electromagnetic energy if dielectrics of different permittivity and geometry can be excited appropriately [48-51]. The modes within the guide are the plane waves reflecting at an angle from the boundaries. The new field patterns are formed within the dielectric slab by the interaction of the field components. The differences in wave patterns are due to the in-phase components of reflections and the generation of the evanescent mode. If the

angle of reflection (θ_1) > the critical angle (θ_c), where [52, 53]

$$\theta_c = \sin^{-1}\left(\frac{\varepsilon_2}{\varepsilon_1}\right)^{\frac{1}{2}} \tag{2.1}$$

then the mode will be confined within the guide. For a steeper angle, when there is energy transmission into the outer medium from the core, each reflection creates the formation of the leaky wave. A Linear combination of Bessel's functions defined the wave within the structure. Hankel's function characterizes traveling waves in the outward direction[54]. The reactance slope parameter (α) is:

$$\alpha = \frac{\omega_0}{2}\frac{dX}{d\omega_0} \text{ (ohm)} \tag{2.2}$$

$$b = \frac{\omega_0}{2}\frac{dB}{d\omega_0} \text{ (mho)} \tag{2.3}$$

$$\left(\frac{\omega}{\omega_0} - \frac{\omega_0}{\omega}\right) = 2\left(\frac{\omega-\omega_0}{\omega_0}\right) \tag{2.4}$$

The resonant circuit may be lumped or distributed in every quarter cycle [55, 56].

2.2 DIELECTRIC RESONATOR

2.2.1 Dielectric

Dielectrics are materials having bounded electrons. Though atoms and molecules are neutral but there is possibility to have dipole moment under the application of electric field, which constitute polarization.

$$\mathrm{P} = \frac{\mathrm{dp}}{\mathrm{d}\tau} \tag{2.5}$$

where, P is the polarization and it is a vector field, $\frac{\mathrm{dp}}{\mathrm{d}\tau}$ (dipole moment/ volume). Dipole moment & polarization are different at a different place in a dielectric. Based on properties, dielectric and insulators can be differentiated. By applying the electric field when dipole moment and polarization are measured then it is called dielectric, and if the current density is measured then it is called an insulator. The behavior of the dielectric can be realized through the atomic concept. A good dielectric is one for which a.c capacitivity (ε') remains almost constant at all radio frequencies and the dielectric loss factor (ε'') is very small. In a lossy dielectric a.c, capacitivity and dielectric loss factor are varying with the variation of frequency. There are three possible ways through which dielectric responds to the applied field [57, 58]:

(i) On the quantum scale, charges are displaced through rotation or separation.

(ii) Under the application of the applied field, the atomic and molecular bonds get stretched up and relaxed. This is called ionic polarization.

(iii) Stretching of electron orbital or cloud around the nucleus and is called electronic polarization.

It takes a non-zero amount of time to bring forth the relevant changes. In a dielectric, when the period of the applied field is matched to the time required to have a relative change, then it can come back to its original position resulting change in effective relative tracking. Below the f_r, the dielectric can track the applied frequency of the field. Whereas above the resonant frequency, the dielectric will never track the applied frequency. So polarization will never occur above the resonant frequency. Due to atomic displacement, there occurs a loss of energy, especially due to heat. Heat loss becomes optimum at the resonant frequency. The presence of roughness and impurities that is electrically large constitutes scattering and absorption. In dielectric, the electric displacement current $\frac{\delta D}{\delta t}$ is a motion of the bound charge.

$$\varepsilon(\omega) = \varepsilon^{'} - j\varepsilon^{''} = |\varepsilon| e^{-j\delta} \tag{2.6}$$

Where, $\varepsilon^{'}, \varepsilon^{''}, \delta$ are real quantities, $\varepsilon^{'}$ is the a-c capacitivity, $\varepsilon^{''}$ is the dielectric decay factor, and δ is the dielectric loss tangent. The time average power dissipation and electric energy will be:

$$P_d = \iiint \omega\varepsilon^{''} |E|^2 \, d\tau \tag{2.7}$$

$$W_e = \frac{1}{2} \iiint \varepsilon^{'} |E|^2 \, d\tau \tag{2.8}$$

Here $\varepsilon^{'}$ contributes to stored energy and $\omega\varepsilon^{''}$ contributes to power dissipation. In a good dielectric a-c capacitivity $\varepsilon^{'}$ is almost constant whereas dielectric loss factor $\varepsilon^{''}$ is very small. DRA is operating at fundamental lower order modes usually radiate like a magnetic dipole [59-61].

2.2.2 Radiation in a Dielectric

While studying the resonance and relaxation of the dielectric materials, the resonant frequency can be compared with the microscopic dipoles. In a dielectric d.c conduction current is negligibly small whereas appreciable alternating current in phase with the applied field is present within the dielectric due to the effect of dielectric hysteresis. The Maxwell's curl equation from Ampere's circuit law [62, 63]:

$$\nabla \times H = J + \frac{\partial D}{\partial t} = \sigma E + j\omega\varepsilon E \quad (2.9)$$

$$\nabla \times H = \sigma E + j\omega(\varepsilon^{'} - j\varepsilon^{''})E \quad (2.10)$$

where, $\varepsilon = (\varepsilon^{'} - j\varepsilon^{''})$, $\varepsilon^{'}$ is the real or lossless part and $\varepsilon^{''}$ imaginary or lossy part of ε.

$$\nabla \times H = [(\sigma + \omega\varepsilon^{''}) + j\omega\varepsilon^{'}]E \quad (2.11)$$

$$\nabla \times H = [\sigma^{'} + j\omega\varepsilon^{'}]E = J_{total}\, E \quad (2.12)$$

At d.c, $\omega = o$ and $\omega\varepsilon^{''}$ is low, therefore power loss is low. At high frequency losses increase as $\omega\varepsilon^{''}$ becomes large. $\tan\delta = \frac{\sigma^{'}}{\omega\varepsilon^{'}}$, and power factor (PF)$cos\theta = \frac{\sigma^{'}}{\omega\varepsilon^{'}}$

The power dissipated per unit volume will be:

$$P = \sigma^{'}E^2 = (\sigma + \omega\varepsilon^{''})E^2 \;\; in\,(\frac{W}{m^2}) \quad (2.13)$$

2.2.3 Field configuration within and outside of the DR

As

$$\theta_i > \theta_c = \sin^{-1}\frac{1}{\varepsilon^{'1/2}} \quad (2.14)$$

Therefore, a dielectric in the air will have high Q and can become a microwave resonator if the loss is significantly small. There exist two types of mode in an anisotropic medium. They are (i) Electric field type mode, which is similar to electric multipole (ii) H-field type mode [64, 65].

2.2.4 Equation of the resonant frequency (First order):

Let the boundary coincides with a node and antinode of electric and magnetic field. The dimension of the resonator > the effective ● in the crystal i.e. $\left(\frac{\bullet}{\varepsilon^{'1/2}}\right)$, $\mu = 1$, and dielectric constant along the three axes are $\varepsilon_x^{'}$, $\varepsilon_y^{'}$, and $\varepsilon_z^{'}$.

Maxwell's equation implies:

$$\nabla \times E = -\dot{H} \tag{2.15}$$

$$\nabla \times H = \varepsilon \dot{E} \tag{2.16}$$

The solution for the electric field in x, y, and z direction will be [66, 67]:

$$E_x = A_x \begin{matrix}\cos\\ \sin\end{matrix} \boxtimes x \begin{matrix}\cos\\ \sin\end{matrix} \approx y \begin{matrix}\sin\\ \cos\end{matrix} \cmd z e^{j\omega t} \tag{2.17}$$

$$E_y = A_y \begin{matrix}\sin\\ \cos\end{matrix} \boxtimes x \begin{matrix}\sin\\ \cos\end{matrix} \approx y \begin{matrix}\sin\\ \cos\end{matrix} \cmd z e^{j\omega t} \tag{2.18}$$

$$E_z = A_z \begin{matrix}\sin\\ \cos\end{matrix} \boxtimes x \begin{matrix}\cos\\ \sin\end{matrix} \approx y \begin{matrix}\cos\\ \sin\end{matrix} \cmd z e^{j\omega t} \tag{2.19}$$

There are three cases to be considered:

Case-I: The permittivity $\varepsilon_z = \varepsilon_{parallel}$ and $\varepsilon_x = \varepsilon_y = \varepsilon_{perpendicular}$

Case-II: The permittivity $\varepsilon_x = \varepsilon_{parallel}$ and $\varepsilon_y = \varepsilon_z = \varepsilon_{perpendicular}$

Case-III:$\varepsilon_y = \varepsilon_{parallel}$ and $\varepsilon_x = \varepsilon_z = \varepsilon_{perpendicular}$

Where, $\varepsilon_{parallel}$ and $\varepsilon_{perpendicular}$ are perpendicular to the optic axis.

The solutions which satisfy the **non-zero** $E_x, E_y,$ and E_z field are:

$$\left(\frac{2}{\bullet}\right)^2 = \frac{1}{\varepsilon_{perpendicular}}\left[\left(\frac{l}{a}\right)^2 + \left(\frac{m}{b}\right)^2 + \left(\frac{n}{c}\right)^2\right] \tag{2.20}$$

$$\left(\frac{2}{\bullet}\right)^2 = \frac{1}{\varepsilon_{parallel}}\left[\left(\frac{l}{a}\right)^2 + \left(\frac{m}{b}\right)^2\right] + \frac{1}{\varepsilon_{perpendicular}}\left(\frac{n}{c}\right)^2 \tag{2.21}$$

$$\left(\frac{2}{\bullet}\right)^2 = \frac{1}{\varepsilon_{perpendicular}}\left[\left(\frac{l}{a}\right)^2 + \left(\frac{m}{b}\right)^2 + \left(\frac{n}{c}\right)^2\right] \tag{2.22}$$

$$\left(\frac{2}{\bullet}\right)^2 = \frac{1}{\varepsilon_{perpendicular}}\left[\left(\frac{l}{a}\right)^2\right] + \frac{1}{\varepsilon_{parallel}}\left[\left(\frac{m}{b}\right)^2 + \left(\frac{n}{c}\right)^2\right] \tag{2.23}$$

$$\left(\frac{2}{\bullet}\right)^2 = \frac{1}{\varepsilon_{perpendicular}}\left[\left(\frac{l}{a}\right)^2 + \left(\frac{m}{b}\right)^2 + \left(\frac{n}{c}\right)^2\right] \quad (2.24)$$

$$\left(\frac{2}{\bullet}\right)^2 = \frac{1}{\varepsilon_{parallel}}\left[\left(\frac{l}{a}\right)^2 + \left(\frac{n}{c}\right)^2\right] + \frac{1}{\varepsilon_{parallel}}\left[\left(\frac{m}{b}\right)^2\right] \quad (2.25)$$

Where,

$\boxtimes = \frac{l}{a}\pi$, $\approx = \frac{m}{b}\pi$, $\text{⌘} = \frac{n}{c}\pi$ and l, m, n are integers.

The first equation for each case implies isotropy of permeability (❍) and second equation implies anisotropy of permittivity (ℳ). These solutions identify different modes and will be useful for the calculations of frequency. The boundary condition can be applied by converting volume based three dimensional (3D) analysis into the surface based two dimensional (2D) analysis. The inside (E_{ix})and outside (E_{ox}).

$$E_{ix} = E_{ox} \quad (2.26)$$

where, $E_{ix} = e_{ix}\cos \text{⌘}_i z\, e^{i\omega t}$ and $E_{ox} = e_{ox}\, e^{-\text{⌘}oz}\, e^{i\omega t}$

$$\text{⌘}o = \text{⌘}_i \tan \text{⌘}_i \frac{c}{2} \quad (2.27)$$

$$\rho_i{}^2 + \text{⌘}o^2 = \beta^2 \text{ : for outside} \quad (2.28)$$

$$\rho_i{}^2 + \text{⌘}i^2 = \varepsilon\beta^2 \text{ : for inside} \quad (2.29)$$

Here $\beta = \frac{2\pi}{\bullet} = \frac{\omega}{c}$ =Intrinsic phase constant. If the dielectric constant along z direction $\text{⌘}_i \gg \text{⌘}_0$then **wave equation** will be:

$$\left(\frac{c\text{⌘}_i}{2}\right)^2 \tan^2 \frac{c\text{⌘}_i}{2} = (\beta^2 - \rho_i{}^2)\left(\frac{c}{2}\right)^2 \quad (2.30)$$

If $\rho_i$is of the order of $\frac{2\sqrt{\varepsilon}}{\bullet}$ and $\rho_i \gg \beta$ then

$$(\beta^2 - \rho_i{}^2)\left(\frac{c}{2}\right)^2 \cong \left(\frac{c\rho_i}{2}\right)^2 \cong \left(\frac{c\sqrt{\varepsilon}}{\bullet}\right)^2 \quad (2.31)$$

If the physical dimension of the resonator is thinner than $\bullet/\sqrt{\varepsilon}$ and it is comparable to that of wavelength, then more electric field extends outside the resonator. Therefore resonator can be considered as **a point source radiator**. The desired radiation pattern can be obtained by controlling the aspect ratio and dielectric constant.

2.2.5 Second order approx of the magnetic field mode

The 2nd order approx H-field is accurate only for the fundamental mode. The fundamental magnetic mode is $TM_{11\delta}$ mode. $\delta = (c/\pi)\text{⌘}$ along z axis inside the resonator. The electric field inside the resonator will be [66]:

$$E_{xi} = A_x(z)\cos \boxtimes x \sin \text{≈} y\, e^{i\omega t} \tag{2.32}$$

$$E_{yi} = A_y(z)\sin \boxtimes x \cos \text{≈} y\, e^{i\omega t} \tag{2.33}$$

$$E_{zi} = 0 \tag{2.34}$$

Putting these values in the Maxwell's equation, we get

$$\frac{d^2A_x}{dz^2} + \left(\varepsilon_x\beta^2 - \text{≈}^2\right)A_x + \boxtimes_{\text{≈}}A_y = 0 \tag{2.35}$$

$$\frac{d^2A_y}{dz^2} + \left(\varepsilon_y\beta^2 - \text{≈}^2\right)A_y + \boxtimes_{\text{≈}}A_x = 0 \tag{2.36}$$

$$\boxtimes\frac{dA_x}{dz} = -\text{≈}\frac{dA_y}{dz} \tag{2.37}$$

$$A_x = C_- \sin\alpha_i e^{i\text{⌘}i-z} + C_+ \cos\alpha_i e^{i\text{⌘}i+z} \tag{2.38}$$

$$A_y = C_- \cos\alpha_i e^{i\text{⌘}i-z} + C_+ \sin\alpha_i e^{i\text{⌘}i+z} \tag{2.39}$$

$$\text{⌘}_{i\pm}{}^2 = \frac{1}{2}\left[\beta^2\left(\varepsilon_x + \varepsilon_y\right) - \left(\boxtimes^2 + \text{≈}^2\right)\right] \pm \left\{\left\{\beta^2\left(\varepsilon_x - \varepsilon_y\right) - \left(\boxtimes^2 - \text{≈}^2\right)\right\}^2 + 4\boxtimes 2\text{≈}212 \right. \tag{2.40}$$

The angle α_i should be

$$\tan\alpha_i = \frac{-1}{2\boxtimes_n}\left[\beta^2(\varepsilon_y - \varepsilon_x) - (\approx^2 - \boxtimes^2)\right] + \left\{\{\beta^2(\varepsilon_x - \varepsilon_y) - (\boxtimes^2 - \approx^2)\}^2 + 4\boxtimes^2\approx^2\right\}^{1/2} \quad (2.41)$$

Where, $\boxtimes = \frac{\pi l}{a}, \approx = \frac{\pi m}{b}$ are propagation constant along x and y direction, l and m are the integer. If the field inside and outside the resonator are matched along the x-y plane and at $\pm\frac{c}{2}$. The outside electric field exactly at the boundary will be:

$$E_{x0} = B_x(z)\cos\boxtimes x \sin\approx y\, e^{j\omega t} \quad (2.42)$$

$$E_{y0} = B_y(z)\sin\boxtimes x \cos\approx y\, e^{j\omega t} \quad (2.43)$$

$$E_{z0} = 0 \quad (2.44)$$

The wave equation for the electric field present outside the resonator will be:

$$B_x = D_- \sin\alpha_0 e^{i\text{⌘}0-z} + D_+ \cos\alpha_0 e^{i\text{⌘}0+z} \quad (2.45)$$

$$B_y = D_- \cos\alpha_i e^{i\text{⌘}0-z} - D_+ \sin\alpha_i e^{i\text{⌘}i+z} \quad (2.46)$$

Where,

$$\left(\frac{\text{⌘}_{0^-}}{\pi}\right)^2 = \left(\frac{2}{\bullet}\right)^2 - \left[\left(\frac{l}{a}\right)^2 + \left(\frac{m}{b}\right)^2\right] \quad (2.47)$$

$$\left(\frac{\text{⌘}_{0^+}}{\pi}\right)^2 = \left(\frac{2}{\bullet}\right)^2 \quad (2.48)$$

$$\tan\alpha_0 = -\frac{\approx}{\boxtimes} = \frac{-ma}{lb} \quad (2.49)$$

Here $i\text{⌘}_{0^-}$ represents exponentially damped wave outside the resonator and $i\text{⌘}_{0^+}$ shows propagation without attenuation. Now we will apply the boundary condition to the field present within and outside of the dielectric resonator. From the boundary conditions:

$$A_x = B_x \text{ at } z = \frac{c}{2} \quad (2.50)$$

$$A_y = B_y \text{ at } z = \frac{c}{2} \tag{2.51}$$

$$\frac{\partial A_x}{\partial z} = \frac{\partial B_x}{\partial z} \text{at } z = \frac{c}{2} \tag{2.52}$$

$$\frac{\partial A_y}{\partial z} = \frac{\partial B_y}{\partial z} \text{at } z = \frac{c}{2} \tag{2.53}$$

Now applying the value of A and B from the above calculated field equations, we get four linear equations for C and D. The following relation will be established [31]:

For $\varepsilon_z = \varepsilon_{parallel}$ and $\varepsilon_x = \varepsilon_y = \varepsilon_{perpendicular}$ and $\alpha_i = \alpha_0$

For inside field:

$$\frac{C_+}{C_-} = \frac{⌘_{i-}(⌧\sin\alpha_i - ⌀\cos\alpha_i)}{⌘_{i-}(⌀\sin\alpha_i + ⌧\cos\alpha_i)} e^{i(⌘_{i-} - ⌘_{i+})z} \tag{2.54}$$

This inside field will couple to the outside field with a significant variation in propagation constant. For the outside field [32]:

$$\frac{D_+}{D_-} = \frac{⌘_{i-}(⌧\sin\alpha_0 - ⌀\cos\alpha_0)}{⌘_{i-}(⌀\sin\alpha_0 + ⌧\cos\alpha_0)} e^{i(⌘_{0-} - ⌘_{0+})z} \tag{2.55}$$

It is observed that there exists a monotonically decreasing mode D_outside of the resonator. Further analysis reveals the following:

$$\left|\frac{⌘_{0+}}{⌘_{0-}}\right|^2 \cong \frac{\left(\frac{2}{●}\right)^2}{\left(\frac{l}{a}\right)^2 + \left(\frac{m}{b}\right)^2} \cong \frac{1}{\varepsilon} \cong 0 \tag{2.56}$$

We have

$$⌘_{0-}(\alpha⌘_{i-}\tan\frac{c}{2}⌘_{i-} + \beta⌘_{i-}\tan\frac{c}{2}⌘_{i+}) \cong ♑⌘_{i+}⌘_{i-}\tan\frac{c}{2}⌘_{i+}\tan\frac{c}{2}⌘_{i-} \tag{2.57}$$

Where, $\alpha = \sin^2(\alpha_i - \alpha_0)$, $\beta = \sin^2(\alpha_i - \alpha_0)$, $\gamma = 1$

When $\varepsilon_z = \varepsilon_{parallel}$ and $\varepsilon_x = \varepsilon_y = \varepsilon_{perpendicular}$ then propagation constant outside and inside of the dielectric resonator may be represented as:

$$\text{⌘}_{0^-} = \text{⌘}_{i^-} \tan \text{⌘}_{i^-} \frac{c}{2} \quad (2.58)$$

There are other set of $TE_{11\delta}$ mode which satisfy the boundary conditions. $\delta = (c/\pi)$⌘ along z axis inside the resonator. The magnetic field inside the resonator will be:

$$H_{xi} = L_x(z) \cos \text{⊠}x \sin \text{≈}y \, e^{i\omega t} \quad (2.59)$$

$$H_{yi} = L_y(z) \sin \text{⊠}x \cos \text{≈}y \, e^{i\omega t} \quad (2.60)$$

$$H_{zi} = 0 \quad (2.61)$$

Where,

$$L_x = M_- \cos \alpha_i \cos(\text{⌘}i - z) + M_+ \sin \alpha_i \cos(\text{⌘}i - z) \quad (2.62)$$

$$L_y = M_- \sin \alpha_i \cos(\text{⌘}i - z) - M_+ \cos \alpha_i \cos(\text{⌘}i - z) \quad (2.63)$$

At the outside electric and magnetic field can be interchanged. The boundary condition remains same but the coefficient will be altered for the magnetic field. The field in x-y plane is quite complicated due to its anisotropic nature. The field pattern which will be generated in the dielectric resonator will be elliptically polarized. There has to be a strong coupling between resonator field, radiation field, and the free space field. For magnetic dipole, the radiation impedance will be [33]:

$$R_H = 7.9 \times 10^2 \left(\frac{R_1}{\bullet}\right)^2 \text{Ohms} \quad (2.64)$$

$$R_E = 3 \times 10^{-27} \left(\frac{\bullet}{R_1}\right)^2 \text{Ohms} \quad (2.65)$$

The magnetic pole field couples strongly than that of the electric pole field. Therefore the radiation pattern is being controlled by DR as a **magnetic dipole**. However, the radiation fields for the higher-level modes are complex due to the formation of the multipole.

2.3 MAJOR CHARACTERISTICS OF DRA

(i) DRA has better bandwidth to footprint ratios with an acceptable height.

(ii) The f_0 and radiation Q will be decided by the aspect ratio of the DRA for a constant dielectric constant ε_r. It provides high design flexibility.

(iii) DRA has good electrical characteristics but non-electrical characteristics like low profile, lightweight, miniaturized and conformal design make it suitable for integration with microwave integrated circuits (MICs).

(iv) DRA is easy to excite. It has high power handling capability, good cross-polarization characteristics, high radiation efficiency, and low feed network losses.

(v) Dielectric as a radiator has a high displacement current and low conduction current. Because of the small skin depth in the dielectric materials conductor losses (ohmic losses and metallic losses) and surface wave losses are very low. It results in high radiation efficiency at microwave and millimeter-wave frequency band.

(vi) Wide range of dielectric constant ($\varepsilon_r = 8\ to\ 100$) allows the designer to have control over the dimensions, bandwidth, and feeding mechanisms.

(vii) DRA can be designed for the low frequency of 1.3 GHz to the high frequency of 40 GHz covering both microwave and millimeter wave domains.

(viii) The radiation mechanism of the DRA is completely different and depends upon the property of dielectric hysteresis. It provides a uniform and stable radiation pattern over the entire impedance bandwidth.

(ix) Multi-functional DRA can be realized without altering its physical dimension.

(x) DRA can employ various feeding mechanisms, such as a probe, slots, microstrip line, DIG, coplanar waveguide, etc.

(xi) The DRA behaves as short electric or magnetic dipoles depending upon the types of lower-order modes produces within it to radiate broadside and omnidirectional patterns.

(xii) DRA is powered by Hybrid LSE and LSM field mode, which addresses issues like degenerate mode and inefficient mode coupling.

(xiii) High impedance bandwidth (up to 60%) can be realized with a DRA array. DRA array configuration offers gain enhancement, high directivity, and beam steering capabilities at high frequency.

(xiv) The radiation pattern of the DRA can be predicted accurately without any extensive computation.

However, the DRA technology experiences inherent challenges like

(i) DRA requires a complex fabrication process. These limitations in fabrication can limit the characteristics of the antenna.

(ii) It is tough to design a modified shape due to material rigidity.

(iii) The high cost of dielectric material.

(iv) DRA uses an insufficient and un-matured numerical technique for its performance analysis (especially Rectangular DRA). It is required to improve RDRA's mathematical modeling to analyze its design characteristics.Certain applications demand accuracy and precision based performance rather than cost. DRA will fulfill the criteria as an efficient radiating and sensing front end device.

2.4 FUNDAMENTAL STRUCTURAL ANALYSIS OF DRA

It is necessary to develop numerical techniques to predict different field configurations to calculate the resonant frequency, radiation Q-factor, input impedance, matching profile, and output characteristics such as gain, directivity, polarization, etc. Detailed knowledge of the internal field configuration leads to thorough analysis and precise prediction of different modes within the DRA [68-70]. Three fundamental structures are hemispherical, cylindrical, and rectangular, are considered first for detailed analysis, and then the complex hybrid structure develops from them.

(i) In hemispherical DRA radius of the hemisphere decides the f_r and the Q_{rad}. The single degree of freedom limits the size, matching profile, and the enhanced performances.

(ii) In cylindrical DRA, aspect ratio, various modes can be excited and controlled to optimize the performance.

(iii)In rectangular DRA, length, width, and depth constitute two degrees of freedom (length/width and depth/width), which provides several aspect ratios and radiation Q-factor for a fixed resonant frequency.

2.4.1 The Hemispherical DRA

The hemispherical DRA of radius 'a' with ε_r is mounted on a substrate as shown in Fig. 2.1. Image theory can be used to replace an isolated spherical shape DRA into a hemispherical DRA. The field patterns or modes can be described with the help of a spherical coordinate system in radius r, azimuth(θ), and elevation($\emptyset$). There exist two types of mode in a dielectric sphere that is TE and TM. In TE_{nmp} the first subscript 'n' refers to the order of the spherical Bessel function (**Schelkunoff type**)[71, 72].

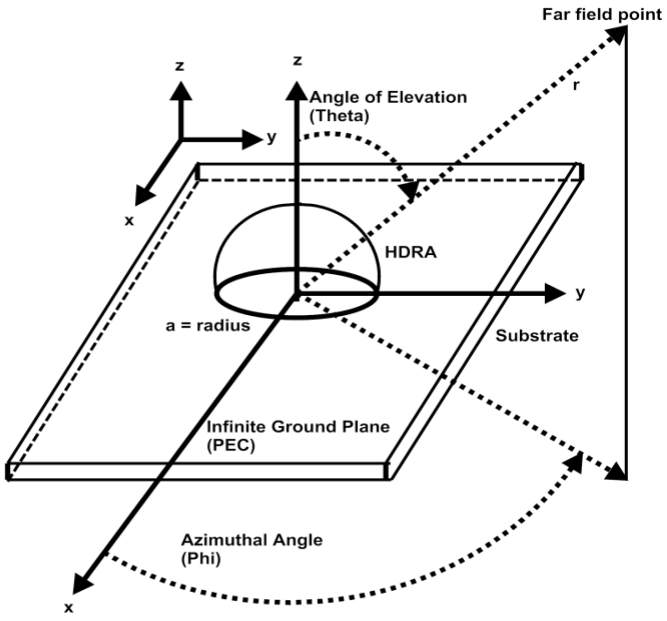

Fig. 2.1: Hemispherical DRA over an infinite ground plane

So there exist 02 modes TE_{111} and TM_{101}. The characteristics equation of an isolated dielectric sphere placed over an infinite ground plane excited by probe or aperture provides a reasonable fair accuracy of the resonant frequency [73-76]. However Q-

factor of the isolated DRA difficult matches with the fabricated DRA due to the impedance matching profile of the feeding mechanism.

The TE_{111} mode:

The characteristics equation of the hemispherical DRA in TE_{111} mode can be written as [77]:

$$\frac{J_{1/2}(\sqrt{\varepsilon_r}k_a a)}{J_{3/2}(\sqrt{\varepsilon_r}k_a a)} = \frac{H^{(2)}{}_{1/2}(k_a a)}{\sqrt{\varepsilon_r}H^{(2)}{}_{1/2}(k_a a)} \tag{2.66}$$

After getting the value of k_0 the resonant frequency can be determined by:

$$f_{GHz} = \frac{4.7713\ Re(k_0 a)}{a_{cm}} \tag{2.67}$$

Here resonant frequency is expressed in GHz and the radius of the hemisphere 'a' is in cm. The radiation Q factor will be:

$$Q = \frac{Re(k_0 a)}{2Im(k_0 a)} \tag{2.68}$$

Therefore the Q-factor of the hemispherical DRA is equal to the radiated Q-factor. The resonant frequency of the hemispherical DRA with constant dielectric constant and radius can be calculated by finding the value of $Re(k_0 a)$ from the graph and given table and further resonant frequency can be calculated [77, 78]. Fig. 2.2 shows the plot of the real part of (k_0a) of the TE_{111} mode of the hemispherical DRA and Fig. 2.3 shows the response of the Q-factor of the TE_{111} mode of the hemispherical DRA.

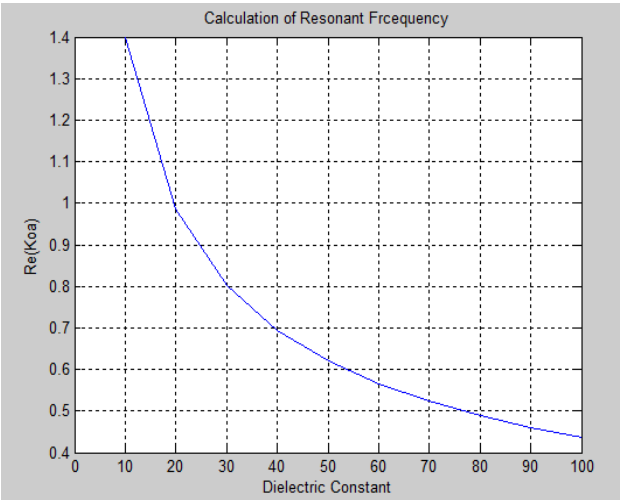

Fig. 2.2: Real part of $(k_0 a)$ of the TE_{111} mode of the hemispherical DRA

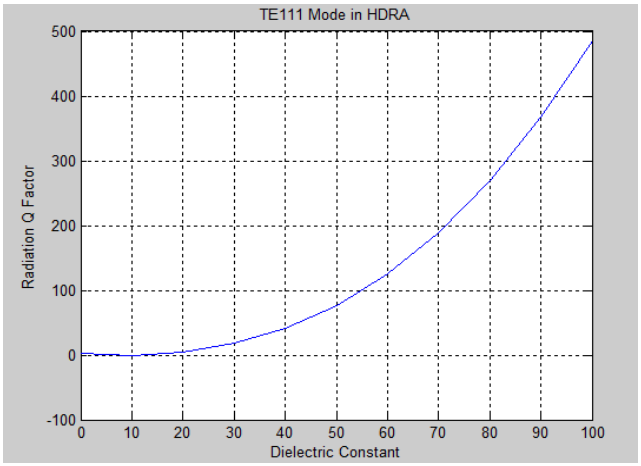

Fig. 2.3: The Q-factor of the TE_{111} mode of the hemispherical DRA

Value of the $Re(k_0 a)$ and radiation Q-factor can be obtained from **curve fitting technique** of the traces.

$$Re(k_0 a) = 2.831\ {\varepsilon_r}^{-0.47829} \tag{2.69}$$

$$Q = 0.08 + 0.796\varepsilon_r + 0.01226\ {\varepsilon_r}^2 - 3.10^{-5}{\varepsilon_r}^3 \tag{2.70}$$

$$BW = \frac{\Delta f}{f_0} = \frac{s-1}{\sqrt{S}Q} \tag{2.71}$$

2.4.2 The Cylindrical DRA

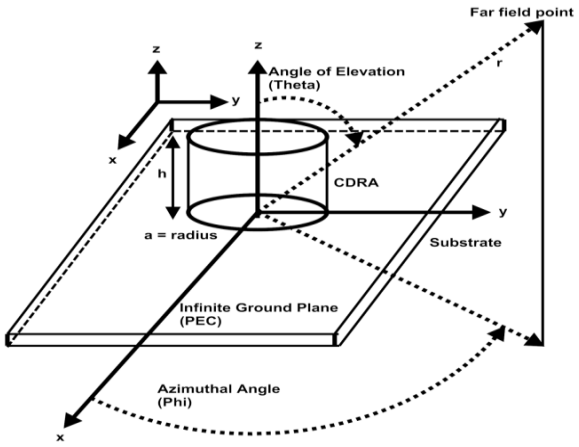

Fig. 2.4: Cylindrical DRA over an infinite ground plane

The cylindrical dielectric resonator is a suitable candidate for circuit applications like oscillator, filter etc. as it shows properties like high Q-factor, high stability, good coupling characteristics, miniaturized design and compatibility to the micro-strip

technology. The radiation characteristic of the cylindrical DRA shows its ability as a radiator. The cylindrical shape is characterized by radius 'a' and height 'h' which provides two degree of freedom with aspect ratio of a/h. Therefore a short and thick CDRA is similar to a long and slender CDRA having the same resonant frequency but Q-factor may somehow drift. On a designer prospective CDRA provides high design flexibilities to that of hemispherical DRA. The field pattern of a cylindrical DRA is similar to that of an isolated cylindrical dielectric waveguide. There are 03 types of modes present in CDRA; they are TE, TM, and Hybrid modes. Hybrid mode is of two types that is hybrid electric, HE, and hybrid magnetic, EH. If E_z field component dominates then it is hybrid electric and if H_z field component dominates then it is hybrid magnetic. Both the TE and TM modes are axially symmetrical with constant azimuth whereas hybrid mode depends upon the azimuth as well. The lowest order modes for radiation applications are $TM_{01\delta}$, $TE_{01\delta}$and $HE_{11\delta}$ modes. Here the subscript shows field variation along azimuth (ϕ), radius (r), and axis (z) directions, respectively. The field component δ is very small and its values lie between 0 and 1 and $\delta \rightarrow 1$ for the high dielectric constant material.[79, 80].

$$\delta = \frac{k_{direction}}{\pi/_d} \tag{2.72}$$

Therefore this mode is called magnetic dipole mode. $TM_{01\delta}$ radiates like an electric dipole oriented along its axis. Under unloaded and isolated condition the resonant frequency will be [81]:

$$f_{GH_z} = \frac{34}{a_{mm}\sqrt{\varepsilon_r}}\left(\frac{a}{h} + 3.45\right) \tag{2.73}$$

where, a = radius of the CDRA, h = height of the CDRA

Table 2.1: The relation between modes within and at the far field of DR

Mode	Field inside the resonator	Far field magnetic dipole
$TE_{01\delta}$	$H_z = J_0(hr)\cos\beta z$ $E_z = 0$	Magnetic dipole
$TM_{01\delta}$	$E_z = J_0(hr)\cos\beta z$ $H_z = 0$	Electric dipole
$HE_{01\delta}$	$E_z = J_1(hr)\cos\beta z\cos\varphi$ $H_z = 0$	Magnetic dipole
$EH_{01\delta}$	$H_z = J_1(hr)\cos\beta z\cos\varphi$ $E_z = 0$	Electric dipole

Table 2.2: A comparative analysis of modes in the fundamental shaped DRAs

Hemispherical DRA		Cylindrical DRA		Rectangular DRA	
Radiating	**Non-radiating**	**Radiating**	**Non-radiating**	**Radiating**	**Non-radiating**
TM_{101}, TE_{111}	TE_{101}	$TM_{01\delta}$, $HE_{11\delta}$	$TE_{01\delta}$	TE^{y}_{111}, TE^{y}_{113}	TE^{y}_{211}, TE^{y}_{112}

2.4.3 The Rectangular DRA

The RDRA has two degrees of freedom with aspect ratios (w/d) and (w/h) based on the resonant frequency [82, 83]. The field pattern within RDRA is similar to an isolated rectangular dielectric waveguide having width w and height b= h/2. By applying 'Image Theory' total height of the RDRA is reduced by half.

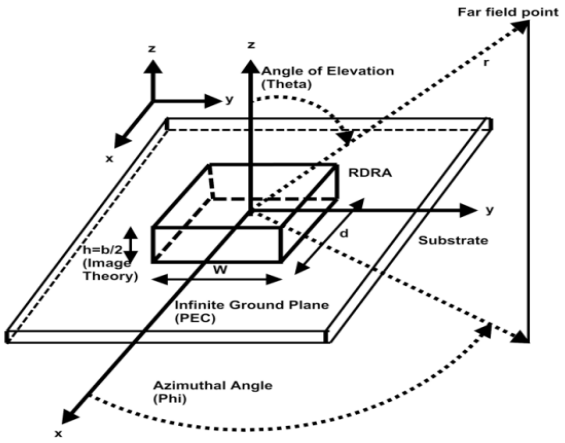

Fig.2.5: Rectangular DRA over an infinite ground plane

Fundamentally there exist two dominant modes on an RDRA that is TE and TM. Small loop whose radius is smaller than the wavelength, RDRA will behave like a magnetic dipole However, the polarization is vertical. Therefore, RDRA will support TE^{x}, TE^{y}, and TE^{z} mode in x,y,z direction. The lowest order mode will be $TE^{x}_{\delta 11}$, $TE^{y}_{1\delta 1}$, and $TE^{z}_{11\delta}$. If w> d > b, then $f_x < f_y < f_z$. Practically due to complex rectangular shapes, there may be the generation of some arbitrary higher-order and evanescent modes, which may create difficulty while fixing the i/p & o/p characteristics of the radiating structure [84, 85].

$$k_x \tan\left(\frac{k_x d}{2}\right) = \sqrt{(\varepsilon_r - 1){k_0}^2 - {k_x}^2} \quad (2.74)$$

Where, $k_0 = \frac{2\pi}{\lambda_0} = \frac{2\pi f_0}{c}, k_y = \frac{\pi}{w}, k_z = \frac{\pi}{b}$

$${k_x}^2 + {k_y}^2 + {k_z}^2 = \varepsilon_r {k_0}^2 \quad (2.75)$$

The transcendental equation can be solved for selected ratio of w/b as a function of d/b w.r.t normalized frequency F. The normalized frequency F can be defined as

$$F = \frac{2\pi w f_0 \sqrt{\varepsilon_r}}{c} \quad (2.76)$$

Here f_0 is the resonant frequency. The value of the normalized frequency F can be determined from the F vs. (d/b) plot for different value of (w/b) [86, 87]. The above equation can be effectively written as

$$f_{GHz} = \frac{15F}{w_{cm}\,\pi\sqrt{\varepsilon_r}} \quad (2.77)$$

Where, resonant frequency is represented in GHz scale and w is in cm.

By using **curve fitting technique** following equation is obtained for the normalized frequency F.

$$F = a_0 + a_1\left(\frac{w}{b}\right) + a_2\left(\frac{w}{b}\right)^2 \quad (2.78)$$

Where, $a_0 = 2.57 - 0.8\left(\frac{d}{b}\right) + 0.42\left(\frac{d}{b}\right)^2 - 0.05\left(\frac{d}{b}\right)^3, a_1 = 2.71\left(\frac{d}{b}\right)^{0.282}$, and $a_2 = 0.16$, The Q_{rad} of the rectangular DRA:

$$Q = \frac{2\omega W_e}{P_{rad}} \quad (2.79)$$

where W_e= Stored energy, P_{rad} = Radiated power

$$W_e = \frac{\varepsilon_0 \varepsilon_r wbd\, A^2}{32}\left(1 + \frac{\sin(k_x d)}{k_x d}\right)\left({k_x}^2 + {k_y}^2\right) \quad (2.80)$$

$$P_{rad} = 10{k_0}^4 |p_m|^2 \quad (2.81)$$

The magnetic dipole moment: $p_m = \frac{-j\omega\, 8\varepsilon_0(\varepsilon_r - 1)A}{k_x k_y k_z} \sin\left(\frac{k_x d}{2}\right)\hat{x}$ (2.82)

'A' represents the maximum amplitude of the fields. As there exist two degrees of freedom in rectangular DRA, the radiation Q-factor is difficult to plot. The graph plots between normalized Q-factor (Qe) as a function of w/b and d/b. The calculated resonant frequency through Dielectric Wave Guide Model and measured values differ by around 3 to 12%. However, radiation Q-factor can deviate up to 100% from the calculated value. Here, the loading effect occurs due to the presence of the

transmission line, incorrect positioning of the source. But by the application of the radar cross technique, the difference between the calculated and measured radiation Q_{rad} isolated RDRA can be reduced to 35% and resonant frequency to 7%. The normalized Q-factor (Qe) can be defined as

$$Q_e = \frac{Q}{{\varepsilon_r}^{3/2}} \tag{2.83}$$

Further, to improve the accuracy "Modified Dielectric Wave Guide Model is used [88]. In this model, physical dimension will be replaced by the effective dimension by multiplying a scaling factor (α). Where,

$$\alpha = 1 - \frac{1}{\varepsilon_r} \tag{2.84}$$

The fringing field causes calculation error to fix the dimension of the RDRA. In modified DWM the obtained resonant frequency will be multiplied by a factor of 1/α. It has been observed that modified model is better suited to dielectric material with high dielectric constant, but for low dielectric constant material traditional dielectric wave guide model is accurate [89]. To get high accuracy in calculation full wave analysis will be considered which takes factor like feeding techniques and influence of finite and infinite ground plane upon the radiating structure.

Design procedure for the Rectangular DRA in $TE^{x}_{\delta 11}$ Mode by using DWM Method:

Let desired dimensions w, d, b=2h and ε_r are given to design the RDRA. We have to find f_r and Q_{rad}.

Step I: To calculate: ratio of (w/b) and (d/b).

Step II: To calculate the normalized frequency (F) by using

$$F = \frac{2\pi w f_0 \sqrt{\varepsilon_r}}{c} \tag{2.85}$$

Here f_0 is the resonant frequency. The value of the normalized frequency F can be determined from the F vs. (d/b) plot for different values of (w/b).

Step III: To calculate the resonant frequency f_0 in GHz by using:

$$f_{0(GHz)} = \frac{15F}{w_{(cm)}\pi\sqrt{\varepsilon_r}} \tag{2.86}$$

Step IV: To calculate the radiation Q-factor by using the plot of normalized Q-factor as a function of d/b for different values of w/b.

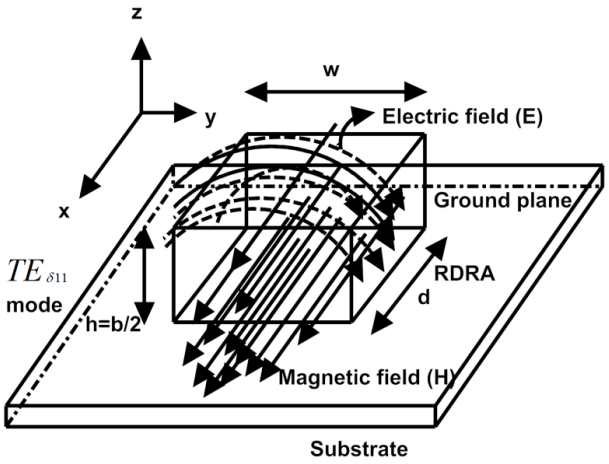

Fig.2.6: The direction of electric and magnetic field in Rectangular DRA

Design procedure for the Rectangular DRA in $TE^{x}_{\delta 11}$ Mode by using MDWM Method:

Step I: Determine the Q-factor:

$$Q = \frac{s-1}{\sqrt{S}\,(BW)} \tag{2.87}$$

Step II: Determine the Dielectric constant: At first convert radiation Q-factor into normalized Q-factor. Select the value of ε_r , below which RDRA will meet the bandwidth requirements.

Step III: Determine the value of normalized frequency F.

Step IV: Determine the dimensions (w,b,d) of the RDRA.

Field within the Rectangular DRA:

The field distribution of the lowest order mode of the RDRA is determined by the dielectric wave guide model (DWM) [90, 91]. The field components of the lowest order mode $TE^{x}_{\delta 11}$ [92]:

$$k_x \tan\left(\frac{k_x d}{2}\right) = \sqrt{(\varepsilon_r - 1){k_0}^2 - {k_x}^2} \tag{2.88}$$

$$H_x = \frac{({k_y}^2 + {k_z}^2)}{j\omega\,\mu_0} \cos(k_x x)\cos(k_y y)\cos(k_z z) \tag{2.89}$$

$$H_y = \frac{(k_y k_x)}{j\omega\,\mu_0} \sin(k_x x)\sin(k_y y)\cos(k_z z) \tag{2.90}$$

$$H_z = \frac{(k_z k_x)}{j\omega\,\mu_0}\sin(k_x x)\cos(k_y y)\sin(k_z z) \quad (2.91)$$

$$E_x = 0 \quad (2.92)$$

$$E_y = k_z \cos(k_x x)\cos(k_y y)\sin(k_z z) \quad (2.93)$$

$$E_z = -k_y\, cos(k_x x)\sin(k_y y)\cos(k_z z) \quad (2.94)$$

Where,

$k_x = \frac{m\pi}{a}$

$k_y = \frac{n\pi}{b}$

Where, $k_0 = \frac{2\pi}{\lambda_0} = \frac{2\pi f_0}{c}, k_y = \frac{\pi}{w}, k_z = \frac{\pi}{b}, {k_x}^2 + {k_y}^2 + {k_z}^2 = \varepsilon_r {k_0}^2,$

$and\ k_z \tan\left(\frac{k_z d}{2}\right) = \sqrt{k_0^2(\varepsilon_r - 1) - k_z^2}$

The output field is sinusoidal in nature.

2.4.4 Hybrid DRA

The combinations of DRA with other antenna technology give rise to Hybrid DRA. Fig.2.14 shows the top view of Hybrid Rectangular DRA. Here an RDRA is placed over a microstrip patch antenna embedded with meta-materials. A hybrid DRA reduces the gaps between the traditional technology and the emerging wireless broadband and ultra-wideband technology. The focus is mainly on developing a miniaturized low-profile device with a high impedance bandwidth response for wireless applications. HDRA supports degenerate resonant mode, because of which there is an increment in cross-polarization.

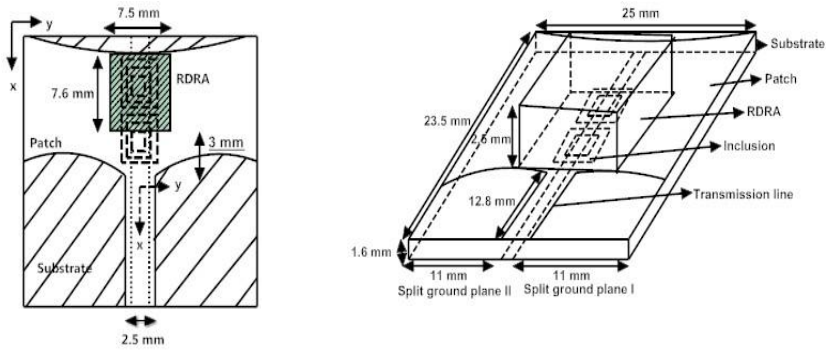

Fig.2.7: Top and side view of Hybrid Rectangular DRA

2.5 FEEDING AND COUPLING MECHANISM IN DRA

The performance of the feed is more important than the performance of the antenna. Proper matching provides a tradeoff between loaded resonance, forced resonance, and self-resonance. The excitation scheme has to be matched with the polarization to achieve good coupling. Coupling problem does not arise in coaxial and planar transmission lines due to coupling of Quasi-TEM mode [93-99].

2.5.1 Coaxial probe feed

The coaxial probe radiates a fountain shape pattern (Donut shaped). The major advantages of the coaxial probe feed directly into the 50 Ohms system without any matching device. It is best at the low frequency of operation where aperture coupling is impossible to apply due to the requirement of a bigger aperture.

2.5.2 Micro-strip line feed

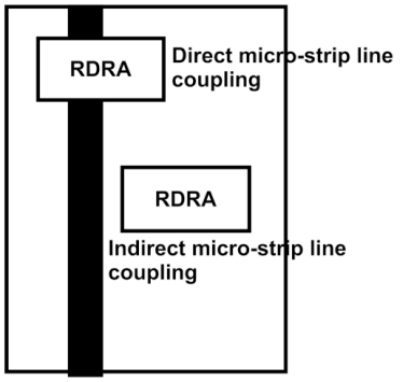

Fig.2.8: Top view of microstrip line direct and indirect coupled Rectangular DRA

Q. However, the microstrip line is unsuitable for broadband microwave and millimeter-wave circuit design because of the following reason. They are: (i) Inaccessibility of the ground plane, (ii) The difficulty associated with making a shunt connection between the strip and the ground plane. (iii) Undesired radiation for the thicker substrate. (iv) These effects affect the frequency of operation. Here singular ground plane occupies the entire lower side of the structure.

2.5.3 Co-planar waveguide feed

Coplanar waveguide is based on the planar topologies (uni-planar configuration). It is useful for high Q applications. It provides an anti-phase electric field to mitigate the effect of the surface wave. The CPW feed is required when the antenna is to be integrated with the embedded active circuit. Various feeding techniques have been presented in Figures 2.16 to 2.20.

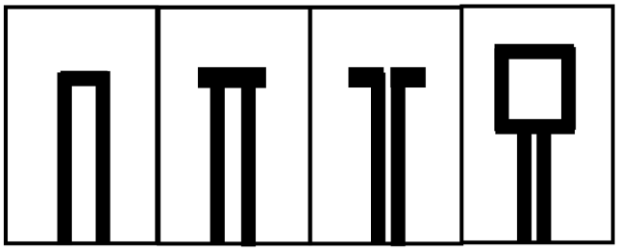

Fig.2.9: Top view of CPW capacitive feed (C1, C2), inductive feed, and square loop feeding arrangement

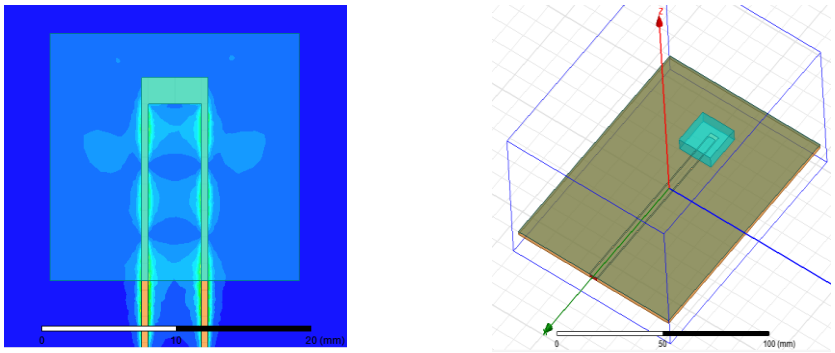

Fig.2.10: CPW capacitive fed

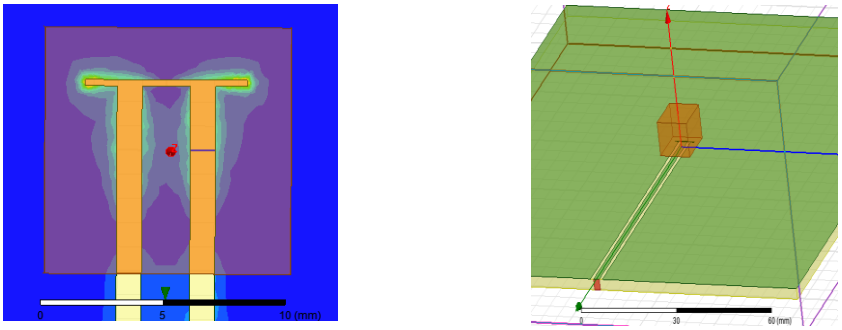

Fig.2.11: CPW capacitive fed

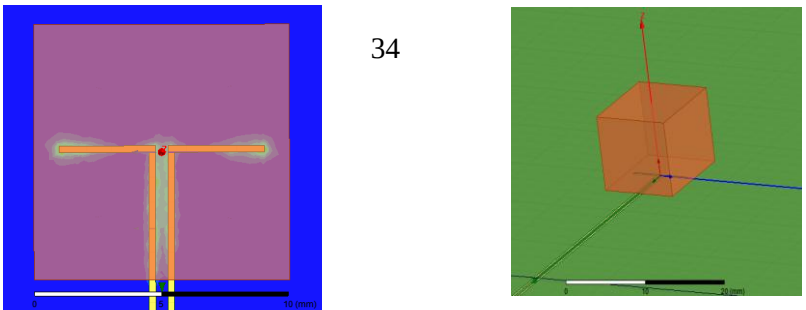

Fig.2.12: CPW inductive fed

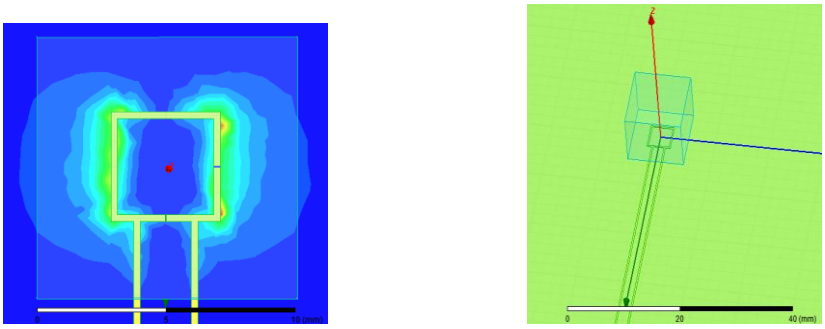

Fig.2.13: CPW square-loop

It is a planar transmission line having arrays of conductors placed on the same geometric plane. It has the following advantages:

(i) Accessible to the surface-mounted components.

(ii) Minimum loss through dispersion for miniaturized geometry.

(iii)Low radiation loss.

(iv)Minimum impact of substrate thickness.

The drawbacks of the CPW line are:

(i) It is prone to spurious mode.

(ii) The resistive loss is more than that of the microstrip line.

2.5.4 Dielectric image guide Feed

DIG is formed by placing a strip of the dielectric slab with a backing sheet of the conductor. It propagates various TE and TM modes trapped within it. It provides high unloaded Q-factors and operates well above 100 GHz. The DIG has the following advantages:

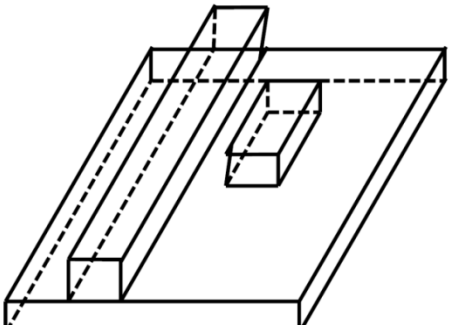

Fig.2.14: Dielectric image guide fed Rectangular DRA

(i) Minimum radiation loss at the bend.

(ii) High line packing density.

(iii)Non restrictive tolerance.

2.5.5 Aperture coupled feed

The slot acts as a resonating cavity. It is complicated as it sees both the transmission line as well as the waveguide. The transmission line is a planar technology, whereas the waveguide is

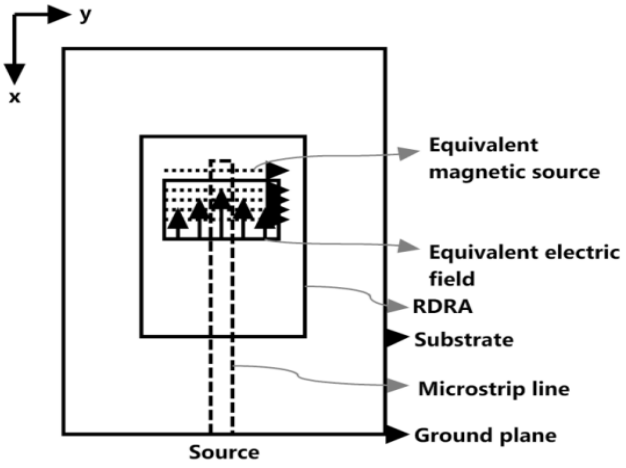

Fig.2.15: Aperture coupled microstrip fed Rectangular DRA

based on non-planar technology. Therefore slot provides the unification of both the planar and non-planar technologies. The non-planar feed provides high power transfer and reduced interference, whereas the planar structure allows Quasi TEM to enable easy coupling of energy into the DRA structure. The important challenge is to

position the slot. The slot has to be placed, where the magnetic field is maximum and where the ground plane current is maximum. Slot coupling produces a broad-shaped pattern.

2.6 COUPLING MECHANISMS

At resonance, the phase will be zero, and below the resonance, there will be a -90 degrees phase shift. There is a +90 degree phase shift for magnetic coupling and a -90 degree phase shift for electrical coupling. The internal field structure provides information about the modes of operation and approximate field distribution. It is suitable for the selection of the feed structure. The performance of a DRA is a function of the compatibility of the port to the antenna, the amount of power that can be fed and coupled from the transmission line, and the frequency response of the impedance [100-102].

The design equation to determine the f_r and Q_{rad} is for the unit cell of the DRA or DRA in isolation, mounted over an infinite ground plane. It did not consider the feeding mechanisms for excitation and coupling of appropriate power to the radiator. Selection of the right kind of feeding mechanism, positioning of the feed, and its matching profile play a pivotal role in deciding the internal as well as external field pattern of the DRA. The feeding structure and coupling mechanism control the formation of mode and decide the f_r and Q_{rad} of the DRA. Depending upon the type of applications it is essential for the designer to decide the number of ports, its power handling capabilities, positioning of the ports, etc. To decide the above, the following things need to be addressed [103-108]:

(i) The excited lowest order modes

(ii) Frequency response of the impedance

These quantities are calculated through detail numerical analysis of the internal E and H field distributions. To represent the source, the field equation can be amended to include impressed currents, electric and magnetic. These current is the source of the field. The amount of coupling is represented by coupling coefficient ($\boldsymbol{X}$) between source and the field.

$$\iiint (E^a \cdot J^b - H^a \cdot M^b)\, dv = \iiint (E^b \cdot J^a - H^b \cdot M^a) dv \tag{2.95}$$

There exist two a-c current sources,J^a,M^a and J^b,M^b. The field produces by the source a isE^a,H^a and by the source b isE^b,H^b. Here the integration extends all over space. Consider electric and magnetic field present within the DRA are E_{DRA}, H_{DRA} respectively. Consider an electric source J_s and magnetic source M_s the coupling coefficient will be

$$\mathcal{X} = \iiint (E_{DRA} \cdot J_s) dV \quad (2.96)$$

$$\mathcal{X} = \iiint (H_{DRA} \cdot M_s) dV \quad (2.97)$$

To achieve strong coupling when the source is electric (probe feed) or magnetic (loop or aperture) in nature. The point of excitation is said to be a sensitive point. So we need to nullify the imaginary part by placing the source at the point of [109-112]:

(i) Maximum electric field (at $\bullet/_4$) within the DRA

(ii) Polarization matching

(i) $A = \pi r^2$impedance matching

(ii) 50 Ω impedance matching

(iii)The point of minimum mode coupling & mode degeneracy

(iv)Excitation of desired lower order mode

Coupling mechanism not only controls the amount of power transfer from the source but also provide loading effect that will have strong impact upon the Q-factor of the DRA.

$$Q_{ext} = \frac{Q}{\mathcal{X}} \quad (2.98)$$

$$Q_L = \left(\frac{1}{Q} + \frac{1}{Q_{ext}}\right)^{-1} = \frac{Q}{1+\mathcal{X}} \quad (2.99)$$

At critical coupling when $\boldsymbol{\mathcal{X}}$=1, maximum power will be coupled from the port to the DRA. Below the coupling coefficient ($\boldsymbol{\mathcal{X}}$<1) and above the coupling coefficient ($\boldsymbol{\mathcal{X}}$>1) coupled energy reduces considerably.

In general the antenna Q-factor depends upon four loss factors. They are losses due to formation of surface wave on the conductor coated with dielectric, dielectric losses due to arbitrary heating within the dielectric, copper losses due to heating of the

conductor and the ground plane [113-116]. Thus

$$\frac{1}{Q} = \frac{1}{Q_{rad}} + \frac{1}{Q_{sw}} + \frac{1}{Q_{dl}} + \frac{1}{Q_{cu}} \quad (2.100)$$

Surface wave losses can further calculated for a thicker dielectric by calculating the energy stored in the fringing field and total field distribution within the structure. Here $Q_{dl} = \frac{1}{\tan \delta}$ and$Q_{cu} = \frac{t}{d_S}$, where skin depth(d_s) $= \frac{1}{\sqrt{\pi f \mu \sigma}}$. For a dielectric resonator antenna these quantities have least contribution. Thus radiation Q-factor of a DRA will be $Q_{rad} = \frac{2\omega W_e}{P_{rad}}$, where, $W_e$the stored energy and P_{rad} is the radiated power.

The stored energy will be:

$$W_e = \frac{\varepsilon_0 \varepsilon_r wbd\, A^2}{32}\left(1 + \frac{\sin(k_x d)}{k_x d}\right)\left(k_y^2 + k_z^2\right) \quad (2.101)$$

Where w, b & d are the length, height & breadth of the DRA. 'A' represents maximum amplitude of the field. Image theory makes the height equal to b/2. The radiated power will be

$$P_{rad} = 10{k_0}^4 |p_m|^2 \quad (2.102)$$

The magnetic dipole moment: $p_m = \frac{-j\omega\, 8\varepsilon_0(\varepsilon_r - 1)A}{k_x k_y k_z} \sin\left(\frac{k_x d}{2}\right)\hat{x}$ (2.103)

The field within the guide varies sinusoidal and field components can be approximated as $k_x = \frac{m\pi}{a}$, $k_y = \frac{n\pi}{b}$& $k_z = \sqrt{\varepsilon_r k_0^2 - k_x^2 - k_y^2}$.

The computational time required to compute the input impedance can be reduced by a factor of about 100 for probe coupled DRA. The computational time required for the same can be reduced by a factor of about 37 for micro-strip slot coupled DRA. But for the center-fed DRA, the overall computation time can be reduced by a factor of about 319.

2.7 IMPEDANCE MATCHING TECHNIQUES

It is paramount to have a precise design while selecting, rejecting controlled time delay, and channelizing maximum energy to transfer with minimum reflection over a broad range of frequency bands. An impedance matching network having minimum insertion loss is to be inserted between the load and generator so that the forward power dominates over the reflected power [117].

Reflection coefficient (Γ) $= \frac{Z_{in} - R_g}{Z_{in} + R_g}$ (2.104)

The reflection coefficient is a function of frequency:

$$\int_0^{\infty} ln\left|\frac{1}{\rho}\right| d\omega = \frac{\pi}{R_L C_L} \tag{2.105}$$

where, R_L, C_L are the resistor and capacitor at the load end.

For a passive circuit: $0 \leq \rho \leq 1$. For perfect transmission: $|\rho| = 0$ and for total reflection: $|\rho| = 1$. Therefore larger $ln\left|\frac{1}{\rho}\right|$ better will be the transmission and area under the curve of $ln\left|\frac{1}{\rho}\right|$ vs ω is no greater than $\frac{\pi}{R_L C_L}$. To get good impedance match within the range of frequency, the best result can be obtained if for that band of frequency $|\rho| = 0$ and $|\rho| = 1$ for all other frequency. Then $ln\left|\frac{1}{\rho}\right| = 0$, for all the frequency except the allowed band $(\omega_2 - \omega_1)$. Therefore, the area under the curve $ln\left|\frac{1}{\rho}\right|$ within the band will be:

$$\int_{\omega_1}^{\omega_2} ln\left|\frac{1}{\rho}\right| d\omega = \frac{\pi}{R_L C_L} \tag{2.106}$$

For ideal impedance matching network for the load will be a bandpass filter. Therefore, an efficient broadband impedance matching structure is the filter structure. Most of the slow-wave structure can be used as a filter for impedance matching networks.

The impedance of a circuit will be the function of complex frequency (p) and can be represented as:

$$Z(p) = \frac{E_n}{I_n} = \frac{a_n p^n + a_{n-1} p^{n-1} + \cdots + a_1 p + a_0}{b_n p^n + b_{n-1} p^{n-1} + \cdots + b_1 p + b_0} \tag{2.107}$$

By factoring the numerator and denominator polynomial:

$$Z(p) = \left(\frac{a_n}{b_n}\right) \frac{(p-p_1)(p-p_3)\ldots}{(p-p_2)(p-p_4)\ldots} \tag{2.108}$$

Here 'p' is the complex frequency and is equal to $(\sigma + j\omega)$. At p= p1, p3,… the numerator polynomial goes to zero, therefore the impedance $Z(p) = 0$. The frequencies are the zeros of the function. These zeros are all frequency in the natural mode of vibration. At p= p_2, p_4,… the numerator polynomial goes to infinite.

Quarter wave transformer:

The quarter-wave transformer is an impedance transformer. It requires to function with flat or equal ripple characteristics in the stopband [118, 119]. The fractional bandwidth

$$W_q = 2\left(\frac{\lambda_{g1}-\lambda_{g2}}{\lambda_{g1}+\lambda_{g2}}\right) \quad (2.109)$$

λ_{g_1} and λ_{g_2} are the longest and shortest guided wavelength. The length of the quarter wave transformer (L) is:

$$L = \frac{\lambda_{g1}\lambda_{g2}}{2(\lambda_{g_1}+\lambda_{g_2})} = \frac{\lambda_{g0}}{4} \quad (2.110)$$

$$W_q = 2\left(\frac{\lambda_1-\lambda_2}{\lambda_1+\lambda_2}\right) = 2\left(\frac{f_2-f_1}{f_2+f_1}\right) \quad (2.111)$$

$$L = \frac{\lambda_1\lambda_2}{2(\lambda_1+\lambda_2)} = \frac{\lambda_0}{4} \quad (2.112)$$

2.8 ANALYTICAL TECHNIQUE: AN INTRODUCTION TO HIGH FREQUENCY STRUCTURE SIMULATOR (HFSS)

The most common technique to analyze the DRA is the FEM. The main aim of the analysis is to find the electric and magnetic field with high accuracy when charge distribution and flow of current are given. The FEM contains features like geometrical adaptability and is a convenient time-domain technique for transient analysis. It describes irregular boundaries and non-homogeneous material properties of the radiator and feeding mechanisms [120, 121]. It helps to reduce the dimensionality of the problem by resolving the 3D problem, through the 2D approach. Therefore, an arbitrary structure can be better tracked and shaped with high accuracy while reducing the cost of the computation. DRA and its entire volume, surroundings can be discretized to increase the computational size of the problem.

A High-frequency structured simulator (HFSS) is a three-dimensional (3D) commercial, high-frequency electromagnetic field solver-based simulation tool [122]. It uses the Finite element method (FEM) and other integral equations-based computing technologies. It is used to calculate field intensity, potential difference, energy, charge, and current densities. In FEM, the total structure is divided into many segments called finite element which, is in the form of a tetrahedron. When tetrahedrons are small, fields are strong, and when it is large, then fields are weak. The total field is an amalgamation of tetrahedrons connected in series and parallel to form the finite element mesh. On a circuital note, it provides an integrated value of capacitance, inductance, and resistance. The field is associated with Laplace's and Poisson's equation, which is in differential form. Laplace's equation implies the space

free of charge [123].

$$\nabla^2 V = 0 \tag{2.113}$$

$$\frac{\partial^2 V}{\partial x^2} + \frac{\partial^2 V}{\partial y^2} + \frac{\partial^2 V}{\partial z^2} = 0 \tag{2.114}$$

By using separation of variable method, the general solution of Laplace's equation will be:

$$V = (C_1 e^{a_1 x} + C_2 e^{-a_1 x})(C_3 e^{a_2 y} + C_4 e^{-a_2 y})(C_5 e^{a_3 z} + C_6 e^{-a_3 z}) \tag{2.115}$$

Poisson's equation implies the space with charge.

$$\nabla^2 V = \frac{-\rho}{\varepsilon} \tag{2.116}$$

The field configuration that satisfies Laplace and Poisson's equation depends on the boundaries, and its solution is unique. FEM is used to solve Laplace's equation over the specified region. It introduces a quantization of the potential contours as the solution of the finite number of elements.

The fundamental equation that controls the electromagnetic phenomenon is formulated by James Clerk Maxwell. Except for all the problems related to Quantum Electro-Dynamic, it addresses almost all the problems related to electromagnetism. The fundamental equations in electromagnetic were inconsistent. Therefore, Maxwell added the term displacement current $\frac{\partial D}{\partial t}$ to make all the equations consistent and the resultant modified equation survives with the theory of relativity. Because of this displacement current, 'Quantum optics' is believed to be similar to that of electromagnetic. The solution of the following linear equations predicts the behavior of the wave from one point to another [124].

$$\nabla \times E = -\frac{\partial B}{\partial t} \tag{2.117}$$

$$\nabla \times H = J + \frac{\partial D}{\partial t} \tag{2.118}$$

The solution can be obtained by solving Helmholtz's equation:

$$\nabla^2 A + K^2 A = -J \tag{2.119}$$

$$H = \nabla \times A \tag{2.120}$$

$$E = \frac{\nabla(\nabla.A)}{j\omega\varepsilon} - j\omega\mu A \tag{2.121}$$

The solution for the electric field can be obtained by solving:

$$\nabla \times \left(\frac{1}{\mu_r}\nabla \times E\right) - k_0^2 \varepsilon_r E = J \tag{2.122}$$

For continuous wave analysis, both the phase and amplitude will be considered.

$$k_0^2 = {\omega^2}/{c^2} \quad (2.123)$$

The magnetic field can be calculated:

$$H = \frac{1}{\mu\varepsilon}(\nabla \times E) \quad (2.124)$$

$$D = \varepsilon E \quad (2.125)$$

$$B = \mu H \quad (2.126)$$

$$J = \sigma E \quad (2.127)$$

Steps to find the E and H field in the DRA of various shapes:

A geometric structure is classified into different finite tetrahedron element mesh. A testing function W_n will be defined for each tetrahedron. It results in many basis functions. (The testing function W_n are curl conform, it means the tangential continuity is being maintained). The field equation is multiplied with W_n and integrated over the entire volume.

$$\int \left(w_n . \nabla \times \left(\frac{1}{\mu_r} \nabla \times E \right) - k_0^2 \varepsilon_r w_n . E \right) dV = 0 \quad (2.128)$$

Using Green's and Divergence's theorem 3D problem can be converted into 2D problem.

$$\int \left(\nabla \times w_n \right). \left(\frac{1}{\mu_r} \nabla \times E \right) - k_0^2 \varepsilon_r w_n . E \Big) = \iint (\text{boundary terms}). dS \quad (2.129)$$

for n = 1, 2, 3,....,N the electric field will be:

$$E = \sum_m x_m w_n \quad (2.130)$$

$$\sum x_m \int \left(\nabla \times w_n \right). \left(\frac{1}{\mu_r} \nabla \times E \right) - k_0^2 \varepsilon_r w_n . E \Big) d = \iint (\text{boundary terms}). dS \quad (2.132)$$

The equation will be in the form:

$$\sum_m x_m A_{n,m} = b_n \quad (2.131)$$

or,

$$Ax = b \quad (2.132)$$

where, A is a known N×N matrix that includes any applied boundary conditions and 'b' is the port excitation. Then full 3D can be calculated for the entire volume. The error can be calculated by using the following procedure: Let we have calculated approximate electric field (E^{approx}) from the above defined procedure, then the outcome will be replaced in:

$$\nabla \times \left(\frac{1}{\mu_r}\nabla \times E\right) - k_0^2 \varepsilon_r = 0 \quad (2.133)$$

$$\nabla \times \left(\frac{1}{\mu_r}\nabla \times E^{appox}\right) - k_0^2 \varepsilon_r E^{appox} = \text{residue} \quad (2.134)$$

High values of residues indicate high degree of error. Based on the solution HFSS locates that tetrahedron where there are high residues. It will refine those meshes with high residues in an intelligent manner through adaptive mesh refinement process.

2.9 SUMMARY

This chapter provides a broad background on the Dielectric Resonator Antenna. It explains the overall objective of the work and various sub-objectives and computational techniques to attain the major objective of the Design, Development, and Analysis of Low Loss Rectangular Dielectric Resonator Antennas for Wireless Applications. It summarizes the current state of knowledge of fundamental DRA structures and points out the gaps and opportunities.

CHAPTER 3
DESIGN AND DEVELOPMENT OF PLANAR AND NON-PLANAR DIELECTRIC RESONATOR ANTENNA

3.1 INTRODUCTION

The last few decades have seen exponential growth in wireless devices for communication, navigation, and sensing purposes. It is supported by significant growth in front end device technology such as antenna arrays in stacked conformal, and planar configurations, along with smart antenna technologies. The performance of these techniques is deeply affected by the channel's response to noise, the wave propagation environment, various sources of interference, and compatibility with the EMI/EMC environment. These limitations can be mitigated and addressed by minimizing losses, adopting simple design, miniaturized structure, suitable impedance matching, etc.

DRA is an open radiating structure, fabricated from a low loss dielectric material having low dielectric constant. It provides a high degree of freedom and versatility. It has certain efficient radiating mode with low radiation quality factor [125]. Different resonating frequency can be easily realized by setting different aspect ratio at some effective dielectric constant with infinite, finite, and defected ground plane. Effective energy coupling can be achieved by considering the source as electric and magnetic current with different modes excitation. The radiation pattern of the standard shape of the DRA can be predicted accurately without complicated computational process. DRA is suitable in those applications where there is a requirement of continuous change in frequency such as software-defined radio, military communication, etc.

Leaky wave based resonator antenna is a periodic, line source based, high efficient travelling wave antenna. It leaks **non spectral wave** all along its length. The prime focus of the design is to make leaky wave radiation much greater than the space wave radiation. This antenna provides high antenna gain with narrow beamwidth. At mm wave leaky wave antenna is based on new low loss waveguides that include non-radiative dielectric [126, 128].

In this chapter, design concentration is towards designing front end narrow band and leaky wave radiating and receiving structure. Most of the dedicated applications

like global positioning system, high secure military communication, etc. prefer narrow operating bandwidth. Narrowband design offers a distinct advantage when there is hardly a clear cut demarcation between near field and far-field radiation, which is quite common at microwave and millimeter-wave antenna. As noise power is directly proportional to the system bandwidth, therefore by employing narrowband technique high channel capacity, high signal to noise ratio (more than 30 dB), and high directive gain can be achieved. Industry demands miniaturized design, which can be obtained by using materials with high permittivity. But with high permittivity material, there is an increment in quality factor, which may turn the radiating structure into a kind of reservoir of electromagnetic energy. Physical size can be reduced by adopting a stacked design. Modes or field pattern plays a significant role in deciding the radiated field pattern.

3.2 DESIGN AND ANALYSIS OF EMBEDDED RECTANGULAR DIELECTRIC RESONATOR ANTENNA

3.2.1 Introduction

The design of a split microstrip-fed embedded rectangular dielectric resonator antenna for near-field communication is presented. In this design, the impedance bandwidth is expanded by merging multi-resonant frequencies. The broadband response is realized by placing two RDRA appropriately to create the loading effect of one w.r.t other [129-132]. The finite ground plane is considered for the design. There is a consistent radiation pattern at both bands over the entire tuning range.

This work focuses on designing a dedicated, multi-resonant, miniaturized, multipurpose DR antenna having a single resonant dimension with high bandwidth and efficiency. The antenna is being supported by a finite ground plane to create an efficient radiating mode. The antenna has a small electrical size while creating an efficient radiation mode in the ground plane. The wideband response is being realized by the overall effective loading effect and providing a suitable matching profile. The prototype of the RDRA is fabricated and measured by using Agilent Technologies N 5247A: A.09.90.02 Vector Network Analyzer (VNA). The antenna shows dual-band response. The first resonant dip occurs from 3.9 GHz to 5.1 GHz, and the second return loss dip occurs from 8.8 to 10.3 GHz. Measured 10 dB impedance bandwidths

($S_{11} < 10\,dB$) are 26.66% and 15.71 % in the lower and upper band of operation. Radiation patterns in both the bands are similar and stable with frequency tuning. It has been observed that the cross-polarized field is very weak and 30 dB less than the co-polarized field in the broadside direction.

3.2.2 Antenna Configuration

The structure of the proposed fabricated proto-type RDRA shown in Fig. 3.1 and 3.2 This antenna is configured on Roger Rd 3003 dielectric substrate with dielectric constant (ε_r) equal to 3, loss tangent ($\tan\delta$) of 0.003, and having a dimension of $0.39● \times 0.98● \times 0.02●$ m^3at 9.8 GHz. A finite ground plane of dimension $0.39● \times 0.31●$ m^2 at 9.8 GHz is placed at the bottom of the antenna towards the excitation side of the feed line. Copper with finite conductivity of 5.8×10^7 Siemens/ meter is used for the finite ground plane for the simulation. The substrate with lower dielectric materials has a lower loss tangent and the wave number is smaller [19]. The loss multiplier in the exponent is equal to the wave number times the loss tangent, for dielectric losses. 99.7% Alumina having ε_r of 9.8 with $\tan\delta$ of 0.0013 is used as the radiating rectangular dielectric resonator antenna. The ceramic alumina has very low loss but is somehow brittle. It offers excellent electrical and mechanical parameters. It is power efficient, robust, bondability, and non-porousness which play a significant role in design considerations. As shown in Fig. 3.1 and 3.2 the dimension of the miniaturized RDRA is $0.45● \times 0.21● \times 0.19● \; m^3$at 9.8 GHz. Two RDRAs' are placed side to side on the substrate, one within the electrical periphery of another RDRA. Here the distance of separation between two nearby points of the RDRA is around $0.045●$ to achieve maximum field coupling. The dimension of RDRA is calculated by using a dielectric waveguide model under unloaded conditions. Optimization is being done under the loaded condition to achieve accurate the simulated and measured result. The split transmission line has three open-circuited stubs. The length of the stub plays a crucial role as it controls the impedance matching profile, the maximum co-polarized ($\theta = 0°$)and cross polarized field ($\theta = 90°$) in the H-plane [20]. The length of the stub at both the end is crucial to calculate the resonant frequency and bandwidth.

The antenna design is simulated by High-Frequency Structured Simulator (HFSS

14.0) under unloaded conditions. Here Silicon sealant, a non-permanent adhesive is used to bond the RDRA over the substrate. Through cleanliness, miniaturized air gaps can be reduced to have reasonable control and accuracy over the variation in the matching profile.

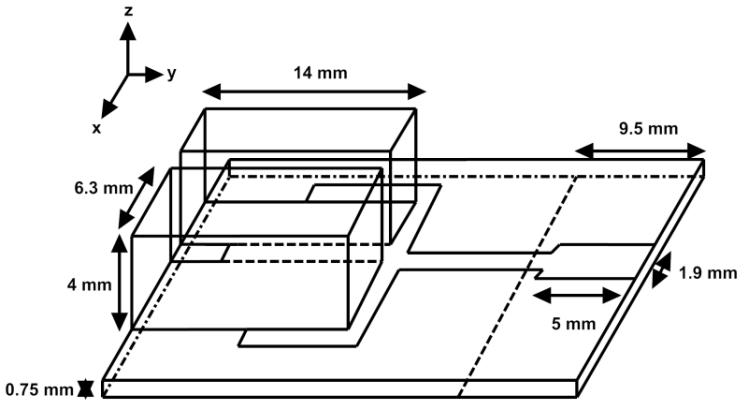

Fig.3.1: Side view of the proposed Rectangular DRA

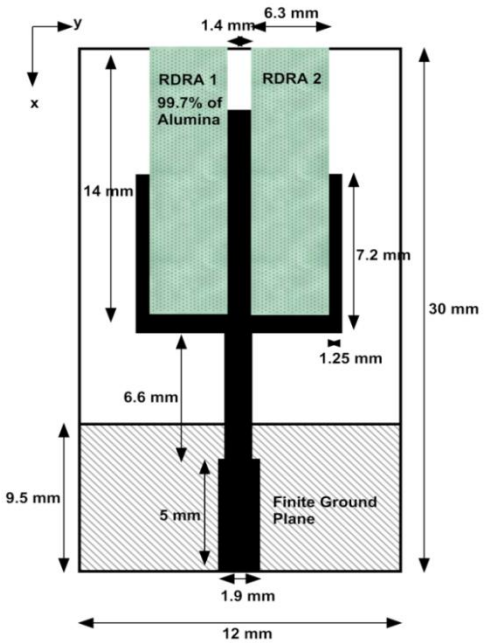

Fig.3.2: Top 2-D view of the proposed Rectangular DRA

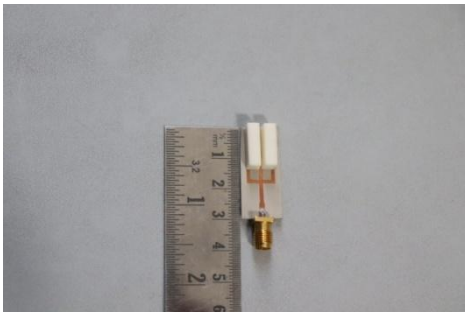

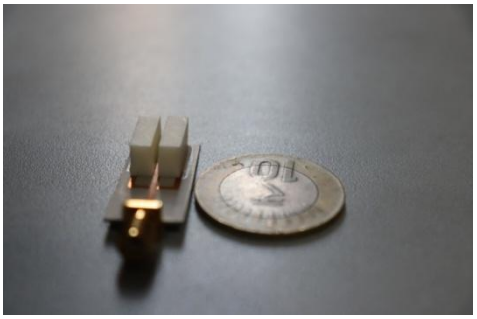

Fig.3.3a and 3.3b: Photograph of the designed embedded Rectangular DRA

Table 3.1: Structural Parameters of RDRA

Structure	Length	Width	Height	Permittivity	Material	$\tan\delta$
Substrate	30 mm	12 mm	0.75 mm	3.0	RO 3003 (tm)	0.0013
DRA 1&2	14 mm	6.3 mm	6 mm	9.8	99.7% Alumina	0.003

3.2.3 Design Methodologies

The complexity of RDRA boundaries and radiation field distributions are addressed by Dielectric Waveguide Model. DWM was first presented by Marcatili to calculate the guided wavelength in dielectric guide [133]. In DWM equation, RDRA is operating at the lowest order mode is modeled as short magnetic dipole [134]. Here the top surface and two sidewalls are behaved as perfect magnetic walls where as the other two side walls are acted as imperfect magnetic walls. Due to the presence of finite ground plane, bottom surface is assumed to be an electrical wall and there is diffraction from the edges. The lowest order mode is $TE^{x}_{\delta 11}$. Modal expansion method is used to describe field in TE and TM modes [135]. The inside and outside of the RDRA are represented in terms of sinusoidal functions. These sinusoidal functions decrease exponentially as distance increases. The wave number and attenuation constant can be determined by matching the boundary walls. However the basic limitations of DWM are:

i. It is useful only for the simple geometries.
ii. It does not consider coupling mechanisms.

These problems can be resolved by using numerical techniques. The field pattern analysis of DRA provides complete information about surface current density, matching profile, and output radiation characteristics after excited by the radiofrequency current. The total surface current density within the DRA is the superposition of various electric (E) and magnetic (H) field components. The current density is represented by the orthogonal Fourier basis functions confined within the boundary at a particular instant of time. The exciting radio frequency current can be

converted into a suitable mode depending upon various parameters like excitation mechanism, coupling techniques, and geometry. The **'resonant mode'** is real current vector that describes the radiating phenomenon. The modes are the field pattern of motion that repeats and oscillate sinusoidally. With suitable impedance matching the RF, excitation current gets converted into surface current.

The radiation field can be evaluated from the displacement current on the antenna and is extremely small and only takes place from the presence of impurities in the dielectric. The accurate estimation of current requires the solution of boundary value problem. A little variation of current is insensitive to the radiation field. Therefore optimum information can be taken from an approximate current distribution. Here current is an harmonic distribution of kz. [39]

$$A_z = \frac{1}{4\pi}\int_{-l/2}^{l/2} \frac{I(z')e^{-jk|r-r'|}}{|r-r'|}dz' \tag{3.1}$$

where, $|r-r'| = \sqrt{r^2 + z'^2 - 2rz'\cos\theta}$

In term of magnetic vector potential (A):

$$E = -j\omega\mu A + \frac{1}{j\omega\varepsilon}\nabla(\nabla.A) \tag{3.2}$$

$$H = \nabla \times A \tag{3.3}$$

The rectangular components of A have corresponding rectangular components of J as their source. From the Maxwell's equations:

$$\nabla \times E = -\mu\frac{\partial H}{\partial t} \tag{3.4}$$

$$\nabla \times H = j + \frac{\partial E}{\partial t} \tag{3.5}$$

In the LHS:

$$\nabla \times E = \begin{vmatrix} i & j & k \\ \frac{\partial}{\partial x} & \frac{\partial}{\partial y} & \frac{\partial}{\partial z} \\ E_x & E_y & E_z \end{vmatrix} = i\left(\frac{\partial E_z}{\partial y} - \frac{\partial E_y}{\partial z}\right) - j\left(\frac{\partial E_z}{\partial x} - \frac{\partial E_x}{\partial z}\right) + k\left(\frac{\partial E_y}{\partial x} - \frac{\partial E_x}{\partial y}\right) \tag{3.6}$$

Thus,

$$i\left(\frac{\partial E_z}{\partial y} - \frac{\partial E_y}{\partial z}\right) - j\left(\frac{\partial E_z}{\partial x} - \frac{\partial E_x}{\partial z}\right) + k\left(\frac{\partial E_y}{\partial x} - \frac{\partial E_x}{\partial y}\right) = -\mu\frac{\partial H_x}{\partial t} - \mu\frac{\partial H_y}{\partial t} - \mu\frac{\partial H_z}{\partial t} \tag{3.7}$$

The components for the Magnetic and Electric field will be:

$$H_x = \frac{1}{-j\omega\mu}\left(\frac{\partial E_z}{\partial y} - \frac{\partial E_y}{\partial z}\right) \quad (3.8)$$

$$H_y = \frac{1}{j\omega\mu}\left(\frac{\partial E_z}{\partial x} - \frac{\partial E_x}{\partial z}\right) \quad (3.9)$$

$$H_z = \frac{1}{-j\omega\mu}\left(\frac{\partial E_y}{\partial x} - \frac{\partial E_x}{\partial y}\right) \quad (3.10)$$

$$E_x = \frac{1}{j\omega\varepsilon}\left(\frac{\partial H_z}{\partial y} - \frac{\partial H_y}{\partial z}\right) \quad (3.11)$$

$$E_y = \frac{1}{-j\omega\varepsilon}\left(\frac{\partial H_z}{\partial x} - \frac{\partial H_x}{\partial z}\right) \quad (3.12)$$

$$E_z = \frac{1}{j\omega\varepsilon}\left(\frac{\partial H_y}{\partial x} - \frac{\partial H_x}{\partial y}\right) \quad (3.13)$$

The total radiated power is estimated by '**Perseval's power theorem'** whereas the magnitude and phase of the radiated field can be calculated by using '**Poynting vector'**. **Eigen function** is used to express the wave within the wave guide. It is used to construct the field. Eigen function is derived from the source free wave equation. It acts as bricks in the rectangular house and is derived from the source free wave equation. Eigen function for the rectangular co-ordinate system will be: $\sin(kx), \cos(kx), e^{\pm j k_x x}$. The first two terms denote reflection where as last function denote wave propagation. **Hankel's function**: $H_n^1(kr)$ represents wave coming from infinity and $H_n^2(kr)$ represents an outgoing field and at infinity the field will decay to zero.

Here the approximate calculation of RDRA's dimension under unloaded condition is made by applying Dielectric Wave Guide Model. The length, width and height of the DRA is calculated by using antenna design equation for Normalized and resonant frequency by using fig 2.17 at page no. 32 of DRA Handbook by A. Petosa [45].

$$F = \frac{2\pi W f_0}{c}\sqrt{\varepsilon_r} \quad (3.14)$$

$$f_{GHz} = \frac{15F}{W_{cm}\,\pi\sqrt{\varepsilon_r}} \quad (3.15)$$

Where, F= Normalized frequency

3.2.4 Experimental And Simulated Result Analysis

It is important to have a precision designing of a circuit while selecting, rejecting controlled time delay, and channelizing maximum energy to transfer with minimum

reflection over a broad range of frequency bands. An impedance matching network having minimum insertion loss is to be inserted between the load and generator so that the reflected power will be extremely less in comparison to that of forwarding power. The simulated and measured return loss characteristic of the antenna is shown in Fig. 3.4. The simulated result shows a wider frequency response from 4.95 GHz to 13.5 GHz. Whereas, the measured result shows two bands of operation. The lower band is from 3.9 GHz to 5.1 GHz and the upper band is from 8.8 GHz to 10.3 GHz. The maximum resonant dip occurs at 9.8 GHz with a return loss of -46 dB. The measured 10 dB impedance bandwidth of the upper and lower bands are 26.66% and 15.71% respectively. However actual operational bandwidth will be influenced by the loading characteristics of the antenna. The measured minimum VSWR is found to be 1.04 at 9.8 GHz. As VSWR is found to be less than 2, an excellent impedance match can be obtained. The substantial difference between a simulated and measured value of the RDRA is due to hypersensitiveness to material tolerance, the manufacturing accuracy, antenna loading effect, indoor measurement conditions, the effect of the SMA connector, losses, etc. However, there is hardly any shift in the resonance frequency.

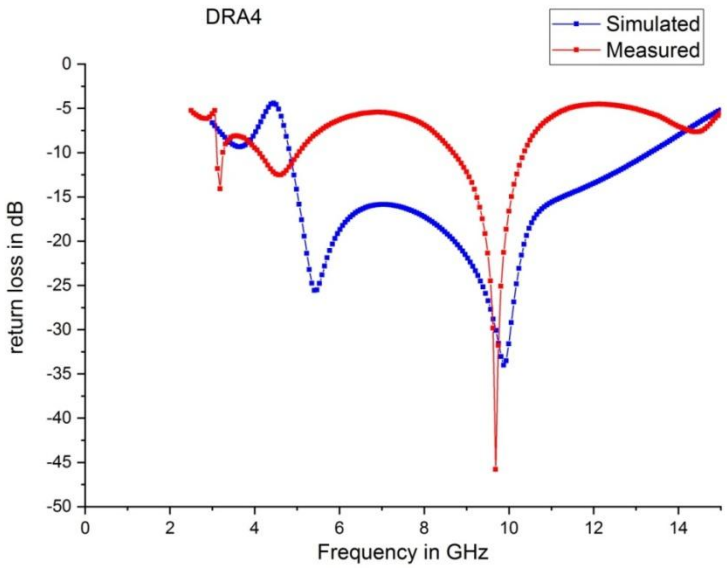

Fig. 3.4: Plot of measured and simulated return loss of the microstrip split fed dual band RDRA

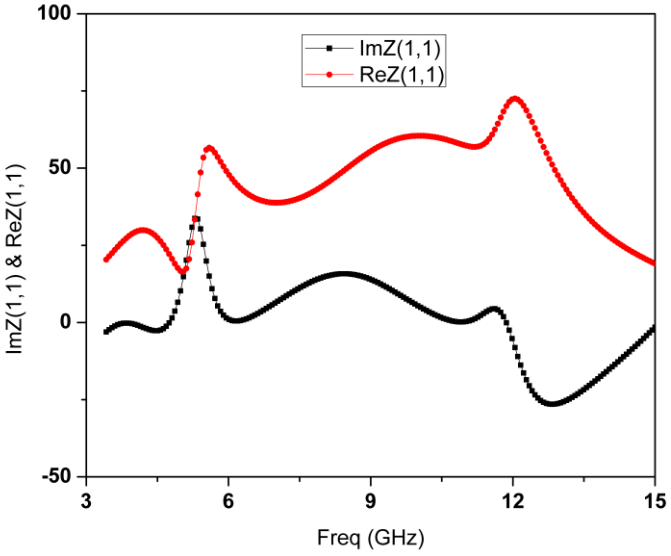

Fig. 3.5: Plot of real and imaginary part of input impedance Z (1, 1)

Further, with appropriate matching and loading conditioning power loss due to the undesired mode can be reduced [136, 137]. Fig. 3.5 shows the plot of real and imaginary input impedance Z (1, 1). It shows input impedance is resistive with a value of 50 Ohms in the entire frequency band of

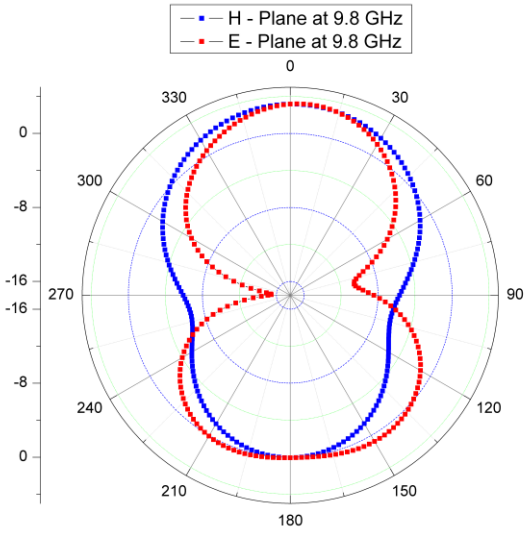

Fig. 3.6 Radiation pattern of the antenna in the E and H plane (10dB/div) corresponds to x-z plane ($\emptyset = 0^{\circ}$) and y-z plane ($\emptyset = 90^{\circ}$) at 9.8 GHz

operation. The radiation field pattern is a plot of $|E|$ and $|H|$ at constant radius 'r' in the radiation zone. Radiation pattern can be plotted by taking [138]

$$|S_r| = \left|E_\theta H_\emptyset^*\right| Vesus\ 'r' \tag{3.16}$$

The E-H plane corresponds to x-z plane ($\emptyset = 0^\circ$) and y-z plane ($\emptyset = 90^\circ$) at 9.8 GHz. The dual resonance with desirable radiation performance is mainly determined by the suitable placement of RDRA, source, and feeding arrangements. The study of co and cross polarization plays a significant role in deciding the performance of the antenna. Hemispherical DRA has a well developed numerical technique. Therefore, behavior of Hemispherical DRA can be used as reference to study the characteristics of RDRA. Ludwig defines the co-polarized probe fed hemispherical DRA as:

$$E_{copol} = E_\theta \cos\emptyset - E_\emptyset \sin\emptyset \tag{3.17}$$

For cross polarized field: $E_{crosspol} = E_\theta \sin\emptyset - E_\emptyset \cos\emptyset$ (3.18)

For $\emptyset = 0°$ in the xz plane$E_{copol} = E_\theta$, $\emptyset = 90°$ in the yz plane $E_{copol} = -E_\emptyset$, $\theta = 0°$, E_{copol} and $E_{crosspol}$ are in x and y direction. Cross polarized field increases with decrease in the value of dielectric constant. The polarization purity is very one of the fundamental requisite characteristics [139-142].

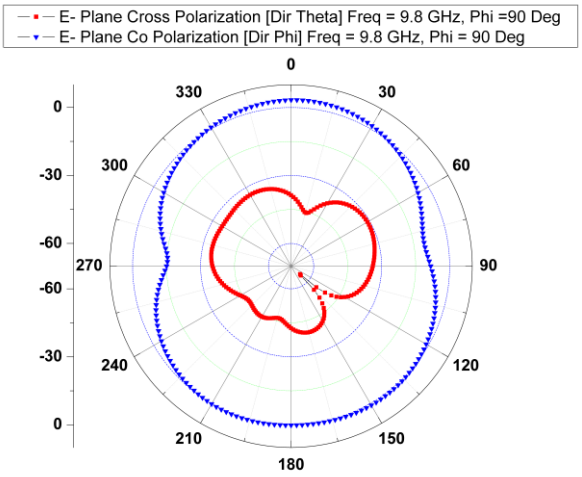

Fig. 3.7: Radiation pattern indicating E-plane co and cross polarization of the antenna (10 dB/div) along the y-z plane ($\emptyset = 90^\circ$) at 9.8 GHz

As described in the figure the maximum E-plane co-polarization is 0 dB and maximum E-plane cross polarization is less than -30 dB. Therefore the desirable co-polarized field is more than 30 dB to that of cross polarized field in the broadside direction that is $\theta = 0^\circ$ and $\theta = 180^\circ$. Low cross polarization is due to matching of the field between the dominant modes $TE^x_{\delta 11}$.

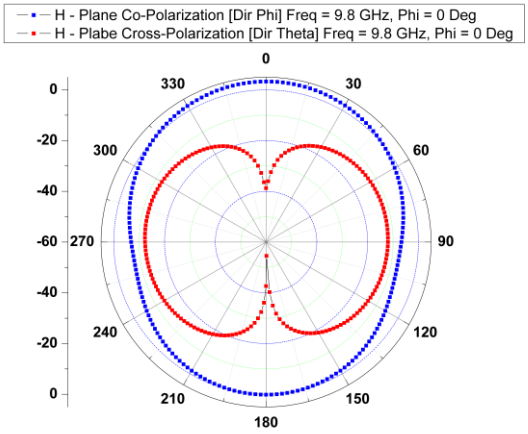

Fig. 3.8: Radiation pattern indicating H-plane co and cross polarization of the antenna (10 dB/div) along the x-z plane ($\emptyset = 0^{\circ}$) at 9.8 GHz

It is found that maximum co-polarized ($\theta = 0^{\circ}$and 180°) is 0 dB and cross polarized ($\theta = 90^{\circ}$and 270°) is -10 dB. In the broadside direction desirable co-polarized field is around 40 dB greater than that of cross polarized field.

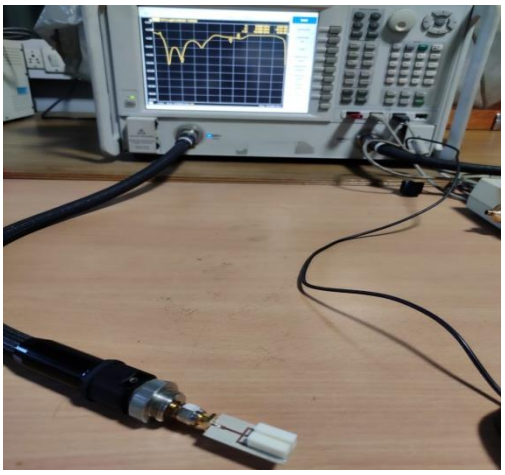

Fig. 3.9: Experimental test set up of the measurement of Return loss, VSWR, Z_{in}, and Smith chart

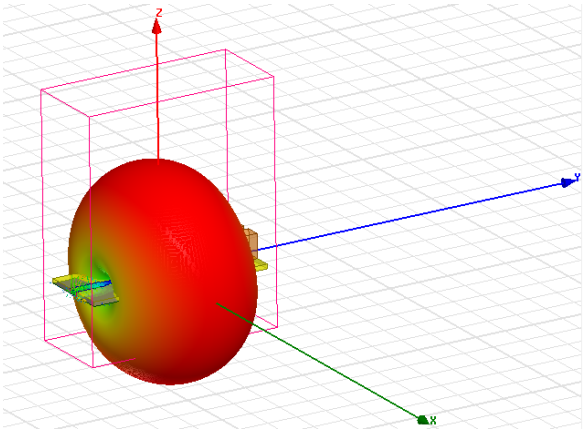

Fig. 3.10: The 3-Dimensional radiation pattern at 9.8 GHz

It is found that polarization efficiency is highest for the co-polarized wave. Fig. 10 shows the 3 dimensional radiation pattern of the proposed RDRA at 9.8 GHz. The symmetric field distribution results output pattern along the broadside direction.

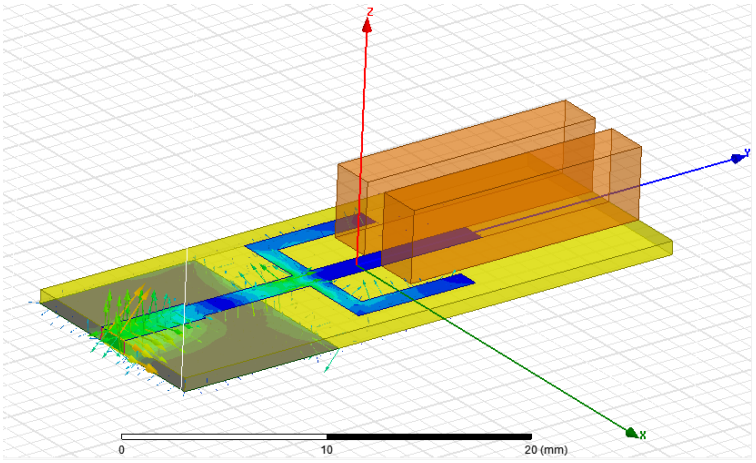

Fig. 3.11: Simulated formation of E-field (V/m), H-field (A/m), and Current density (J) (A/m^2)

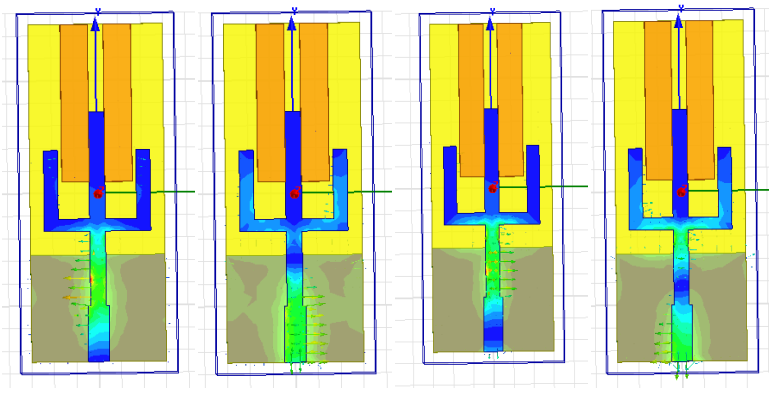

Fig. 3.12: Formation of surface current density (J) in Amp/m^2 on the antenna

Table 3.2: Parameters of RDRA

Efficiency	Peak Gain (dBi)	10 dB Band Width (%)	Frequency Band (GHz)	Resonant Frequency (f_0)	Return loss $\|S_{11}\|$ in dB
42%	2.8 dBi	26.66	Band-I: 3.9 – 5.1	4.6 GHz	12.5
		15.71	Band-II: 8.8 – 10.3	9.8 GHz	46

3.2.5 Conclusion

A novel dielectric resonator antenna for wireless application has been proposed. The designed antenna shows dual band response. The first resonant dip occurs from 4 GHz to 5 GHz with maximum dip occurs at 4.5 GHz. The second return loss dip occurs from 9 GHz to 10.2 GHz with maximum resonating frequency of 9.8 GHz. The measured 10 dB impedance bandwidth ($S_{11} < 10\ dB$) of the first and second band are 22.22% and 12.5% respectively.

3.3 DESIGN OF A NARROWBAND DIELECTRIC RESONATOR ANTENNA FOR WIRELESS COMMUNICATION AND SENSING APPLICATIONS

3.3.1 Introduction

The rectangular dielectric resonator antenna is emerging as a suitable alternative to micro-strip patch antenna technology for the modern high-speed communication system. The proposed radiator operates near to 2.4 GHz. for indoor, short-range, noiseless wireless communication. It provides high radiation stability with a radiation efficiency of 23.52%, impedance bandwidth of around 100 MHz. It provides minimum cross-polarization loss due to the induction of minimum orthogonal current components and surface waves. The radiation pattern is uniform over the impedance bandwidth. Critical coupling is achieved by a slot aperture but due to edge diffraction surface wave is producing comparatively high radiation in the back lobe [143-145].

3.3.2 Methodology

Because of the complex geometrical structure of the rectangular DRA and the distinction of different boundaries, the analytical solution cannot determine the

potential at far-field. Therefore the numerical solution is used to determine the dimensions, radiation Q-factor from the desired resonant frequency, and the electromagnetic far-field. Analytical techniques involve continuous variables. The main theme is to determine the electric and magnetic field when charge distribution and flow of current are known. Here finite element method is used to analyze the rectangular DRA. FEM constitutes the discretization of total geometry into small tetrahedrons. The testing function or shape function is estimated for each tetrahedron resulting in multiple basis functions. Then, the field wave equation is multiplied by the testing function and then integrated over the solution of the volume. This procedure results in thousands of equations for n=1, 2, 3…

From Helmholtz's equation: $\nabla^2 A + \mathrm{K}^2 A = -J$ (3.19)

$$H = \nabla \times A \tag{3.20}$$

$$E = \frac{\nabla(\nabla.A)}{j\omega\varepsilon} - j\omega\mu A \tag{3.21}$$

Where, A is the magnetic vector potential.

$$\nabla \times \left(\frac{1}{\mu_r}\nabla \times E\right) - k_0^2 \varepsilon_r E = J \tag{3.22}$$

$$\int \left(w_n.\nabla \times \left(\frac{1}{\mu_r}\nabla \times E\right) - k_0^2 \varepsilon_r w_n.E\right) dV = 0 \tag{3.23}$$

The dimensionality of the problem can be reduced by using Green's function and by applying Divergence theorem:

$$\int \left(\nabla \times w_n\right).\left(\frac{1}{\mu_r}\nabla \times E\right) - k_0^2 \varepsilon_r w_n.E\Big) dV = \iint (boundary\ t\ erms).dS \tag{3.24}$$

Where, n= 1, 2,…, N

$$E = \sum_m x_m w_n \tag{3.25}$$

Thus,

$$\sum x_m \int \left(\nabla \times w_n\right).\left(\frac{1}{\mu_r}\nabla \times E\right) - k_0^2 \varepsilon_r w_n.E\Big) dV = \iint (boundary\ t\ erms).dS \tag{3.26}$$

$$\sum_m x_m A_m = b_n \tag{3.27}$$

Where, b is the port excitation and A is the N×N matrix that includes any applied boundary conditions. E can be calculated by solving for x. For the rectangular DRA with infinite ground plane with lowest order mode will be $TE^{x}_{\delta 11}$the resulted field components can be obtained by applying the dielectric wave guide model (DWM). The field components of $TE^{x}_{\delta 11}$can be obtained by solving the transcendental equation.

$$k_x \tan\left(\frac{k_x d}{2}\right) = \sqrt{(\varepsilon_r - 1){k_0}^2 - {k_x}^2} \tag{3.28}$$

The resulted sinusoidal field will be:

$$H_x = \frac{({k_y}^2 + {k_z}^2)}{j\omega\,\mu_0} \cos(k_x x)\cos(k_y y)\cos(k_z z) \tag{3.29}$$

$$H_y = \frac{(k_y k_x)}{j\omega\,\mu_0} \sin(k_x x)\sin(k_y y)\cos(k_z z) \tag{3.30}$$

$$H_z = \frac{(k_z k_x)}{j\omega\,\mu_0} \sin(k_x x)\cos(k_y y)\sin(k_z z) \tag{3.31}$$

$$E_x = 0 \tag{3.32}$$

$$E_y = k_z \cos(k_x x)\cos(k_y y)\sin(k_z z) \tag{3.33}$$

$$E_z = -k_y\, cos(k_x x)\sin(k_y y)\cos(k_z z) \tag{3.34}$$

Where,

$k_x = \frac{m\pi}{a}, k_y = \frac{n\pi}{b}$

Where, $k_0 = \frac{2\pi}{\lambda_0} = \frac{2\pi f_0}{c}, k_y = \frac{\pi}{w}, k_z = \frac{\pi}{b}$

$${k_x}^2 + {k_y}^2 + {k_z}^2 = \varepsilon_r {k_0}^2 \tag{3.35}$$

The resonant frequency $f_0$in GHz can be calculated [4]:

$$f_{0(GHz)} = \frac{15F}{w_{(cm)}\pi\sqrt{\varepsilon_r}} \tag{3.36}$$

Design procedure for the Multi-Segment DRA:

i. By using Dielectric Wave Guide Model calculate length, breadth and height of the rectangular dielectric antenna for the given resonant frequency, radiation Q-factor and the location of higher order modes. Higher order mode should

not be responsible for cross polarization level [146, 147].

ii. To choose an insert permittivity between 20-40 and an thickness (t) and H is the height of the DRA such that 0.1<T<0.3 where,$T = {t}/{(t + H)}$.

iii. According to simple static capacitance model [148-151]:

$$\varepsilon_{eff} = \frac{H_{eff}}{\frac{h}{\varepsilon_r}+\frac{t}{\varepsilon_i}+\frac{s}{\varepsilon_s}} \tag{3.37}$$

$$H_{eff} = h + t + s \tag{3.38}$$

where, H_{eff} is the effective height of the MSDRA, h is the height of the DRA, t is the thickness of the insert parameter, and s is the thickness of the substrate. It will replace to DEM with ε_r replaces ε_{eff} and $2H_{eff}$ replaces 'b'. The effective insert thickness is a function of optimal coupling. However insert should not be a radiator.

$$t_{eff} = t\sqrt{\varepsilon_i} \tag{3.39}$$

Higher the permittivity of the insert(ε_i) lower will be the bandwidth and greater will be the sensitivity to position.

The output E and H field in the x,y, and z direction will be:

$$E_z = -Ak_y \cos(k_x x)\sin(k_y y)\cos(k_z z) \tag{3.40}$$

$$E_y = Ak_z \cos(k_x x)\cos(k_y y)\sin(k_z z) \tag{3.41}$$

$$E_x = 0 \tag{3.42}$$

$$H_z = \frac{(k_x k_z)}{j\omega\mu_0} \mathrm{A}\sin(k_x x)\sin(k_y y)\cos(k_z z) \tag{3.43}$$

$$H_y = \frac{(k_y k_x)}{j\omega\mu_0} A\sin(k_x x)\sin(k_y y)\cos(k_z z) \tag{3.44}$$

$$H_x = \frac{({k_y}^2+{k_z}^2)}{j\omega\mu_0} \mathrm{A}\cos(k_x x)\cos(k_y y)\cos(k_z z) \tag{3.45}$$

$$k_x \tan({k_x}^{W}/_2) = \sqrt{(\varepsilon_{r_1}-1)k_0^2 - k_x^2} \tag{3.46}$$

Where, $k_x = \sqrt{(\varepsilon_{r_1} - 1)k_0^2 - k_x^2}$

$k_z = \frac{\pi}{h}$,

$k_y = \frac{\pi}{L}$

$k_y = \frac{2\pi f_0}{Lc}$

3.3.3 Antenna Configuration

Fig 3.13, 3.14 represents the 3-Dside view and top view and detailed geometry of the proposed designed RDRA. The top radiating structure is made up of dielectric Roger RO 3010 (tm), $\tan\delta$ = 0.0035, which has dimension 13×13×6.5 mm^3.The lower structure is made up of RT 6010 with permittivity of 10.2 and a dimension of 13×13×2 $mm^3$and is placed over the rectangular aperture slot. The ground plane is placed over a substrate on which an aperture slot is etched.

The slot has a dimension of 16×1.2 mm^2 designed to provide critical coupling of energy from the micro-strip line to the lower RDRA. The substrate is made up of Roger TMM 6 (tm), ε_r = 6, $\tan\delta$ = 0.0035 having dimension of 30×30×0.762 mm^3. The micro-strip feeding line is placed below the substrate having dimension of 4×17.5 mm^2. The aperture feeding mechanism initiates transverse electric mode, where the lowest order mode is $TE^x_{\delta 11}$.

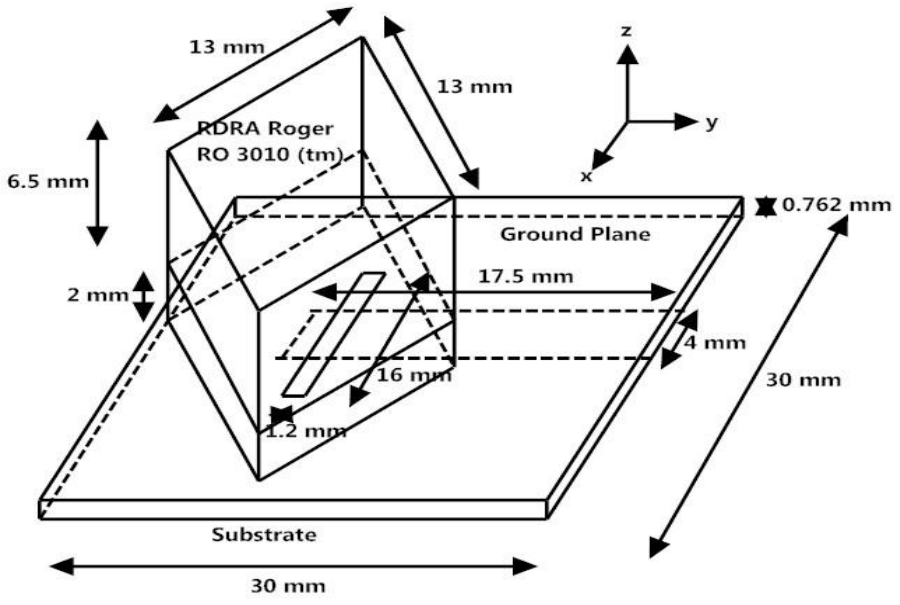

Fig. 3.13: 3-D side view of the proposed antenna

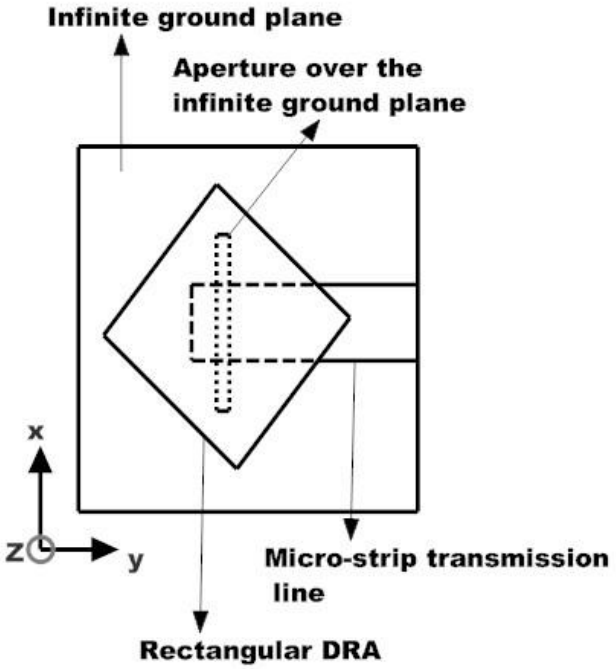

Fig. 3.14: Top view of the proposed antenna

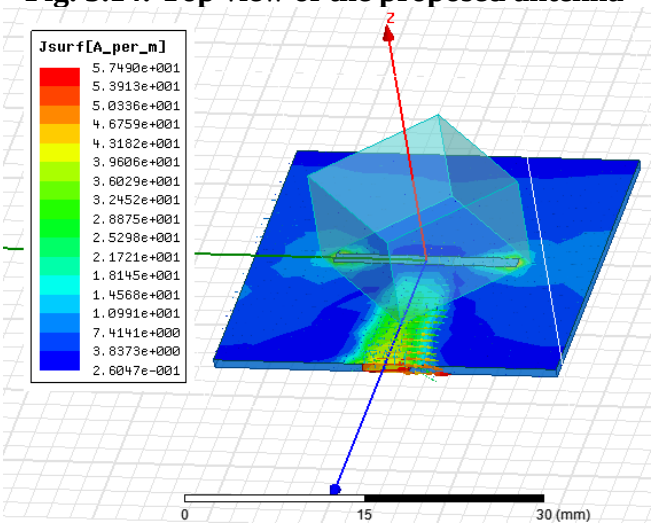

Fig.3.15: Simulated surface current density of the RDRA.

3.3.4 Result Analysis

The input impedance changes along with the microstrip line especially when it is within the aperture's initial or final edges. It indicates that microstrip position can be used as fundamental parameters for matching and tuning of the antenna. From Figure

3.16 it is found that the antenna is resonating at 2.4 GHz and the value of the return loss is around -12 dB. The -10 dB impedance bandwidth is calculated to be around 100 MHz, which provides a narrow band response. Fig. 3.17 indicates VSWR versus frequency. Here open-end stub is used to match the antenna w.r.t the 50 Ω micro-strip

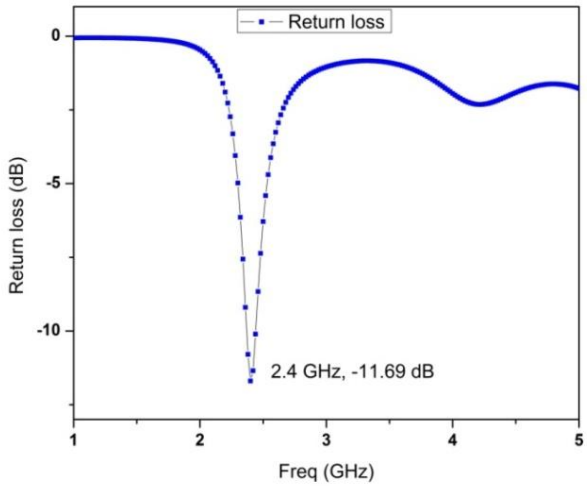

Fig3.16 Reflection coefficient (|S11|in dB) versus frequency plot

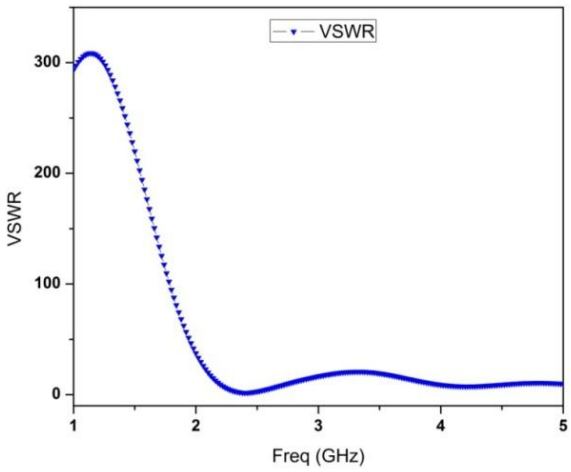

Fig 3.17 VSWR versus frequency plot

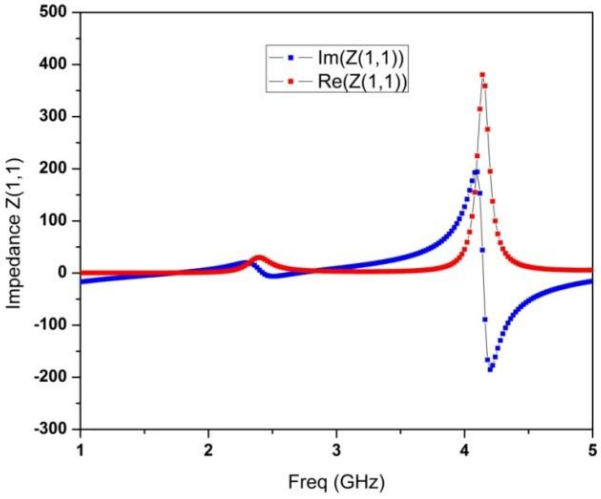

Fig 3.18 Real and imaginary input impedance versus frequency

feeding structure. At resonating frequency of 2.4 GHz there is resistive matching to maximize the power transfer.

The output radiated E and H along yz and xz plane at $\phi = 0^{o}$ and 90^{o} are shown in Fig. 3.19. It is found that 2.4 GHz RDRA is behaving like a perfect magnetic dipole to radiate the field in the broadside direction. However, due to aperture coupling, there is radiation in the back lobe. The resulted front to back ratio is calculated to be around 26.776 dB.

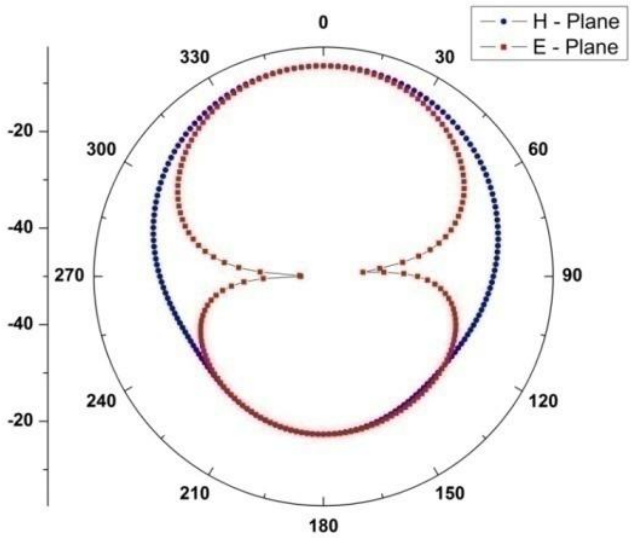

Fig 3.19 Plot of the E and H field in the yz and xz plane

It is observed that in all the plane there is a difference of -20 dB between co and cross polarization.

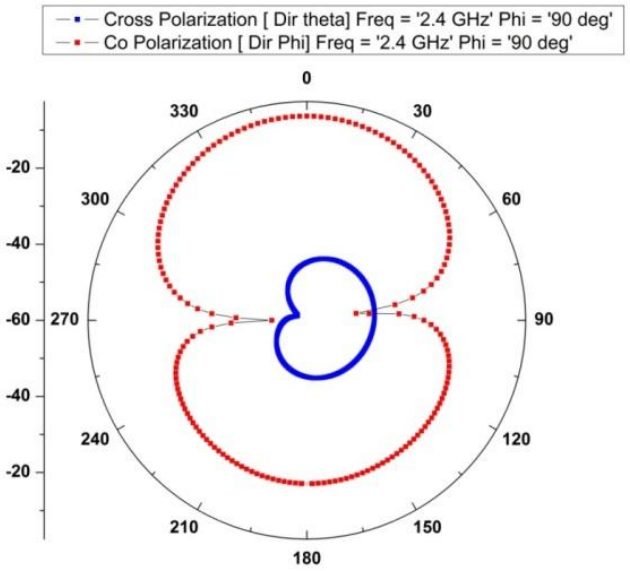

Fig 3.20 Plot of H-plane co and cross polarization

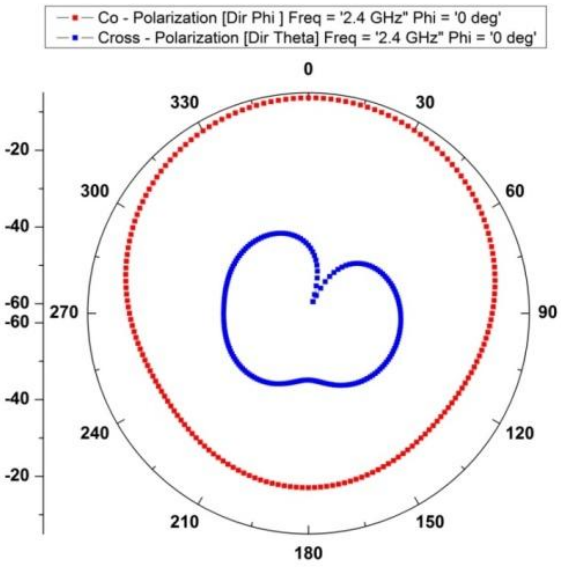

Fig 3.21 Plot of E-plane co and cross polarization

Fig. 3.22 shows the total gain versus frequency. The gain of the antenna can be defined as the sum of the E_θ and E_ϕ components. It is found that at 2.4 GHz the total gain is about -2dBi. But as this device is going to be used for portable wireless communication the average gain is more significant and can be determined along a

specific plane. Fig. 3.23 describes the plot of electric and magnetic field vectors in the designed RDRA.

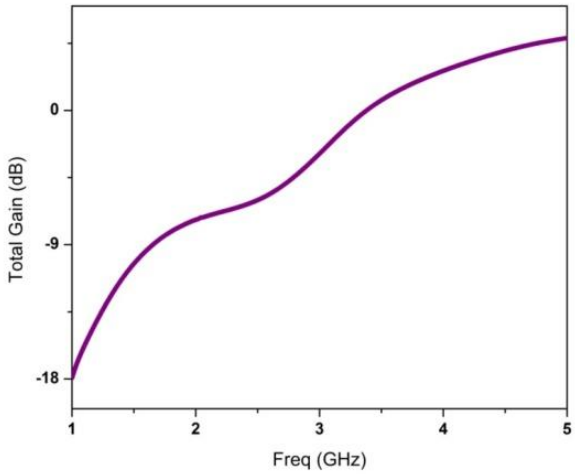

Fig 3.22 Plot of gain in dB versus frequency in GHz

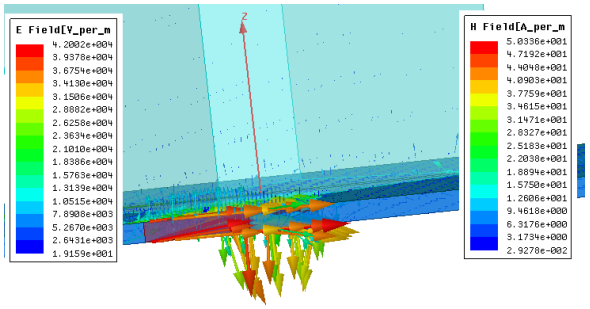

Fig 3.23 Plot of electric and magnetic field vectors in the designed antenna

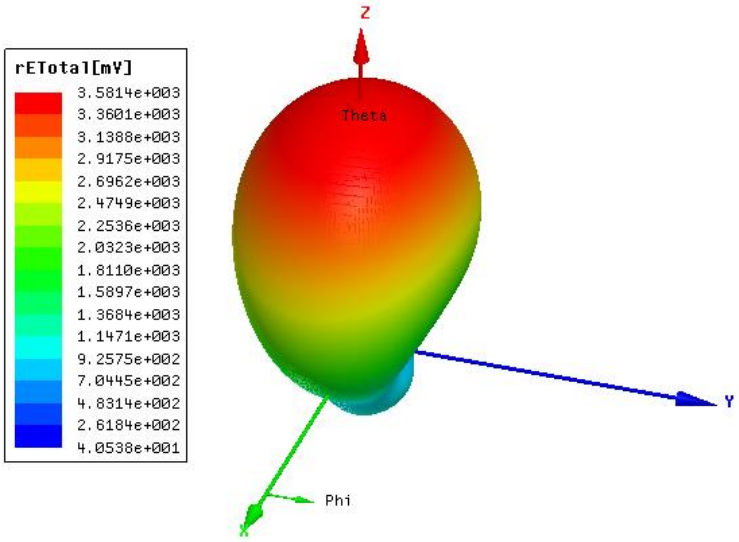

Fig 3.24 Plot of radiated electric field in the broadside direction

3.3.5 Conclusion

In the above work, a narrowband dielectric resonator antenna for wireless communication and sensing application is designed and analyzed by using electromagnetic simulator HFSS 14.0. The designed structure resonates at 2.4 GHz with impedance bandwidth of 100 MHz. This antenna shows front to back ratio of 26.776 dB which indicates considerably power loss in the back lobe. These back radiations can be blocked and made useful by using dielectric material of high permittivity and by using a focusing mechanism to achieve high directive gain.

3.4 LEAKY WAVE-GUIDE BASED DIELECTRIC RESONATOR ANTENNA FOR MILLIMETER-WAVE APPLICATIONS

3.4.1 Introduction

Future wireless communication depends upon front end devices, which is low profile, high radiation efficiency, and efficient at high frequency. Leaky wave DRA may be desirable due to low loss, low surface wave, conductor loss and high radiation efficiency at mm wave frequency. NRD guide was introduced by Yoneyama and Nishida in 1981[152]. NRD guide is non radiating in nature but it can radiate if approximate perturbation is created in the structure so that intrinsic bounded mode can be converted into leaky wave mode [153-155]. This antenna can radiate in the off broadside direction.

Leaky wave based resonator antenna is a periodic, line source based, high efficient travelling wave antenna. It leaks non spectral wave all along its length. This antenna provides high antenna gain with narrow beamwidth. At mm wave leaky wave antenna is based on new lower loss waveguides that include non-radiative dielectric. It is flexible in terms of ease of installation and space allocation. The NRD guide is a transmission line of non-radiative. Therefore different lengths of the NRD as transmission line will produce different cutoff frequency. Multiband can be realized by using different blocks of transmission lines through different switching elements. The NRD guide can suppress radiation at the curved section and the discontinuities. The NRD guide will minimize the surface wave. The surface wave lowers the conductor loss and provides minimum loss tangent at high frequency. Therefore radiation efficiency of the radiator increases significantly. Though the NRD guide does not radiate, it can be leaky-wave in nature if excited suitably with associated

perturbation. The distance between open-end and dielectric slab is made smaller than half of the free-space wavelength. The field will not be allowed to decay completely and so some power will leak out from the open end. The leakage will increase with the decrease in displacement. It means bounded mode should be converted into the leaky-wave mode. The dominant mode within the guide will be the LSE and LSM mode. The dominant mode within the leaky wave can be excited by using aperture coupling. The introduction of asymmetry between the NRD guide will result in a net horizontal field [156-158]. This horizontal field will excite different modes within the guide. Aperture coupling is used for making the leaky-wave radiation in the broadside and off the broadside direction of the E-plane by placing a suitable metal casing. Back radiation can be reduced which may arise due to the presence of the aperture. A flared horn is attached to the open end of the radiator. This open flared horn controls the H-plane beamwidth. Radiation in the E-plane is symmetrical about the broadside direction with narrow beamwidth. In H-plane it is shifted away from the broadside. The vertical height of the parallel plates is used for controlling impedance bandwidth, antenna gain, and radiation pattern. The lower value of magnetic field results in lower antenna gain and the higher value of magnetic field results in higher antenna gain and clear radiation pattern [159, 160].

Here even if the NRD structure is perturbed the major characteristics of the antenna are constant and is symmetrical about the y-z plane. It is suitable for the near field communication (NFC) in the millimeter-wave band [161].

3.4.2 Principle Of Operation

The conventional leaky-wave antenna is used in the forward and backward angles, but show limited efficiency in the broadside direction. Its scanning is restricted to a small range of angles either in the forward or backward direction. In a leaky-wave structure the attenuation constant and phase constant characterize the beam width, and radiation angle respectively. The large value of attenuation constant in the leaky-wave structure results in a small effective aperture and wide beamwidth. Whereas, small attenuation constant in the antenna leads to slow leakage, which resulted in narrow beamwidth. At mm wave new antennas are based on new lower loss wave guides that include NRD [162]:

$$\beta_x = \beta_n = \beta_0 + \frac{2n\pi}{d} \tag{3.47}$$

The radiation angle: $\theta = \sin^{-1}\left(\frac{\beta_n}{k_0}\right) = \sin^{-1}\left(\frac{\beta_0 + \frac{2n\pi}{d}}{k_0}\right)$ (3.48)

When there will be a change in frequency, the phase constant varies and radiation angle can be controlled by the frequency. The attenuation factor along the broadside direction is small therefore field will decay slowly towards the open end. By adjusting the aspect ratio of the NRD and height of the parallel plate, practical radiation patterns can be controlled. It has been observed that broadside radiation occurs when: (i) The operating frequency is nearer to the cut-off frequency of LSE_{11} (ii) The feeding is located at the middle of the dielectric slab (iii) Excitation of the dielectric radiator by a half sinusoidal field distribution (iv) The dominant mode is in fact bounded one but introduction of asymmetry, groove, and perturbation make them leak [163].

A leaky-wave antenna based on two symmetrical NRD guides is studied. The height of the parallel plate is responsible to control the impedance bandwidth, antenna gain, and radiation pattern. If two H-plates are unequal then the beam will be steer towards the shorter plate. The thickness of the dielectric slot will have an impact on the operating frequency. The open waveguide supports slow wave structure, where $\beta > k_0$. The rectangular dielectric rod is placed over the ground plane and the microstrip line. As leaky wave is fast the fundamental surface wave is slow. The feed arrangement introduces spurious radiation that is extended to the air.

For a wave guide:

$$\left(\frac{m\pi}{a}\right)^2 + \left(\frac{n\pi}{b}\right)^2 + {k_z}^2 = \omega^2\mu\varepsilon = k^2 \quad (3.49)$$

The propagation constant in the z direction will be:

$$k_z = k_z^{'} - jk_z^{"} \quad (3.50)$$

$k_z^{'}$ controls the beam direction whereas $k_z^{"}$ detects the directivity of the beam. Therefore frequency scanned leaky wave antenna is a function of $k_z^{'}$ and$k_z^{"}$. Within a dielectric slab field can be written by discrete summation of modes.

$$E_x = \sum_{m=0}^{\infty}\sum_{n=0}^{\infty} A_{mn} \quad (3.51)$$

Assuming $k_y = \frac{n\pi}{b} = 0$

Then, $k_x^2 + k_y^2 = k^2$ (3.52)

The field is:

$$E(x,z) = \int_{-\infty}^{\infty} R\,(k_z) e^{j k_z z} e^{j k_x x} dk_x \quad (3.53)$$

It has been observed that while integrating function does not exist at certain point. It demarcates the existence of surface wave mode through Somerfield's integral. Therefore distinct pole called leaky wave pole will contribute to the surface wave. When there is variation of field wave with respect to x leads to the generation of non-spectral wave or Ghost wave. A. A. Oliner detects the presence of leaky wave. Surface wave travels along the surface and it's energy is concentrated to the boundary. Wave moves by lateral motion charge at the boundary. Inside the conductor the electric field is mainly horizontal and outside the conductor the field is mainly vertical. Therefore there is no net transfer of charges and all the wave energy is getting converted into heat energy.

3.4.3 Structure Of Antenna

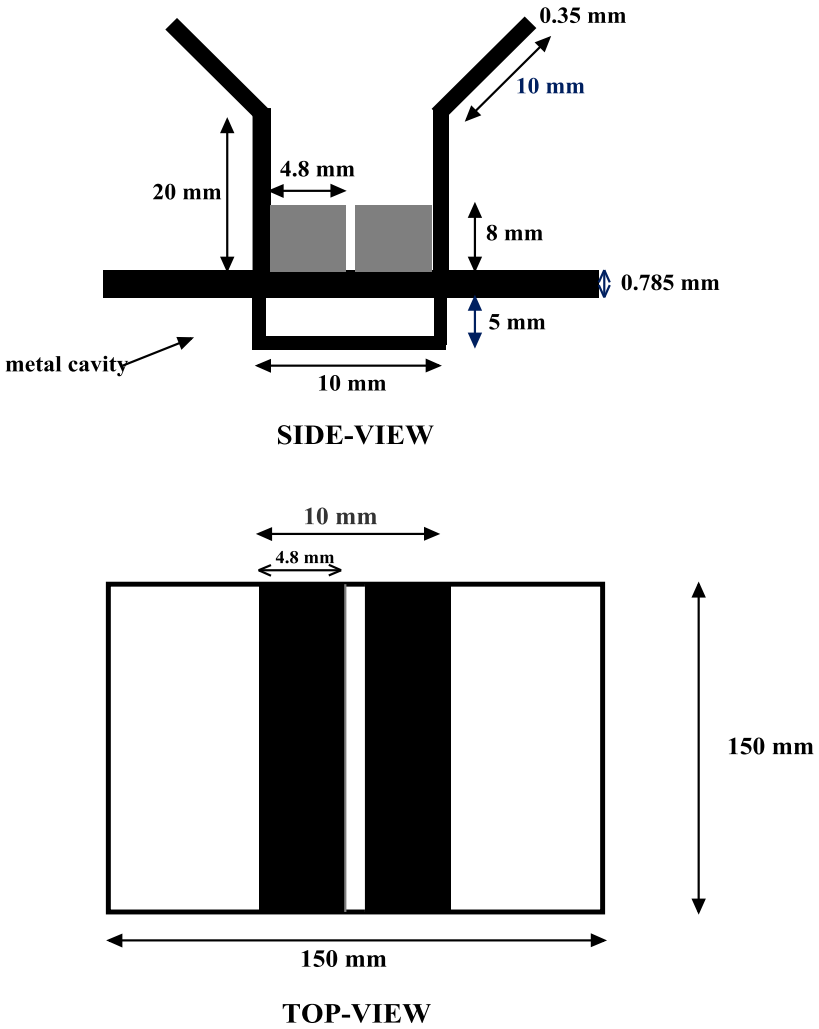

Fig. 3.25 Side view and top view of the proposed antenna.

Table 3.3: Parameters of the leaky wave antenna

Structure	Length	Width	Height	Permittivity	Material	tan δ
Substrate	150 mm	150 mm	0.785 mm	2.55	Arlon AD 255C	0.0014
DRA	150 mm	4.8 mm	8 mm	2.2	Arlon Di Clad 880	0.0009

Flaring of the guide wall approximately results in impedance matching and more focused radiation pattern with the increased directivity. Here it is an E-plane sectorial horn. In this design flaring angle is high and phase distribution over the aperture is non-uniform. It implies directivity and enhanced beam width.

Fig. 3.26 indicates the direction of the E and H field within the dielectric.

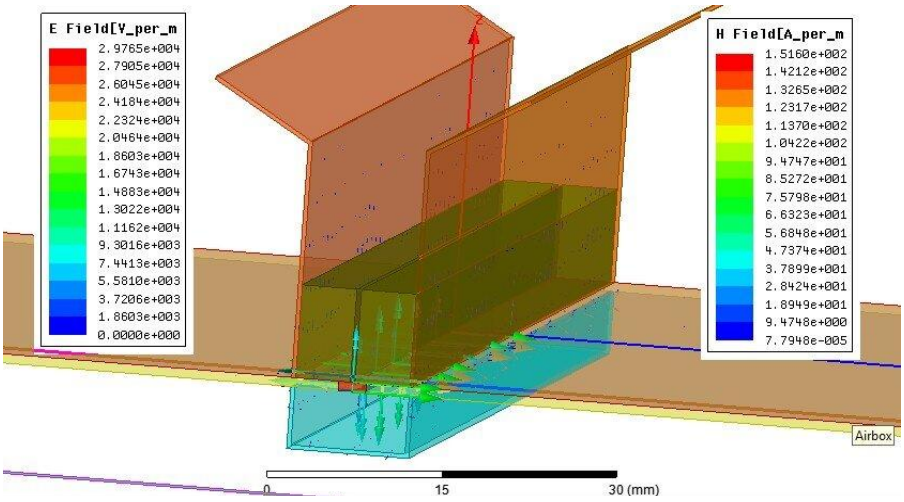

Fig. 3.26 Formation of E and H field within the antenna

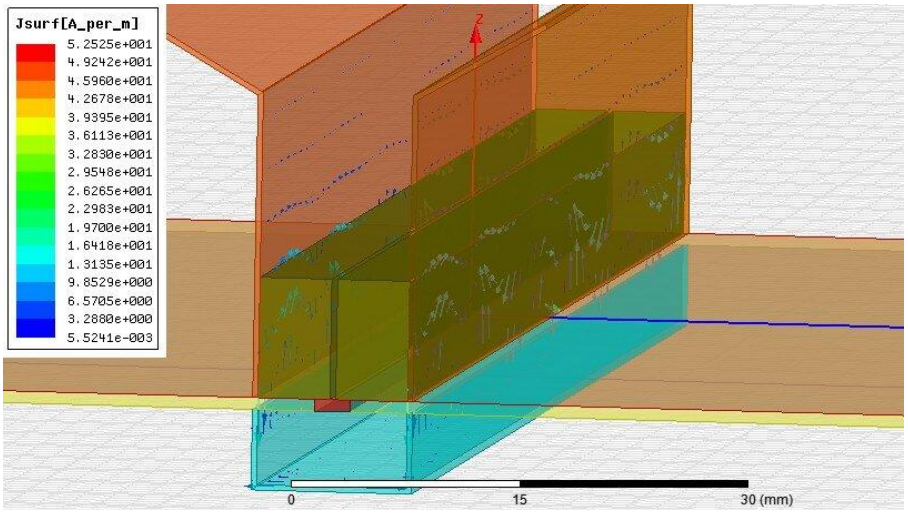

Fig. 3.27 Formation of surface current on the antenna

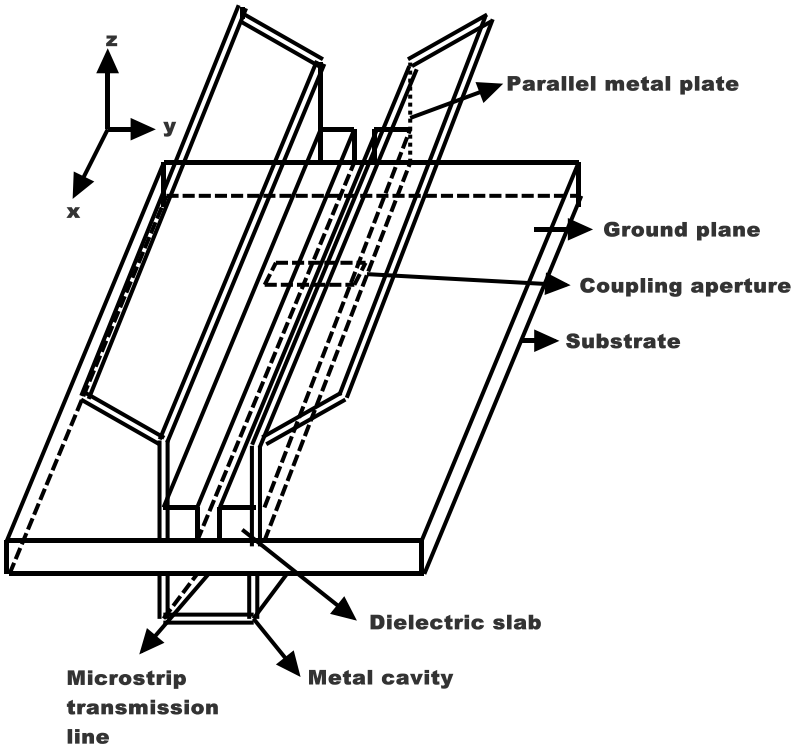

Fig. 3.28 Leaky wave based DRA structure.

3.4.4 Results Analysis

The leaky wave antenna is analyzed in terms of guided electromagnetic wave through the non-radiating dielectric waveguide. The non-confinement of the EM wave can be achieved by deliberate introduction of a slot. The slot is less than half of the operating wavelength. But exact length of the resonance depends upon the position of the slot in the guide. The slot provides inductive reactance within the specified frequency range.

Thus slot cannot extract all the power present in the dielectric wave guide but couple out a fraction of it. But proper impedance matching enhances the power coupling of the slot. The slot is covered by low loss dielectric material. Feeding slot to be located at the middle of the NRD guide. The slot will radiate from both the sides of the x-y plane. As radiation from the back side is undesirable, it is enclosed by a metallic box, which acts as an electrical wall. The electric field line exist parallel to the surface.

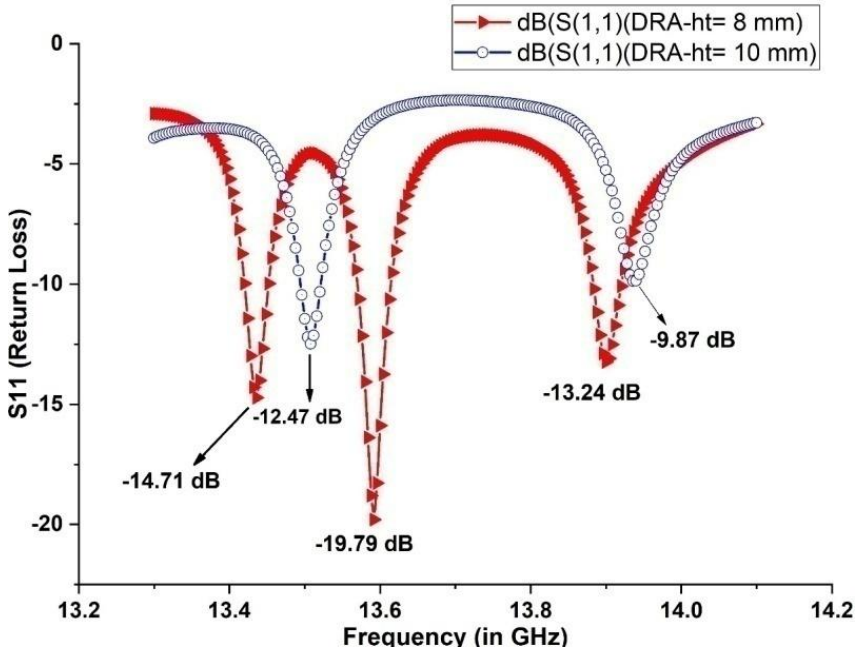

Fig. 3.29 Plot of Return loss versus frequency.

Broad side radiation can be established when operating frequency comes closure to the cut off frequency. Guide length should be twice of the length of the NRD guide. Leaky wave antenna usually generate narrow beam. As the antenna supports standing wave due to the reflected wave at the end of the slab, it is resonant in nature. The side lobes are 15 dB lesser than the major lobes. Side lobe level is due to the presence of minor imperfections in the antenna which cannot be corrected. The total length of the non radiating dielectric be shortened by about 5% of half wavelength to mitigate the standing wave without compromising the output antenna pattern appreciably.

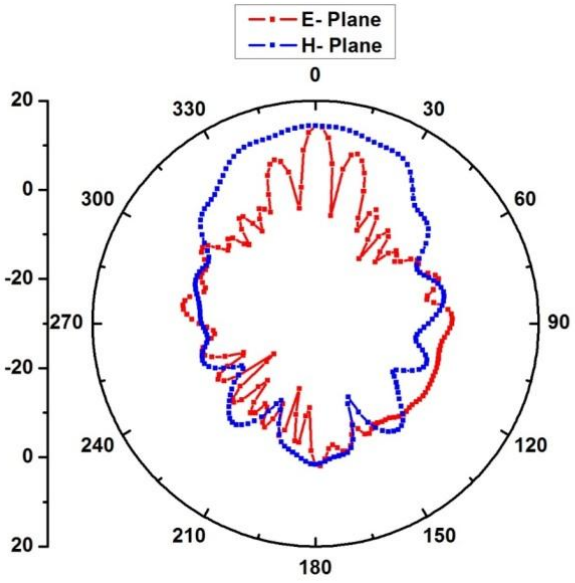

Fig. 3.30: Radiation pattern of the antenna in the E and H plane (10dB/div)

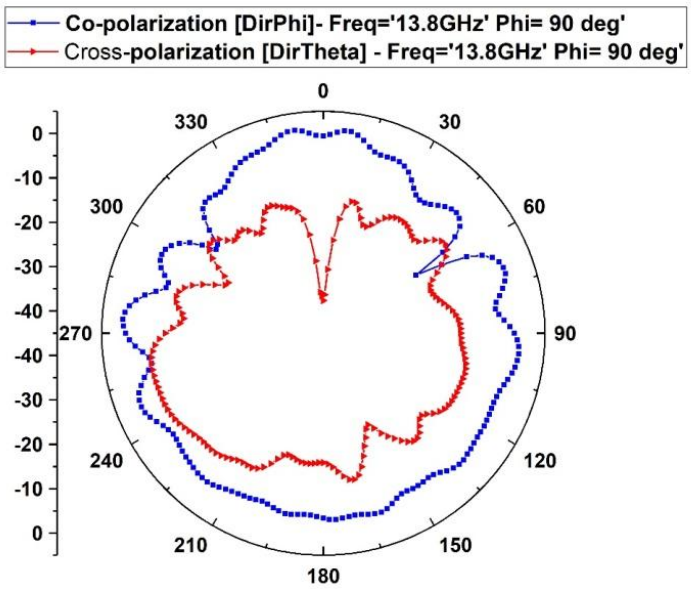

Fig. 3.31 Radiation pattern indicating E-plane co and cross polarization (10 dB/div)

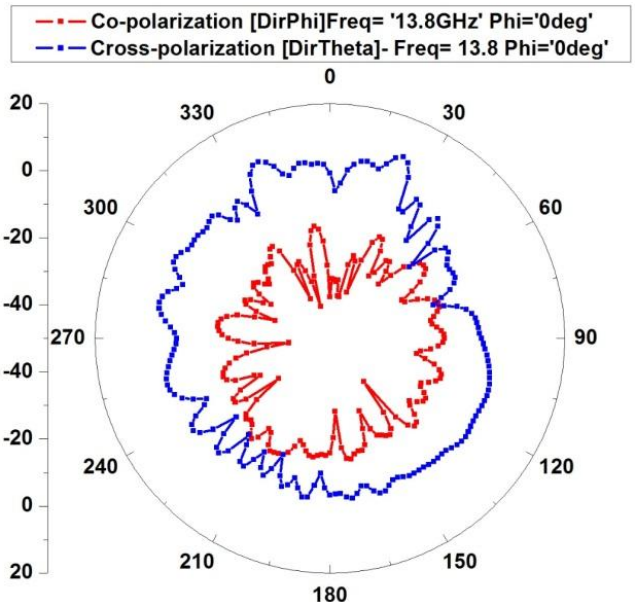

Fig. 3.32 Radiation pattern indicating H-plane co and cross polarization of the antenna (10dB/div)

3.4.5 Conclusion

Here a leaky wave asymmetric based NRD radiator has been proposed. The resonant dip occurs at the frequency of 13.59 GHz, 13.43 GHz, and 13.93 GHz. Leaky wave NRD based dielectric is a usually narrow band in nature which makes it suitable for Narrowband IoT. In this type of antenna 3 dB gain bandwidth is narrower than the impedance bandwidth. Therefore overall usable bandwidth depends upon the gain bandwidth. It has the potential to become a wideband antenna with high radiation efficiency.

CHAPTER 4
DESIGN OF MULTI-FUNCTIONAL HYBRID DRA

4.1 INTRODUCTION

The never-ending quest for higher bandwidth and stability are forcing the high-speed circuit design to scale new heights. However, high-speed digital signal creates unwanted radiation. In a conductor, the electric field is almost shorted and conduction current flows due to the influence of magnetic field. As frequency of operation increases current distribution is over the surface of the waveguide. When frequency of operation increases, electrical thickness of the conductor decreases. As a result radiation power loss increases. The radiation can be minimized by using dielectric slab of high dielectric constant. Usually the dielectric slab with high ε_r is brittle in nature and it can introduce effect like fringing field and evanescent wave due to the presence of air gap. The E and H field will constituting **'Hybrid mode'**. Rectangular DRA when operating in their fundamental mode $TE_{11\delta}$ will behave as a magnetic dipole. It has wider impedance bandwidth as it radiates through the entire DRA surface. The RDRA offers high design flexibility, due to two degree of freedom and the availability of a wide range of aspect ratio for the desired frequency. It is low profile having a small footprint area. RDRA does not allow surface wave and only loss in RDRA is through imperfection in the dielectric [164, 167]. It can be easily integrate with modern surface mounted devices (SMDs).

DRA used to be arranged in an array format to achieve shaped beam radiation pattern and to improve the gain of the device. The number of array elements, their positional co-ordinates, and the magnitude of excitation coefficient are responsible to obtain the desired radiation pattern. The desirable parameters in array is wide beam width radiation pattern, with high front to back ratio, a miniaturized compact foot print to reduce the grating lobe, low mutual coupling to improve the scan blindness, etc.

4.2 DUAL BAND RDRA FOR PORTABLE WIRELESS APPLICATIONS

4.2.1 Introduction

This work presents, a microstrip fed miniaturized, low loss dual-band RDRA for portable wireless applications. The goal is to maximize the tunability range of the RDRA with consistent radiation pattern over the entire tuning range. In this novel design, a rectangular dielectric, made up of 99.7% of Alumina, $\boldsymbol{\varepsilon_r}$ = 9.8 is placed on a substrate of Roger Rd 3003, $\boldsymbol{\varepsilon_r}$ = 3. It operates in two bands, which are from 3.1 GHz to 5.2 GHz in band-I and from 9 GHz to 10.8 GHz in band-II. The measured 10 dB impedance bandwidth of the first and second bands are 50.6% and 18.18% respectively. The dual resonant frequency can be achieved by exciting the RDRA with the split microstrip line. It provides a peak gain of 3 dBi. The RDRA is fabricated and measured by using Agilent Technologies N 5247A: A.09.90.02 Vector Network Analyzer (VNA). It is suitable as a front end device for portable wireless cellular communication system in ultra-wideband application.

Ultra Wide Band technology is recently used in i-phone for spatial awareness allowing device to understand precise location relative to other devices. The aim is to enhance latency, coverage, scalability, diversity and moreover bandwidth performance to bridge the practical gap between the emerging broadband or ultra-wideband system and current technological trend for high-speed communication. The most significant feature of the DRA is to provide a high degree of electrical flexibility to fulfill the varied portable wireless communication requirements. The major variables which determine the working of the DRA are excitation and generation of modes within the DRA, resonant frequency, loaded and unloaded radiation Q-factor, and output radiation patterns in broadside direction. The impedance bandwidth has got some strong impact on these factors. While considering the fundamental structure like cylindrical and hemispherical, the rectangular shape provides the highest design flexibilities as its aspect ratio is proportional to length/width and depth/width. Thus radiating structure can be easily customized according to the bandwidth requirements, and the resonant frequency is the function of the dimension [168-172]. The coupling mechanism is the lifeline of the DRA, which usually affects the output radiation pattern mainly due to loaded cross-polarization level. Based on the pattern of the

mode within the DRA, an electric, magnetic, and hybrid dipole will be formed. If the dielectric has low loss then loss power will be equivalent to the radiated power.

There are numerous ways to enhance the bandwidth of the RDRA. Multi-resonant frequency can be stacked together to realize the broadband nature of the RDRA. Bandwidth can be enhanced by lowering the Q-factor by appropriate impedance matching and combining multiple resonators. However, Q-factor cannot be reduced below a certain limit called the Chu limit. Difference structures can excite different modes, and by the amalgamation of all these modes, broadband can be obtained. Permittivity can be altered from 6 to 100 to realize broadband response. Broadband can be achieved by altering the feeding techniques and matching profile. It can be achieved by creating irregularities, truncation, and splitting in the structure. Therefore there will be rapid altercation of time-harmonic displacement current. Two or more dielectric of the same and different permittivity and shape can create broadband response. DRA array configurations with appropriate switching can generate broadband response. By using sub and super structure-based frequency selective surface, the broadband response can be initiated. DRA will be arranged appropriately to create a loading effect of one w.r.t other to have broadband response. Hybrid design can result in broadband response where there is a combination between DRA and patch. Dimension and dielectric permittivity control the bandwidth. By the optimization of ground, plane bandwidth can be improved [173-182].

4.2.2 Geometry Of Antenna

The detailed geometry and photograph of the novel fabricated proto-type of dual-band RDRA are shown in Fig. 4.1a and 4.1b. This antenna is configured on Roger Rd 3003 dielectric substrate with dielectric constant (ε_r) equal to 3, loss tangent ($\tan\delta$) of 0.003, and having a dimension of$12 \times 30 \times 0.75\ \text{mm}^3$. For the high-frequency design, a lower dielectric constant is preferred to avoid an extreme miniaturized shape which is difficult to fabricate and excite. It may significantly contribute to unwanted radiation to reduce the effective bandwidth of operation. The thinner height of the substrate is useful to reduce the substrate loss which is due to the formation of the high amplitude of the surface wave. It often degrades the radiation efficiency of the

radiator. A finite ground plane of dimension $12 \times 9.5\ mm^2$ is at the bottom of the antenna towards the excitation side of the feed line. Copper with finite conductivity of 5.8×10^7 Siemens/ meter is used is used.

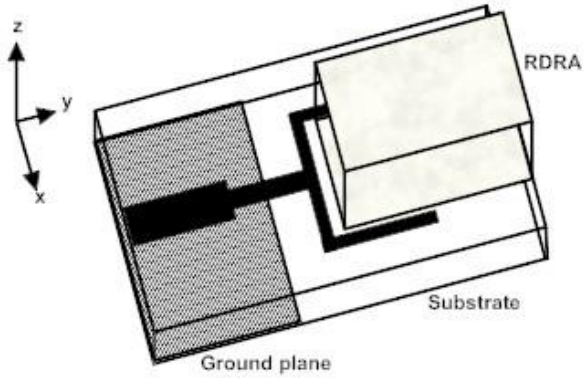

Fig. 4.1a: Structure of the proposed RDRA

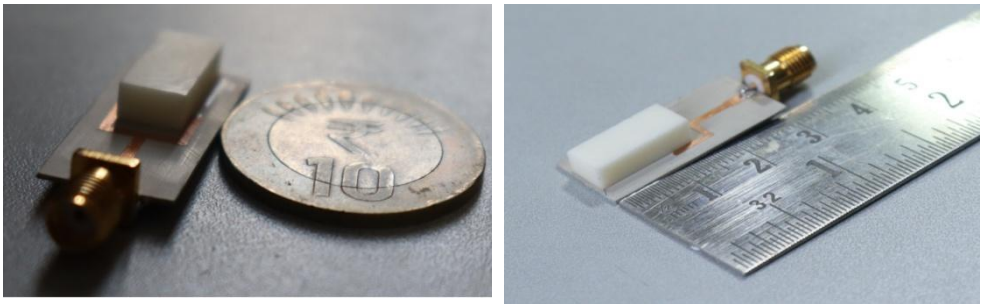

Fig. 4.1b: Photograph of the proposed fabricated prototype RDRA

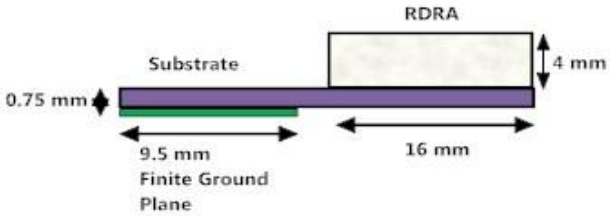

Fig. 4.2: Side view of the proposed RDRA.

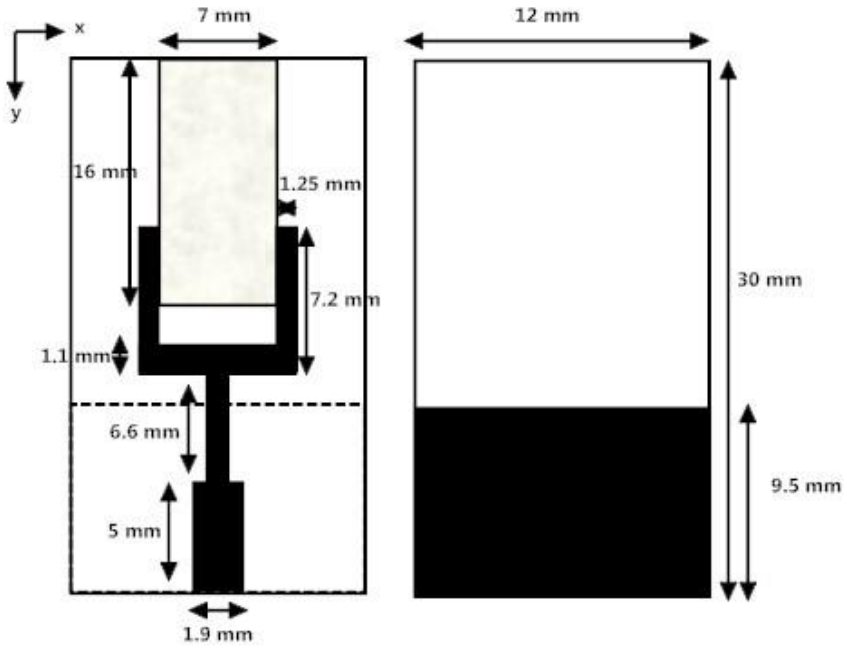

Fig. 4.3a: Top and bottom view of the proposed RDRA.

Fig. 4.3b: Top and bottom view of the fabricated substrate

simulation. The transmission line for the antenna is having a total length 18.8 mm and different specified dimensions as shown in Fig 4.2, 4.3a, and 4.3b. The microstrip transmission line is preferred due to ease of fabrication, ease of active integration, reduction in mode coupling, and low radiation and transmission loss. However, the microstrip transmission line suffers from high dispersion and excitation of the surface wave. The input impedance is found to be capacitive below the resonant frequency. The necessary impedance is provided by quarter guided wavelength. The split line adds the necessary inductance to compensate for the capacitive effect. The different dimension of the split line network is to achieve characteristics Z of 50 Ohms for effective matching and to excite the dominant mode in the RDRA. Proper impedance

matching provides a tradeoff between loaded resonance, forced resonance, and self-resonance. With appropriate matching and loading conditioning power loss due to the undesired mode can be reduced. As shown in Fig. 4.1 the dimension of the miniaturized RDRA is $7 \times 16 \times 4\, mm^3$. It is calculated by using a dielectric waveguide model under unloaded conditions. Optimization is being done under the loaded condition to achieve accurate result. High-Frequency Structured Simulator (HFSS) is used under unloaded conditions. Here Silicon sealant, a non-permanent adhesive is used to bond the RDRA over the substrate. Through cleanliness, miniaturized air gaps can be reduced to have reasonable control and accuracy over the variation in the matching profile.

TABLE 4.1: Structural Parameters of RDRA

Element	**Material used**	**Relative Permittivity**	**Loss Tangent**	**Dimensions (**Tolerance: +/- 0.5 mm)
Rectangular DRA	99.7% Alumina	9.8	0.003	x =7mm, y = 16mm, z(height) = 4 mm,
Substrate	Roger RO 3003 (tm)	3	0.0013	x =12mm, y = 30mm, Z(height) = 0.75 mm

4.2.3 Principle Of Operation

An extreme low value of Q can be realized by selecting lower dielectric constant material with appropriate dimensions. Therefore, theoretically it is possible to design DRA having broad bandwidth. Therefore a magnetic dipole radiates maximum field intensity along the plane of the small loop but in the horizontal directions the polarization is vertical.

Practically due to complex rectangular shape there may be generation of some arbitrary higher order and evanescent modes. It may create difficulty while fixing the input and output characteristics of the radiating structure. Therefore dimension of the rectangular structure plays a significant role in ensuring the mitigation of any unwanted modes especially in the frequency band of operations. By using ‘curve fitting technique’ following equation is obtained for the normalized frequency F.

$$F = a_0 + a_1\left(\frac{w}{b}\right) + a_2\left(\frac{w}{b}\right)^2 \quad (4.1)$$

Where, $a_0 = 2.57 - 0.8\left(\frac{d}{b}\right) + 0.42\left(\frac{d}{b}\right)^2 - 0.05\left(\frac{d}{b}\right)^3$

$a_1 = 2.71\left(\frac{d}{b}\right)^{0.282}$

$a_2 = 0.16$

The radiation Q-factor of RDRA will be [45]:

$$Q = \frac{2\omega W_e}{P_{rad}} \quad (4.2)$$

P_{rad} = The radiated power, W_e = The stored energy

$$W_e = \frac{\varepsilon_0 \varepsilon_r abd}{32}\left(1 + \frac{\sin(k_x d)}{(k_x d)}\right)\left({k_x}^2 + {k_y}^2\right) \quad (4.3)$$

$$P_{rad} = 10{k_0}^4 |p_m|^2 \quad (4.4)$$

p_m is the magnetic dipole moment.

$$p_m = \frac{-j\omega\, 8\varepsilon_0(\varepsilon_r - 1)}{k_x k_y k_z}\sin\left(\frac{k_x}{d}\right)\hat{x} \quad (4.5)$$

The impedance bandwidth = $\frac{S-1}{Q\sqrt{S}}$ (4.6)

The normalized Q-factor '$Q_e = \frac{Q}{{\varepsilon_r}^{3/2}}$ (4.7)

At resonant frequency the acceptable VSWR is 2. It has been observed that calculated resonant frequency through Dielectric Wave Guide Model and measured values differ by around 3 to 12%. Accuracy of the result is controlled by the aspect ratio and dielectric constant of the RDRA. However radiation Q-factor can deviate up to 100% from the calculated value. It is due to the loading effect caused by the addition of transmission line, incorrect positioning of the source. But by the application of radar cross technique, the difference between the calculated and of an isolated RDRA can be reduced to 35% and resonant frequency to 7%.The normalized Q-factor (Qn) can be defined as

$$Q_n = \frac{Q}{{\varepsilon_r}^{3/2}} \quad (4.8)$$

4.2.4 Experimental And Simulated Results

The antenna operates in two bands that are from 3.1 GHz to 5.2 GHz in band-I

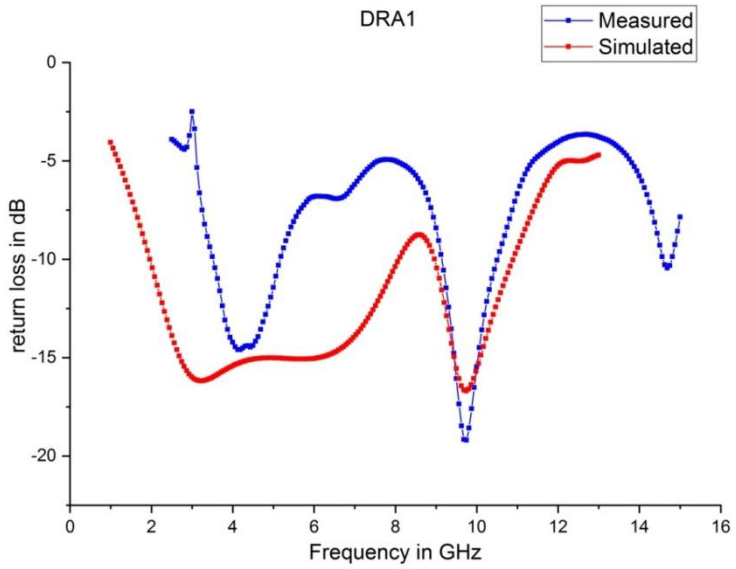

Fig. 4.4: Plot of measured and simulated return loss

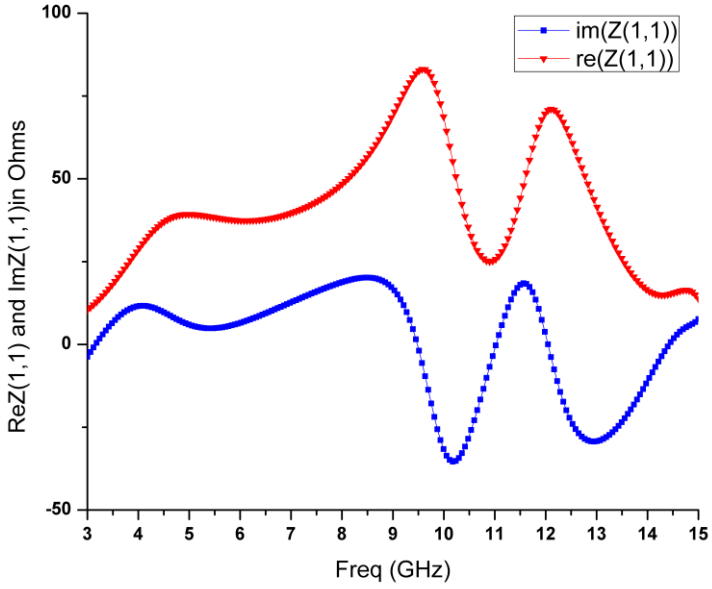

Fig. 4.5: Plot of real and imaginary input impedance Z(1,1) versus frequency

and from 9 GHz to 10.8 GHz in band-II. The first resonant dip occurs at 4.2 GHz. It is caused due to excitation of dominant mode$TE_{11\delta}$. The second return loss dip occurs at 9.8 GHz of the impedance curve corresponding to the loaded microstrip line

resonance. In these bands VSWR is found to be less than 2. Fig 4.5 describes the plot of real and imaginary input impedance Z(1,1) versus frequency.

It results in excellent impedance match over the entire given tunable range. Split transmission line is acting as an open ended stub having much stronger effect on the RDRA resonance. The length of the stub at both the end is crucial to calculate the resonant frequency and bandwidth. $|S_{11}| < 10\ dB$ of the first and second band are 50.6% and 18.18% respectively. However, actual operational bandwidth will be influenced by the loading characteristics of the radiator. The simulated result shows two bands of operation, band I is from 2 GHz to 8.1 GHz and band II is from 9 GHz to 11.1 GHz. It results is due to difference in material tolerances, the manufacturing precision and accuracy, the loading effect on the antenna due to indoor measurement conditions, the creations of miniaturized air gap, the effect of the SMA connector, the effect of Silicon sealant as non-permanent adhesive, and variation in accuracy of placing the RDRA over the substrate. Due to high sensitivity
nature of the impedance matching the measurement set up should be very precise and

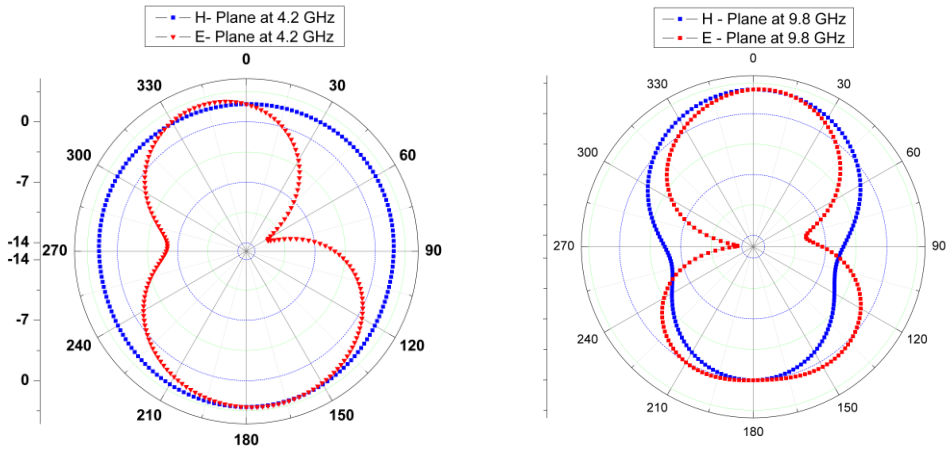

Fig. 4.6 Radiation pattern of the antenna in the E and H plane (10dB/div) corresponds to x-z plane ($\emptyset = 0^{\circ}$) and y-z plane ($\emptyset = 90^{\circ}$) at 4.2 GHz and 9.8

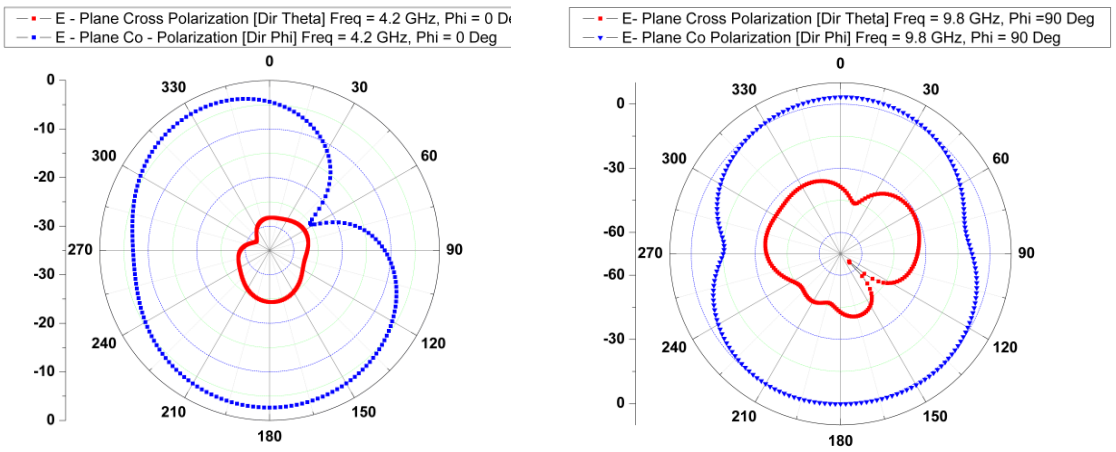

Fig. 4.7: Radiation pattern indicating E-plane co and cross polarization of the antenna (10 dB/div) along the y-z plane ($\emptyset = 90^{\circ}$) at 4.2 GHz and 9.8 GHz

Fig. 4.7 shows the radiation pattern indicating E-plane co and cross polarization of the antenna (10 dB/div) along the y-z plane ($\emptyset = 90^{\circ}$) at 4.5 GHz. As described in the figure the desirable co-polarized field is more than 20 dB to that of cross polarized field in the broadside direction that is $\boldsymbol{\theta = 0^{\circ}}$ and $\boldsymbol{\theta = 180^{\circ}}$. The cross polarized field is found to be at low level that is at least 20 dB less than the co-polarized field in the broadside direction. The cross polar discrimination is the ratio of co-polarized power to that of cross polarized power. The ripple and unwanted harmonics in the radiation pattern is due to the effect of the finite ground plane like reflection, diffraction, and scattering. A metamaterial inclusion, may be added to make the field distribution well more uniform than that of a conventional structure. It leads to improvement in gain as

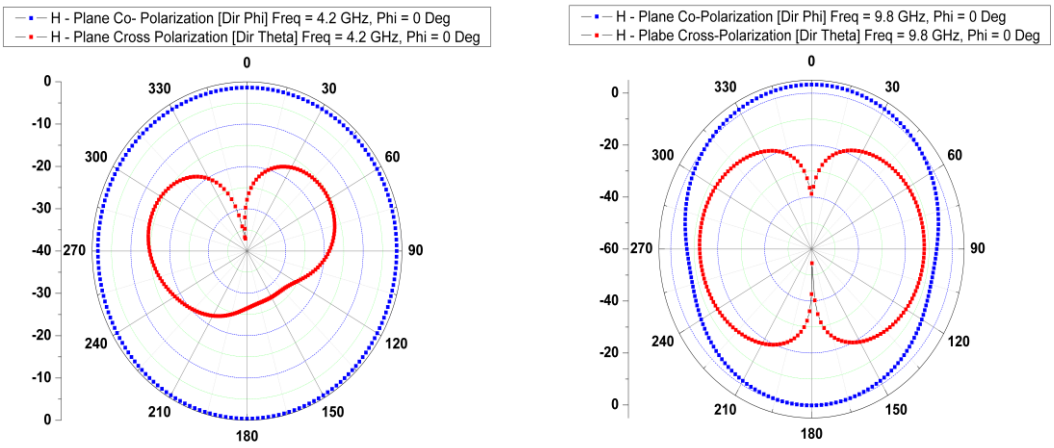

Fig. 4.8: Radiation pattern indicating H-plane co and cross polarization of the antenna (10 dB/div) along the x-z plane ($\emptyset = 0^{\circ}$) at 4.2 GHz and 9.8 GHz

It is found that co-polarized ($\theta = 0^{\circ}$) and cross polarized ($\theta = 90^{\circ}$) H-plane field alters with the change in stub length and there will be altercation in the impedance matching. Therefore split phase transmission line can change the tunable frequency range by altering the VSWR and polarization purity of the radiation field.

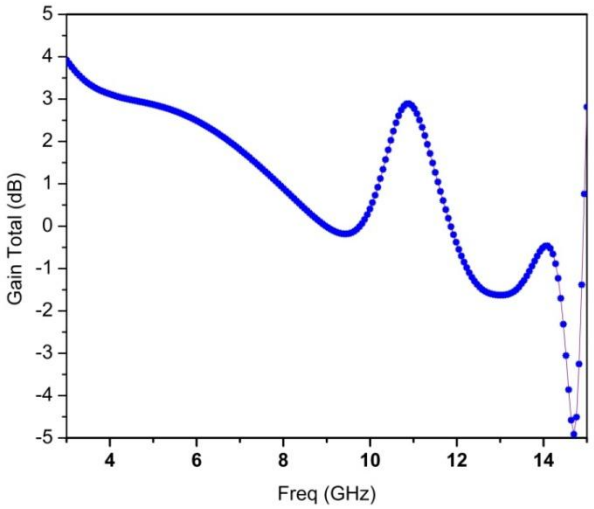

Fig. 4.9: Plot showing the relation between frequency of operation and total gain in dB

Fig. 4.9 shows the relation between frequency of operation and total gain of the antenna in dBi.

Fig. 4.10: Experimental test set up of the measurement of Return loss, VSWR, Z_{in}, and Smith chart

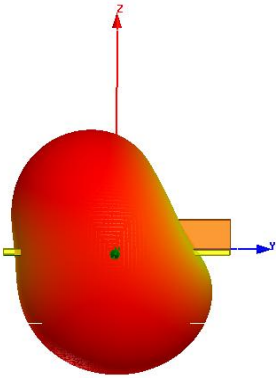

Fig. 4.11: The 3-Dimensional radiation pattern at 4.2 GHz

Required from an omni-directional antenna to the power required from an actual antenna.

$$g(\theta) = \frac{4\pi r^2 S_r(\theta)}{P_f} \tag{4.9}$$

where, the radiated power density $S_r(\theta) = E_\theta H_\emptyset^*$

The power radiated $P_f = \int_0^{2\pi} \int_0^{\pi} S_r r^2 \sin(\theta) d\theta d\emptyset$

The symmetric field distribution results output pattern along the broadside direction.

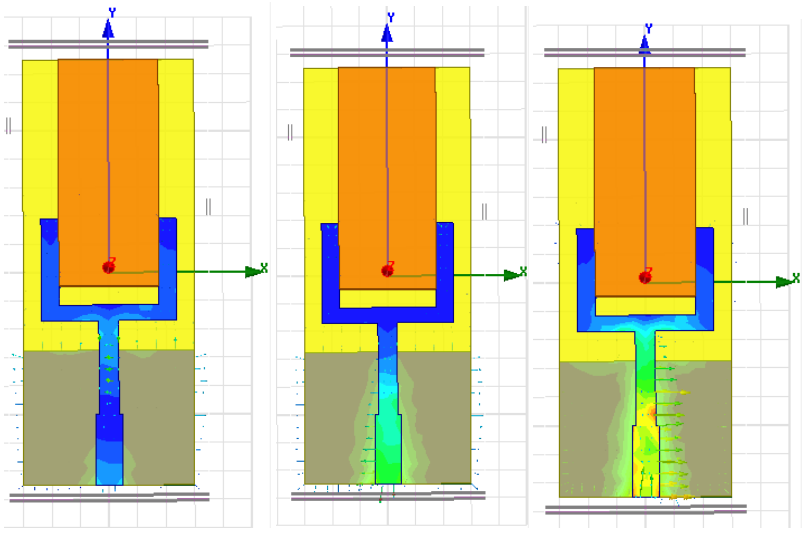

Fig. 4.12: Formation of surface current density (J) in Amp/m^2 within the antenna structure at 4.2 GHz

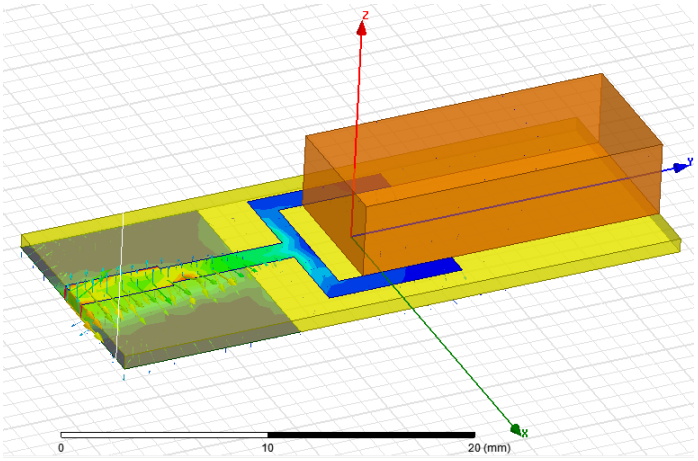

Fig. 4.13: Simulated integrated formation of E-field (V/m), H-field (A/m), and Current density (J) (A/m^2) at 4.2 GHz

Table 4.2: Input and output parameters of the fabricated RDRA

Efficiency	Peak Gain (dBi)	10 dB Band Width (%)	Frequency Band	Resonant Frequency (f_0)
45%	3 dBi	50.6	Band-I: 3.1 – 5.2 GHz	4.2 GHz
		18.18	Band-II: 9 – 10.5 GHz	9.8 GHz

4.2.5 Conclusion

The designed radiating RDRA shows dual band response. Under loaded condition the characteristics of the RDRA like radiation efficiency, directivity is significantly enhanced and good matching profile is obtained by using the finite ground plane at the bottom of the substrate towards the feed side. Radiation bandwidth and pattern bandwidth are balanced to keep the radiation pattern stable in both the band of operation. The symmetric field distribution leads to output radiation patterns in the broadside direction. Front to back ratio at broadside direction is 1.19 dB. Because of its miniaturized design and having operating bandwidth greater than 10%, it is a suitable for portable wireless cellular communication system. Further, a metamaterial inclusion or superstrate may be added to make the field distribution more uniform which leads to improvement in gain as well as in bandwidth. It is required to improve RDRA's mathematical modeling to analyze its design characteristics.

4.3 FILLETED DUAL BAND DIELECTRIC RESONATOR ANTENNA FOR HIGH SPEED APPLICATION

4.3.1 Introduction

The antennas for wireless communication devices have undergone a tremendous expansion from the external monoband resonant antenna to the internal non-resonant multi-band antenna. Due to the complex edge-shaped boundary between the dielectric and air in a rectangular dielectric resonator antenna, a complex closed form of expression is difficult to achieve. To address this problem a half-cut cylinder is placed over the rectangular dielectric to achieve excellent radiation characteristics. This proposed antenna provides a wide dual-band response with fractional impedance bandwidth of 21.92% and 19.09%while operating from7.32 GHz to 9.12 GHz and 10.71 GHz to 12.95 GHz. It provides an average gain of 3dBi with high gain stability in the entire operating frequency band. The radiation efficiency is found to be 96% due to low ohmic and dielectric losses. The cross-polarization is around 20 dB lesser than the co-polarization [182-185]. Its gain and directivity can further be enhanced by implementing serial and parallel array structures.

4.3.2 Structure Of Antenna

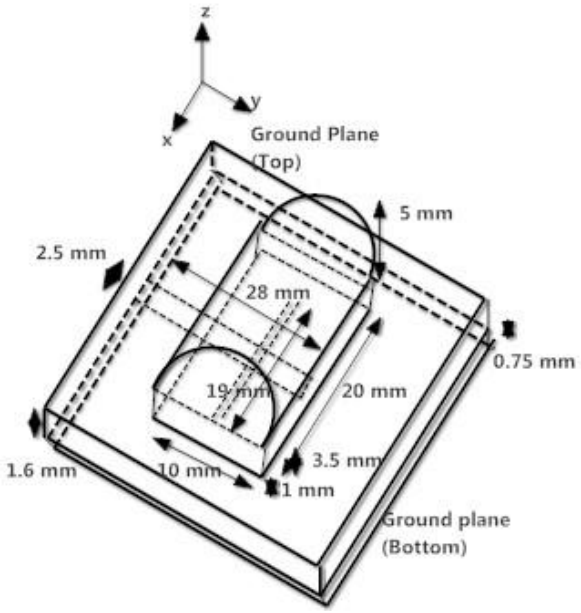

Fig. 4.14: Side view of the proposed radiator

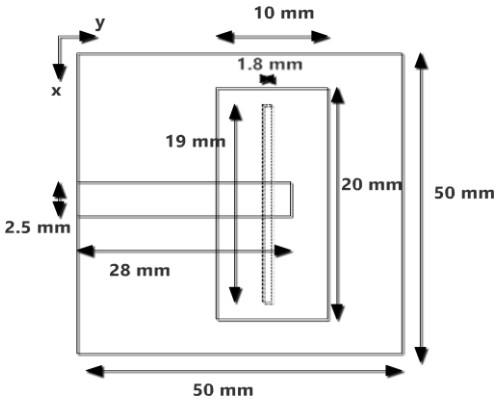

Fig. 4.15: Top view of the antenna

Fig. 4.15 and 4.16 show the structure of the designed dual-band dielectric resonator antenna. The antenna is placed on a Teflon substrate having $\varepsilon_r = 2.1$ having loss tangent $\tan\delta = 0.001$ with a dimension of 50×50×0.75 mm^3 over which micro-strip line as a feeding transmission line is drawn. The dimension of the transmission line, along with the quarter-wave stub, is 2.5×28×0.35 mm^3. The bottom portion of the substrate is covered with a perfect electrical conductor (PEC) as an infinite ground plane.

$$n \times H = J_s \tag{4.10}$$

$$n \times E = 0 \tag{4.11}$$

where, J_s is the source current density. To represent the source, the field equation can be amended to include impressed currents, electric, and magnetic field. This current is the source of the field. It reduces the radiation of energy in an unwanted direction. Thus large probe self-reactance or wide microstrip lines that are artificial at microwave frequency can be avoided. An aperture of dimension 18.9×1.8 mm^2 is placed at the top ground plane of the upper substrate, which is used to couple energy from the feeding transmission line to the radiator. It is based on the coupling theory, derived from the cavity model. The strongest coupling occurs where the termination of the line is slightly less than one-quarter of a dielectric wavelength from the edge of the dielectric. The transmission line is used to excite the lowest order mode, which will be the dominant mode within the resonator. This slot coupler will act as a major contributor to back radiation. Another substrate (Arlon AD 255 A (tm),$\varepsilon_r = 2.55$, $\tan\partial = 0.0015$) is placed over the bottom substrate to reduce the surface wave,

creation of redundant evanescent modes, and to eliminate exposure of field of the microstrip line to the medium of the radiator directly. Therefore, the effect of the feeding mechanisms on the antenna output characteristics can be minimized to a large extent. When the width of the substrate is narrow, it results in high input impedance, much higher than 50Ω, whereas when the width of the substrate is wide, it results in low input impedance of the DRA. So by controlling the width of the substrate, impedance matching can be accomplished. The lower permittivity of the substrate results in increasing the coupling of energy into the DRA. An air gap is introduced at the top of the substrate by placing a thin foam spacer having $\varepsilon_r = 1$ of dimension 50×50×1 mm^3. The air gap is responsible to enhance the resonant frequency and to reduce the radiation Q-factor [6]. Therefore, there is enhancement in the impedance bandwidth and there will be modification of the matching profile. A rectangular dielectric resonator antenna made up of Teflon having ε_r=2.1, $\tan\delta = 0.001$ of dimension 20×10×3.5 mm^3 is placed over the foam spacer. A half cylindrical structure made up of Alumina Al_2O_3 having ε_r= 9.8, $\tan\delta$ = 0.002) of dimension 20×10 mm^2 cut along XY plane having radius 5 mm is placed over the rectangular structure. The half-cut cylindrical structure is used to increase the effective electrical area of the radiator. The calculation of the resonant frequency of this stacked configuration requires certain adjustments. This top cylindrical structure may be useful in providing high mechanical strength when the antenna will be operated in free space.

Table 4.3: Structural parameters of the antenna

Structure	Length	Width	Height	Permittivity	Material	$\tan\delta$
Substrate (bottom)	50 mm	50 mm	0.75 mm	2.1	Teflon	0.001
Substrate (top)	50 mm	50 mm	0.75 mm	2.55	Arlon AD 255 A (tm)	0.0015
RDRA	20 mm	10 mm	3.5 mm	2.1	Teflon	0.001
Half Cylindrical DRA	20 mm	10 mm	Radius = 5 mm	9.8	Alumina (Al_2O_3)	0.002

4.3.3 Input And Output Characteristics

As shown in Fig 4.16 the S_{11} versus frequency graph, the resonating frequency below -10dB comes out to be 8.21 GHz from 7.32 GHz to 9.12 GHz and 11.73 GHz from

10.71 GHz to 12.95 GHz. However, practically it has been observed that more than -8dB the antenna will function quite well. The impedance bandwidth for Band-I is found to be 21.92% and impedance bandwidth for Band-II is found to be 19.09%. This dual wideband response covers the frequency from 3.1 GHz to 10.6 GHz. This embedded stacked configuration is very sensitive to variation in frequency response. Fig 4.17 describes the impedance smith chart, which provides polar form of mapping of the impedance plane and the reflection coefficient. At 8.21 GHz and 11.73 GHz a perfect match is plotted and is a vector of zero length i.e. 1+j0 or 50 Ω.

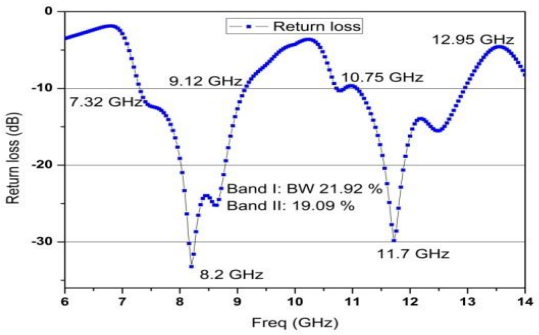

Fig. 4.16: Plot of Return loss versus frequency.

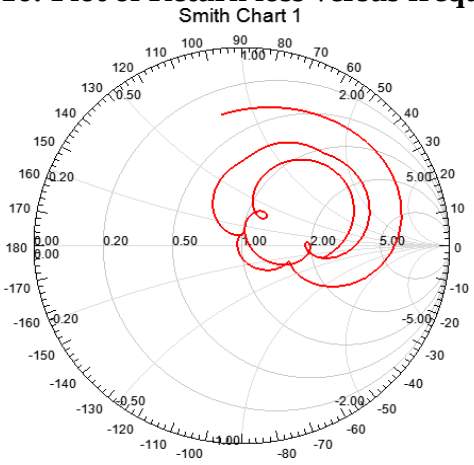

Fig. 4.17: The Impedance smith chart

Fig. 4.18 and 4.19 shows the output radiated E and H field in the yz and xz plane at $\measuredangle = 0°$ and $\measuredangle = 90°$ at 7 GHz. The radiation plot guides how to aim the antenna towards its corresponding receiver. Here the half power beam width is found to be 70°. From this output characteristic graph, it is found that radiation is basically concentrated in the broadside direction with $\theta = 0°$. Though high conductivity infinite ground is placed at the bottom of the antenna but still it is found that there is

considerable back radiation with front to back ratio of around -30 dB. It means power is mainly concentrated in the main lobe and low power is being wasted. Further the ♒ is found to be symmetric along the z-axis.

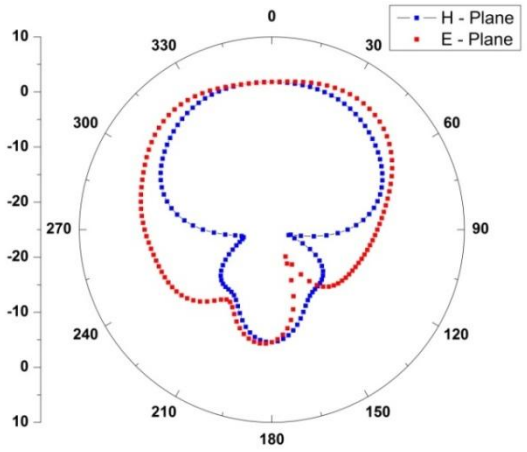

Fig. 4.18: Radiation pattern of the antenna in the E and H plane (10dB/div)

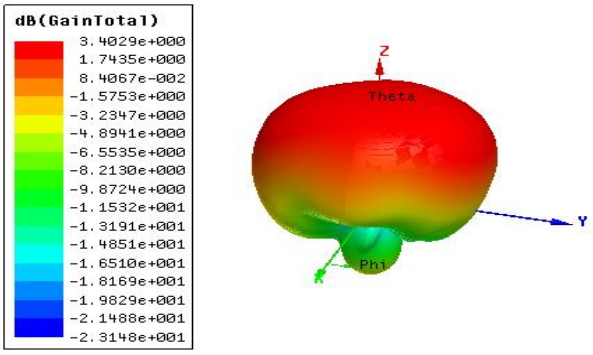

Fig. 4.19: 3 D radiation pattern of the proposed antenna

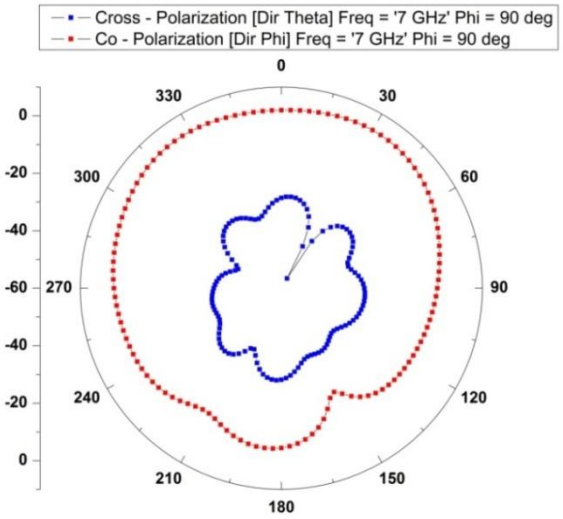

Fig. 4.20: Radiation pattern indicating E-plane co and cross polarization of the antenna (10 dB/div)

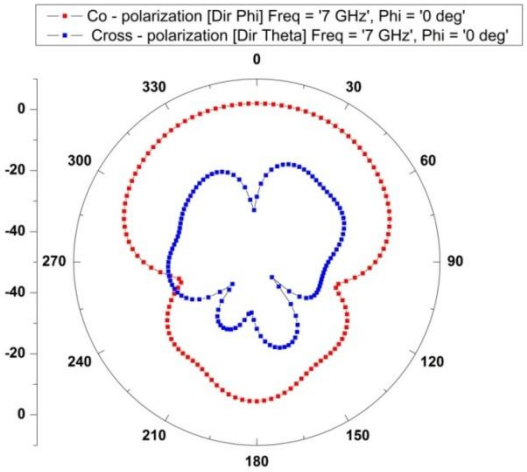

Fig. 4.21: Radiation pattern indicating H-plane co and cross polarization of the antenna (10 dB/div)

Fig 4.20 & 4.21 show the Co and Cross polarization in the electric and magnetic plane. This co and cross-polarization indicate the E and H field between transmitting and receiving platform. The cross-polarization is around 28 dB lesser than the co polarization for the electric plane and around 25 dB lesser for the magnetic plane. Commercial antenna technology demands a co and cross-polarization difference of around 20 dB for effective noiseless communication. This parameter plays a significant role in near field ultra-wideband communication where transmission range is relatively poor due to low transmitted power.

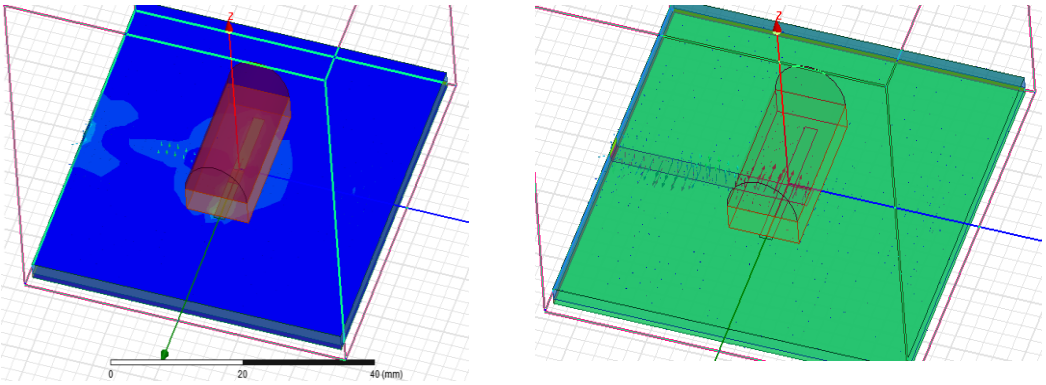

Fig. 4.22: The current density and electromagnetic field in the proposed radiator

4.3.4 Conclusion

Wireless near field ultra-wideband communication has been undergoing tremendous growth in recent time due to the expansion of technologies like Internet of Thing (IoT), Blue tooth, Wireless Local Loop (WLL), Wireless Fidelity (Wi-Fi), Local Multipoint Distributive System (LMDS), which mainly concentrate in the range of 3.1 GHz to 10.6 GHz and expanded up to X-band range. This multifunctional dual-band antenna resonates within 7.32 GHz to 9.12 GHz and 10.71 GHz to 12.9 GHz with -10 dB impedance fractional bandwidth of 21.92% and 19.09% respectively. The radiation efficiency is found to be 96% with high radiation stability. Though due to a double infinite ground plane this structure is somehow bulky its electrical characteristics are found to be very robust. This antenna is suitable for modern high-speed ultra wideband internet of things and enhanced mobile broadband applications.

4.4 DUAL BAND HYBRID RDRA

4.4.1. Introduction

A dual band hybrid rectangular dielectric resonator antenna is designed over a substrate made up of Roger Rd 3003, ε_r = 3.0, 99.7% of Alumina, ε_r = 9.8 is placed on a substrate of. It operates in two bands, which are from 3.1 GHz to 5.2 GHz in band-I and from 9 GHz to 10.8 GHz in band-II. S11 of the first and second bands are 50.6% and 18.18% respectively.

This work uses simplified DWM method to calculate the geometry of the RDRA. The model is initially realized by using 3D electromagnetic software HFSS. Optimization carried out to find a difference of 12% between the calculated and simulated geometry. A prototype is fabricated, followed by measurement and analysis of its performance. It has two resonating modes excited from a single feed and single RDRA. It provides higher degrees of freedom, flexibility in selecting two resonance modes.

4.4.2 Antenna Structure

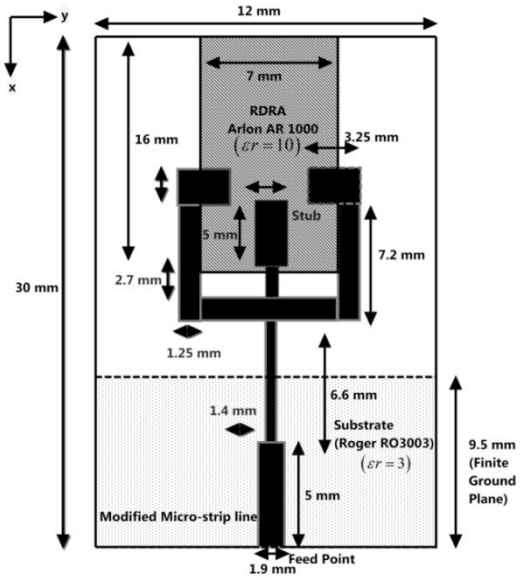

Fig.4.23: Top view of the proposed RDRA

The detailed geometry and photograph of the novel fabricated proto-type of dual-band RDRA are shown in Fig. 4.23 and 4.24. This antenna is configured on Roger Rd 3003 dielectric substrate with dielectric constant (ε_r) equal to 3, loss tangent ($\tan\delta$) of 0.003, and having a dimension of$12 \times 30 \times 0.75\ \text{mm}^3$. For the high-frequency design, a lower dielectric constant is preferred to avoid an extreme miniaturized shape which is difficult to fabricate and excite. It may significantly contribute to unwanted radiation to reduce the effective bandwidth of operation. The thinner height of the substrate is useful to reduce the substrate loss which is due to the

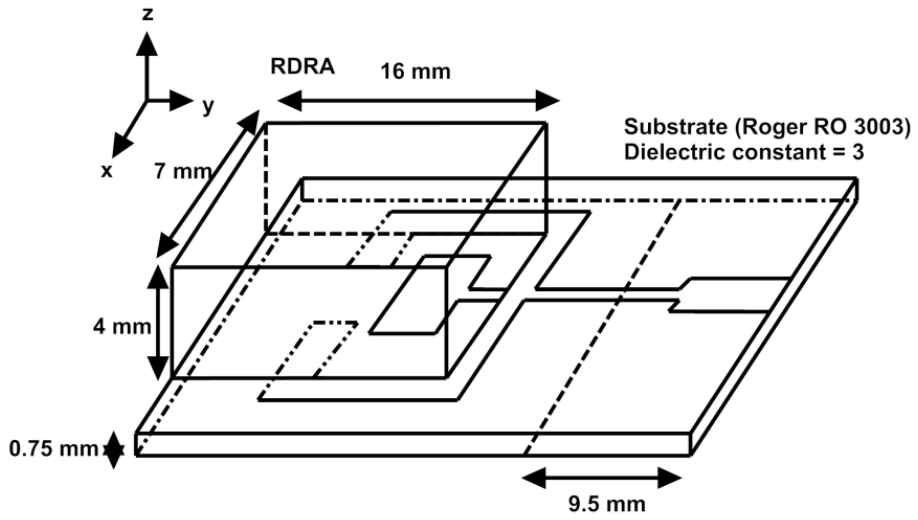

Fig.4.24: Side view of the proposed RDRA

formation of the high amplitude of the surface wave. It often degrades the radiation efficiency of the radiator. A finite ground plane of dimension 12×9.5 mm^2 is placed at the bottom of the antenna towards the excitation side of the feed line. Copper with finite conductivity of 5.8×10^7 Siemens/ meter is used. Transmission line 18.8 mm and different specified dimensions as shown in Fig 4.23 & 4.24. The microstrip transmission line is preferred due to ease of fabrication, ease of active integration, reduction in mode coupling, and low radiation and transmission loss. However, the microstrip transmission line suffers from high dispersion and excitation of the surface wave. The input impedance is found to be capacitive below the resonant frequency. The necessary impedance is provided by quarter guided wavelength. The split line adds the necessary inductance to compensate for the capacitive effect [32]. The different dimension of the split microstrip line network is used to achieve characteristics impedance of 50 Ohms for effective matching and to excite the dominant mode in the RDRA. Proper impedance matching provides a tradeoff between loaded resonance, forced resonance, and self-resonance. With appropriate matching and loading conditioning power loss due to the undesired mode can be reduced. 99.7% Alumina having dielectric constant (ε_r) of 9.8 with loss tangent ($\tan\delta$) of 0.0013 is used as the radiating rectangular dielectric resonator antenna. As shown in Fig. 4.23 the dimension of the miniaturized RDRA is $7 \times 16 \times 4\ mm^3$. It is calculated by using a dielectric waveguide model under unloaded conditions.

Optimization is being done under the loaded condition to achieve accurate the simulated and measured result. The antenna structure is simulated by using High-Frequency Structured Simulator (HFSS) under unloaded conditions. Here Silicon sealant, a non-permanent adhesive is used to bond the RDRA over the substrate. Through cleanliness, miniaturized air gaps can be reduced to have reasonable control and accuracy over the variation in the matching profile.

Table 4.4: Design Parameters of the RDRA

Element	**Material used**	**Relative Permittivity**	**Loss Tangent**	**Dimensions** (Tolerance: +/- 0.5 mm)
Rectangular DRA	99.7% Alumina	9.8	0.003	x =7mm, y = 16mm, z(height) = 4 mm,
Substrate	Roger RO 3003 (tm)	3	0.0013	x =12mm, y = 30mm, Z(height) = 0.75 mm

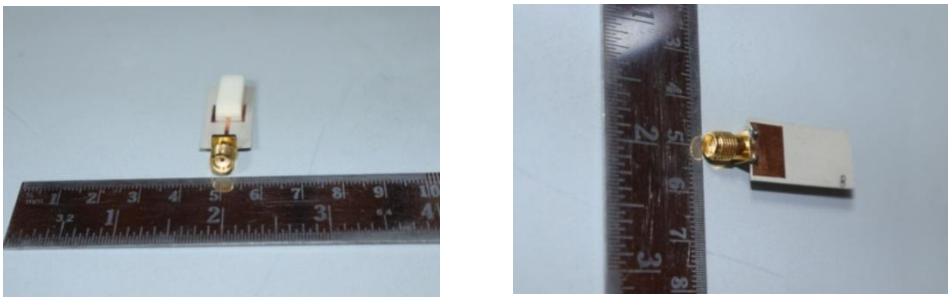

Fig.4.25: Top and bottom view of the fabricated RDRA

4.4.3 Experimental And Simulated Result Analysis

Low radiation resistance plus the presence of dominated capacitive reactance component of input impedance creates a complex feed problem. There are two ways to mitigate this problem [186, 187]. To alter the current distribution to uplift the effective height. As it is well known that if current can be made uniform then effective height will be equal to the actual height and radiation resistance will increase. It reduces the capacitive reactance components from the input impedance. Therefore much less inductance is required in series and high power can be supplied to the DRA from the source [188, 189]. As the antenna is resonating at 8.6 GHz frequency the input impedance is non-reactive and radiation resistance is quite

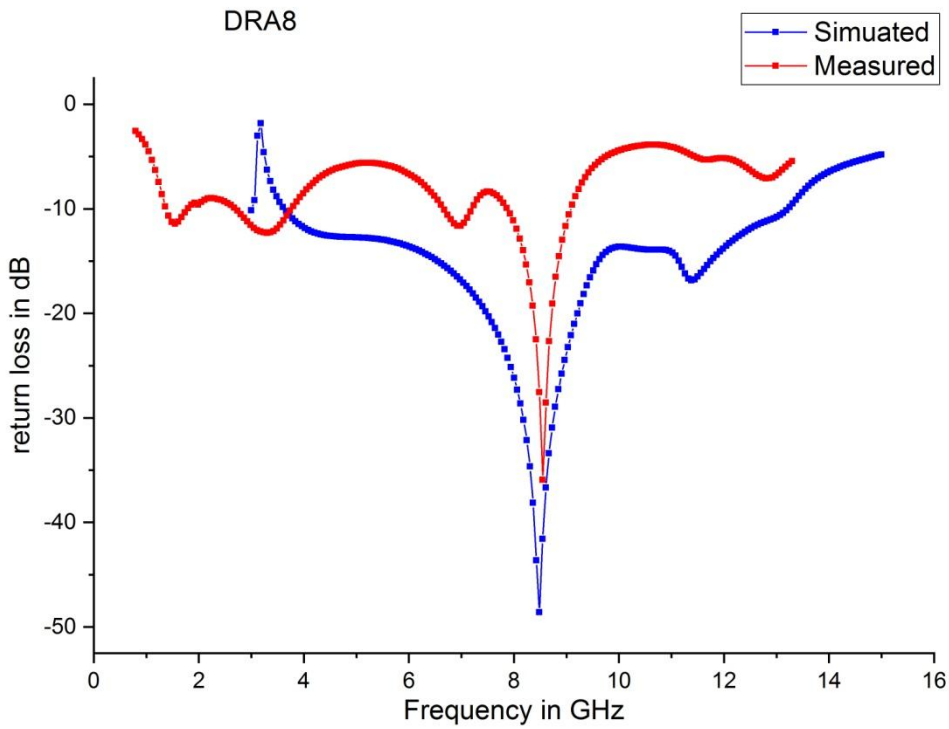

Fig. 4.26: Measured and Simulated return loss of the proposed RDRA

The antenna operates in two bands, that are from 3.1 GHz to 5.2 GHz in band-I and from 9 GHz to 10.8 GHz in band-II. In these bands VSWR is found to be less than 2. Fig. 4.27 describes the plot of real and imaginary input impedance Z(1,1) versus frequency. The studied impedance is purely experimental here. Input impedance versus frequency curve shows the variation of resistance and reactance with respect to the resonant frequency.

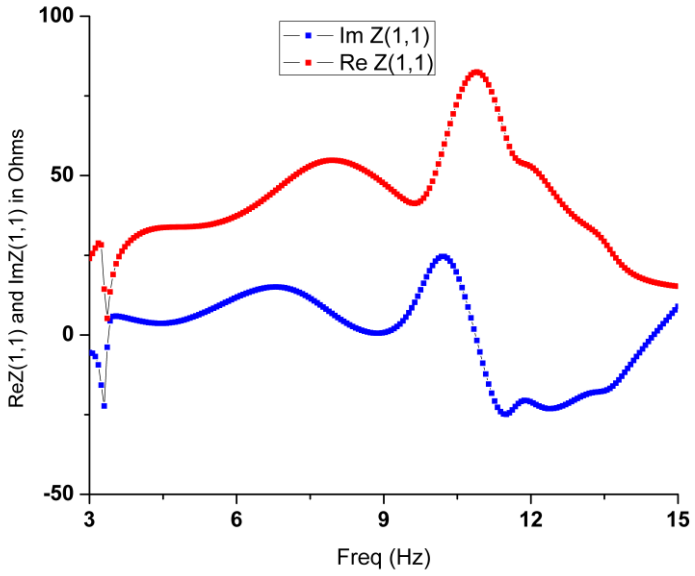

Fig. 4.27: Plot of real and imaginary input impedance Z(1,1) versus frequency

It results in excellent impedance match over the entire given tunable range. Split transmission line is acting as an open ended stub having much stronger effect on the RDRA resonance. The length of the stub at both the end is crucial to calculate the resonant frequency and bandwidth. $|S_{11}| < 10\ dB$ of the first and second band are 50.6% and 18.18% respectively. However, actual operational bandwidth will be influenced by the loading characteristics of the radiator. The simulated result shows two bands of operation, band I is from 2 GHz to 8.1 GHz and band II is from 9 GHz to 11.1 GHz. The non alignment results due to difference in material tolerances, the manufacturing precision and accuracy, the loading effect on the antenna due to indoor measurement conditions, the creations of miniaturized air gap, the effect of the SMA connector, the effect of Silicon sealant as non-permanent adhesive, and variation in accuracy of placing the RDRA over the substrate. Due to high sensitivity nature of the impedance matching the measurement set up should be very precise and accurate.

Output Characteristics: The electromagnetic field for each mode depends upon source orientation, location of the source, and the frequency of operation. These modes are responsible for the induction of E & H current distribution. The variation of field geometry affects the input impedance of the antenna. The far field components E_θ and $E_\emptyset$ can be determined from the current distribution on the external

surface of the dielectric antenna. To radiate appreciably high current density is mandatory. As shown in the Fig. 4.28 the designed antenna is radiating in the broadside direction. Being ground plane of relatively smaller size (<< ●) there is existence of high back radiation.

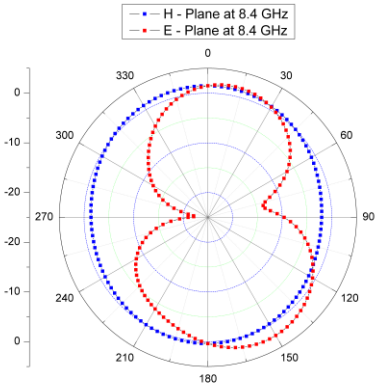

Fig. 4.28a: E & H plane at 8.4 GHz

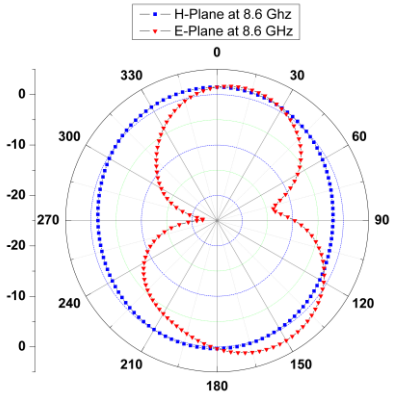

Fig. 4.28b: E & H plane at 8.6 GHz

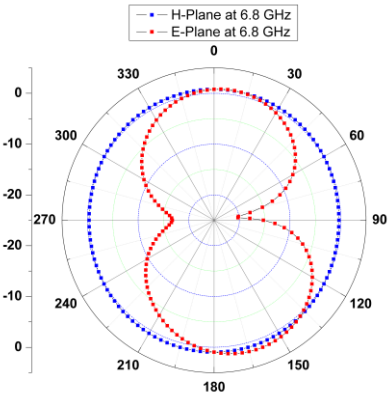

Fig. 4.28c: E & H plane at 6.8 GHz

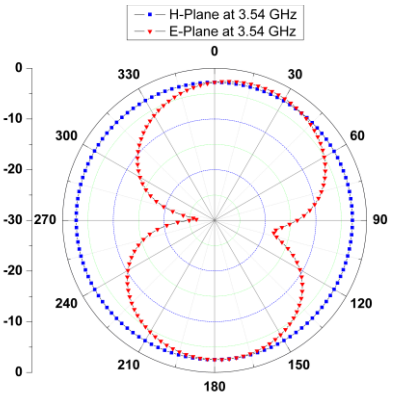

Fig. 4.28d: E & H plane at 3.54 GHz

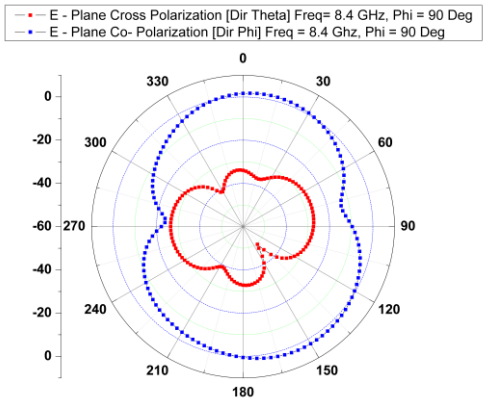

Fig. 4.28e: E plane Cross and Co Polarization at 8.4 GHz

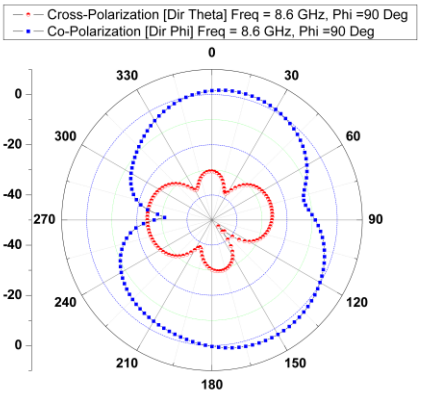

Fig. 4.28f: E plane Cross and Co Polarization at 8.6 GHz

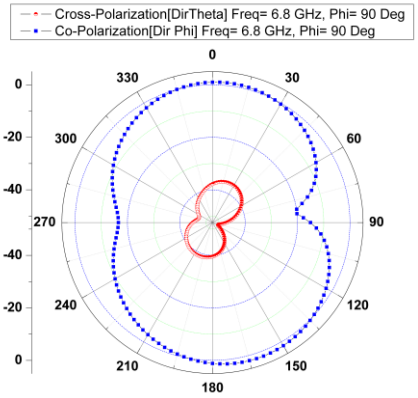

Fig. 4.28g: E plane Cross and Co Polarization at 6.8 GHz

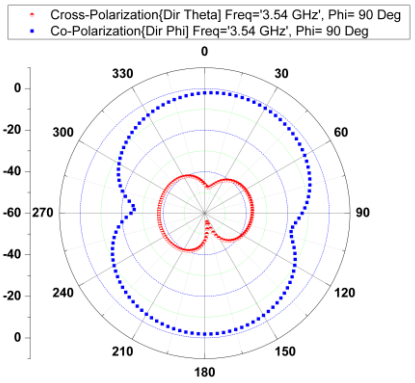

Fig. 4.28h: E plane Cross and Co Polarization at 3.54 GHz

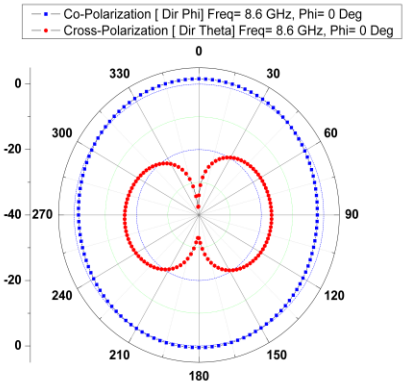

Fig. 4.28i: H plane Cross and Co Polarization at 8.6 GHz

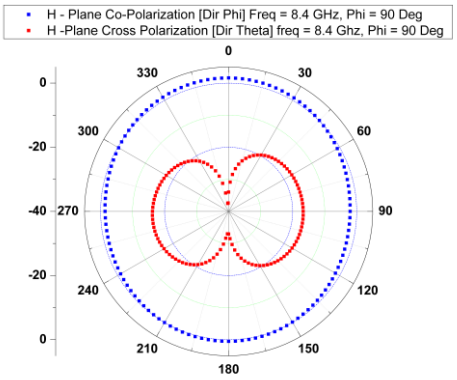

Fig. 4.28j: H plane Cross and Co Polarization at 8.4 GHz

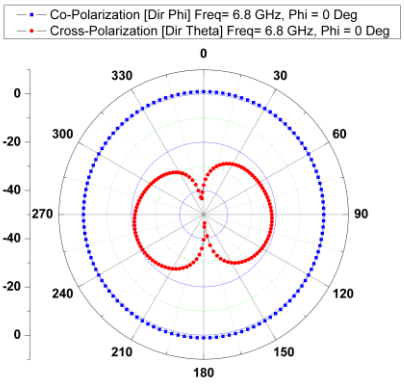

Fig. 4.28k: H plane Cross and Co Polarization at 6.8 GHz

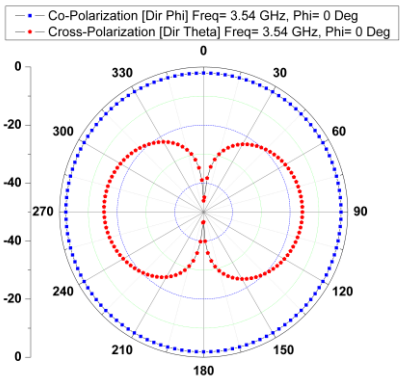

Fig. 4.28l: H plane Cross and Co Polarization at 8.4 GHz

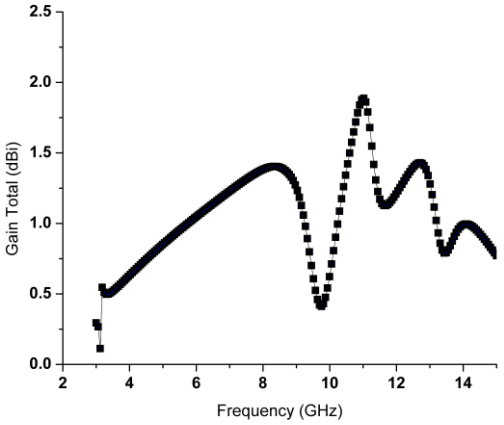

Fig. 4.29: Plot showing the relation between frequency of operation and total gain in dBi

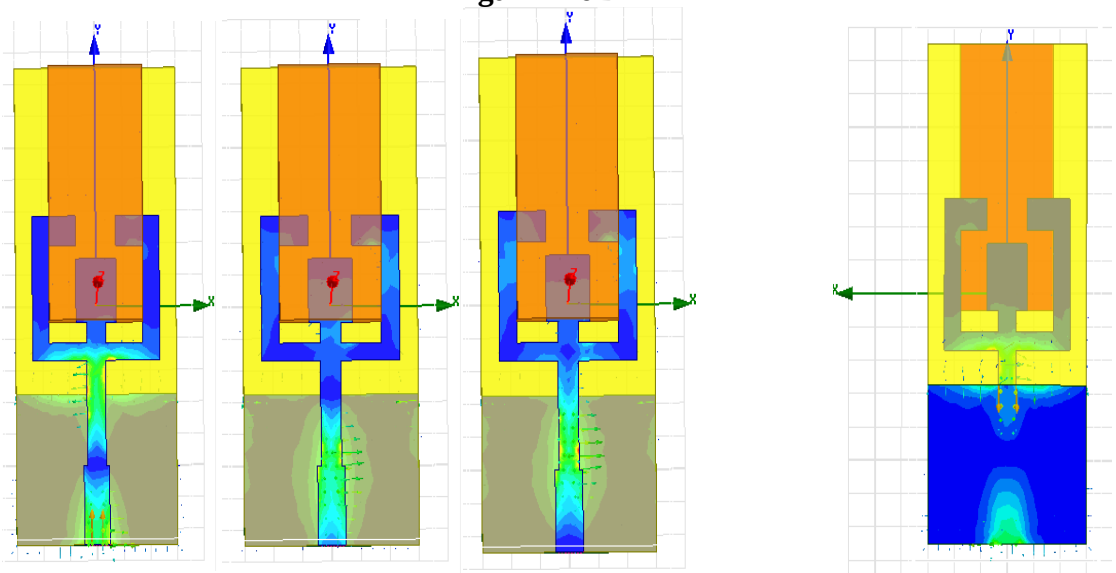

Fig.4.30: Simulated vector and scalar components of the current density in J/m^2

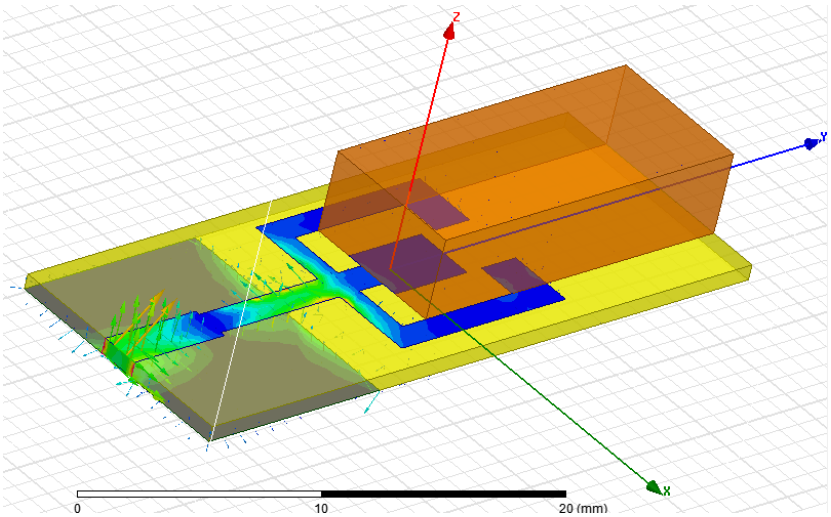

Fig.4.31: Simulated vector and scalar components of the J, E, and H

Fig.4.32: Measurement set up for the proposed RDRA

4.4.4 Conclusion

A novel hybrid RDRA is proposed. The return loss is matching at the resonant frequency of 4.2 and 9.8 GHz. The return loss impedance bandwidths are found to be 50.6 and 18.18%. There is a least variation between them and the result is found to be consistent. The antenna gain is 2 dBi at 9.8 GHz at the resonant frequency and gain is found to be maximum around the resonance. The antenna efficiency is found to be 98.56% with FBR of 2.48 dB. The beam pattern has 03 dimensional axial symmetry, along the horizontal axis. Here the ground plane size is trimmed to optimize the good beam shape and impedance matching in the given bandwidth.

CHAPTER 5
DESIGN AND ANALYSIS OF WIDE BAND DIELECTRIC RESONATOR ANTENNA

5.1 INTRODUCTION

There exist numerous design solutions and mode in a dielectric resonator antenna. These solutions are mainly controlled by the quality factor. If limits of Q-factor can be set then bandwidth can be controlled. A very low Q-factor can be realized by reducingε_r, dimension of the device. Practically bandwidth is limited by various losses, and overall structure of the feeding mechanisms.

There is no concrete definition of bandwidth, as operating criterion of an antenna involves varieties of variables. Therefore based on the input and output characteristics of an antenna, we have impedance bandwidth, pattern bandwidth, gain bandwidth, axial ratio bandwidth or polarization bandwidth.

Impedance bandwidth is usually expressed in terms of return loss and maximum voltage standing wave ratio.

$$BW = \frac{SWR-1}{Q\sqrt{SWR}} \tag{5.1}$$

The inherent limit in impedance bandwidth is '**Chu-Harrington criteria'**. Chu-Harrington theory produces a fundamental limit concerning minimum Q of an antenna of a given size. It states that the Q_{min} of an antenna with hundred percent reductions in efficiency that can be enclosed within a spherical surface of 'R' is given by:

$$Q = \frac{1+3(k_0R)^2}{(k_0R)^3[1+(k_0R)^2]} \tag{5.2}$$

It is important to consider the volume of the enclosing sphere. So impedance bandwidth can be improved through high profile design [190-192]. Pattern bandwidth is the range of frequency over which output characteristics like beam width, side lobe levels and gain of an antenna provides a specified output. It is desirable to have fixed level of polarization at the operating frequency. When maximum cross polarization or axial ratio level is used to find the operating zone of the antenna then that range of frequency is called polarization or axial ratio bandwidth.

Multi-resonant frequency can be merged to realize the broadband nature of the RDRA. Band width can be enhanced by lowering of the Q-factor by appropriate

impedance matching and combining multiple resonators. Difference structures can excite different modes and by the amalgamation of all these modes broadband can be obtained. Permittivity can be altered from 6 to 100 to realize broad band response .Broadband can be achieved by altering the feeding techniques and matching profile. Two or more modes need to be excited in order to have broadband response. It can be achieved by creating irregularities, truncation, and splitting in the structure. Therefore there will be rapid altercation of time harmonic displacement current. Two or more dielectric of same and different permittivity and shape can create broadband response. DRA array configurations with appropriate switching can also generate broadband response. By using sub and super structure based frequency selective surface, broadband response can be initiated. DRA will be arranged appropriately to create loading effect of one w.r.t others to have broadband response. Hybrid design can result in broadband response where there is a combination between DRA and patch. Dimension and dielectric permittivity control the bandwidth. By the optimization of ground plane bandwidth can be improved. Here dielectric wave guide model will be replaced by ADI-FDTD method. Integrated wideband structure can improve the bandwidth.

5.2 DESIGN OF MICRO-STRIP FED APERTURE COUPLED BROADSIDE CYLINDRICAL DIELECTRIC RESONATOR ANTENNA ARRAY

5.2.1 Introduction

Dielectric resonator antenna with single element offered low gain with broad radiation patterns. It can be arrayed to upgrade into a high-gain device with a shaped radiation pattern [193-195]. The output characteristics are required to be controlled and shaped for modern applications like direction-finding, beam shaping, beamforming, creation, and the avoidance of jamming, acquisition, and tracking of the signal, etc. It has been observed that independent control of the beam pattern with desired stability cannot be achieved by controlling the terminal impedance alone. Therefore, the radiation patterns can be most efficiently controlled and high design flexibilities can be obtained by the design of the antenna array. However, the design of the DRA array at high frequency is complicated and challenging.

This works presents a systematic design of a micro-strip fed aperture coupled broadside CDRA array. The magnitude of reflection coefficient, output radiation patterns, and efficiency are calculated for the single, double, three, and nine elements array architecture, and the results are compared. The single element architecture shows a peak gain of 4.56 dB and directivity of 4.52 dB at 8GHz, whereas the nine elements architecture shows a peak gain and directivity of 11.62 dB and 13.67 dB respectively at 8 GHz. For the nine elements array, the first resonant dip occurs at 9.52 GHz, and the second return loss dip occurs at 11.3 GHz. The -10 dB impedance BW for the first band is 5.95% and the second band is 1.41%. Micro-strip split feed network with three apertures is used to achieve maximum coupling coefficient. The proposed radiator is suitable for high resolution, high sensitivity security surveillance sensors in the receiver antenna array, and maximum power output to cover long-range for wireless transmission in the transmitter antenna array applications.

5.2.2 Principle Of Operation

From the fundamental Fourier relationship, it has been observed that there lies a strong relationship between current distribution on the radiator and the output radiation patterns. It means if the current distribution is given there is an existence of a unique radiation pattern and if the radiation pattern is given there is a unique current distribution. When the radiator is excited the overall distributed current on the DRA is the weighted sum of Eigen currents which is obtained from various modes at a particular instant of time. Therefore, to customize the radiation patterns it is essential to have control over the spatial distribution of the magnitude and phase of the antenna current. Amplitude can be adjusted to reduce the side lobes whereas phase can be adjusted to steer the beam patterns. It is essential to improve mutual coupling and to decrease the decoupling of the radiated energy from the input impedance [196-199].

The cylindrical dielectric resonator antenna array is the collection of basic cylindrical DR radiating elements. It is required to place these radiating elements at a specified distance and excite from a common microstrip feed network to achieve the desired shaped superposition of the field. It is required to decouple the terminal characteristics impedance and radiation pattern. When multiple antennas are brought together there will be a strong variation of the input impedance. According to the theory of reflection total reflections are the sum of the first-order reflection. Therefore, there is

reduction in the total reflection coefficient and enhancement in the impedance bandwidth while maintaining the spacing between the DRA near to $\lambda_g/4$ at the center frequency of operation.

For the ultra-high frequency design like X-band applications, the spacing between the DR elements are required to be reduced to mitigate the grating lobe. However close spacing will induce strong mutual coupling which affects the impedance bandwidth and overall performance of the radiator. Major advantage in the dielectric configuration based array is that it does not support surface wave which creates grating lobes.

When antenna elements are arranged uniformly with progressive phases and excited accordingly then pattern multiplication takes place. In this design, arrays are arranged in an irregular rectangular lattice configuration. The array factor will be:

$$AF = \frac{A_0 \sin\left(\frac{N\Psi_x}{2}\right)\sin\left(\frac{M\Psi_y}{2}\right)}{\sin\left(\frac{N\Psi_x}{2}\right)\sin\left(\frac{N\Psi_y}{2}\right)} \quad (5.3)$$

Where, $\Psi_x = k_0 dx \sin\theta + \beta_x$, $\Psi_y = k_0 dy \sin\theta + \beta_y$

This equation can be survived when there are infinite no. of elements in the array and the performance of each element is not a function of spatial co-ordinate, which is practically difficult. Cylindrical DRA is considered here, as it provides high design flexibilities to that of hemispherical DRA and availability of dielectric in the cylindrical shape. The cylindrical shape of the unit cell is characterized by radius 'a' and height 'h'. The aspect ratio decides the (k0a) and the radiation Q-factor for a particular dielectric constant. Where ko is the complex wavenumber. The characterization of CDRA depends upon the initiation of the traveling and evanescent modes. In traveling mode, propagation coefficient is real whereas, in the evanescent mode it is imaginary. The overall characteristics of CDRA is a function of an exciting mode, the amount of energy that can be coupled, and frequency response of the impedance.

The lowest order or fundamental mode for radiations in CDRA is the $HE_{11\delta}$ modes. Here the subscript shows field variation along azimuth ($\nearrow$), radius (r), and axis (z) directions, respectively. The field component δ is very small and its values lie between 0 and 1 and $\delta \rightarrow 1$ for the high dielectric constant material and δ is the fractional half cycle field variation along the corresponding direction.

$$\delta = \frac{k_{direction}}{\pi/d} \tag{5.4}$$

The fundamental mode is the $HE_{11\delta}$ mode and it can be modelled as magnetic dipole. The design procedure of cylindrical DRA in $HE_{11\delta}$ mode are as follows:

Step I: Determination of the Q-factor:

$$BW = \frac{\Delta f}{f_0} = \frac{s-1}{\sqrt{S}\,Q} \tag{5.5}$$

As impedance bandwidth (BW) and resonant frequency f0 is given, Δf and radiation Q-factor can be found. 'S' is the desired VSWR which is 2.

$$Q = \frac{s-1}{\sqrt{S}} \tag{5.6}$$

Step II: Determination of ε_r

To determine the dielectric constant, it is required to put the value of the Q-factor in the Q-factor graph and draw a horizontal line. The dielectric constant to be selected depends upon other factors like material availability, size required, etc.

Step III: Determination of k_0a:

$$k_0a = \frac{f_{GHz} \cdot h_{cm} \cdot (a/h)}{4.7713} \tag{5.7}$$

Step IV: Determination of the radius:

The above equation can be plotted on the k_0a vs. (a/h) for various value of h. The major advantages of this type of structure is design flexibilities due to higher degree of freedom. Input impedance can be determined by finite element method. The length of the slot (ls) is:

$$l_s = 0.4\lambda_0/\sqrt{\varepsilon_e}\,, \varepsilon_e = (\varepsilon_r + \varepsilon_s)/2 \tag{5.8}$$

The width (ws) = 0.2 ls. 'S' to be chosen initially as $\lambda_g/4$ and later it will be adjusted to enhance the matching profile by canceling the reactive components jX. The dimension of the slot controls the loading characteristics and radiation quality factor (Q) of the array architecture. It should be very small to avoid back radiation and unnecessary spillage of energy. However, smaller dimensions of the slot may impose certain fabrication tolerance.

5.2.3 Structure Of The Antenna

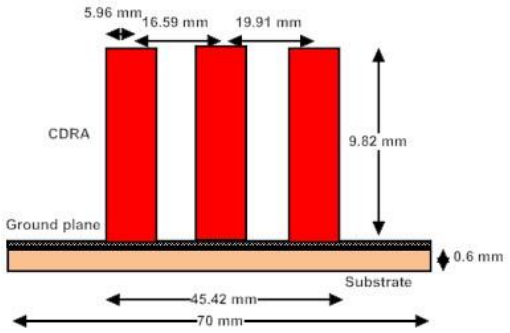

Fig. 5.1: Side view of the proposed antenna.

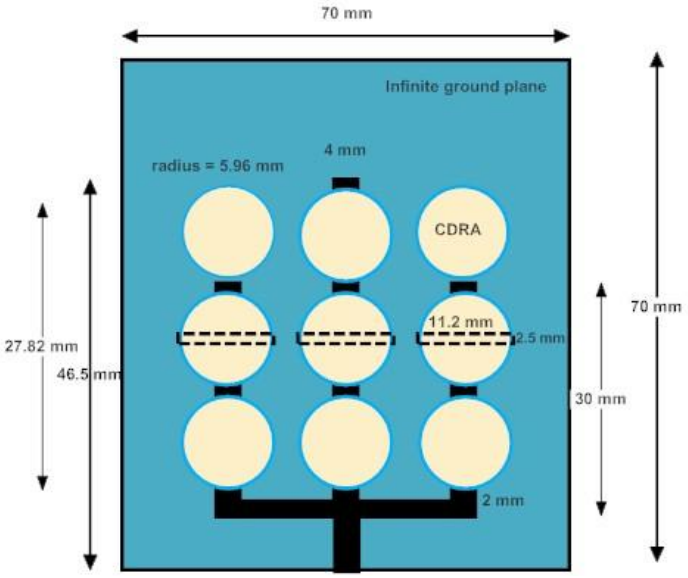

Fig. 5.2: Top 2-D view of the proposed antenna.

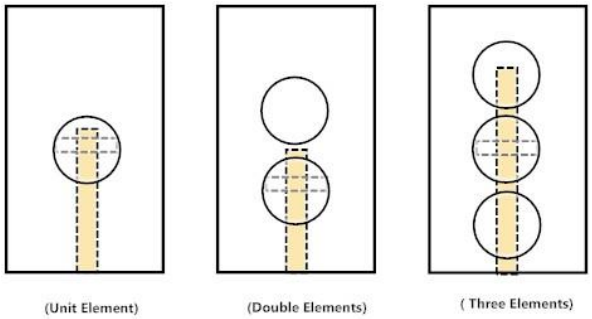

Fig. 5.3: Top 2-D view of the unit, double, and three elements antenna.

Table 5.1: Materials used in the CDRA arrays

Element	Material used	Relative Permittivity	Loss Tangent

Cylindrical DRA	Rogers RT/duroid6010/6010LM (tm)	10.2	0.0023
Substrate	Arlon 25 (tm)	3.38	0.0025

Fig. 5.3 shows the top view of the one, two, and three elements CDRA. These antennas are placed over an infinite ground plane (Perfect Electrical Conductor) XY. The ground plane is drawn over a substrate (Roger RT/duroid 6010/6010 LM (tm), ε_r = 10.2, $\tan\delta$ = 0.0023) of dimension 70×70×1.6 mm^3. Three apertures, each having a dimension of 11.2×2.5 mm^2 are etched on the ground plane for critical electromagnetic coupling of the energy from the source to the radiator. A combination of series and corporate micro-strip line feeding network controls the amplitude and phase excitation by initiating passive phase delay in the feed network. Over the transmission line, nine CDRA elements (radius = 5.96 mm, height = 9.82 mm) are positioned at a distance of $\lambda_g/4$. In the simulation process, the antenna is excited by a delta type source with 50 Ω internal resistance. This architecture supports a short magnetic dipole model. The side by side positioned CDRAs to have E-plane coupling whereas front to back positioned has H-plane coupling.

Table 5.2: Design parameters of the nine elements CDRA array

Structural and input Parameters	Value
Resonant Frequencies	9.52 GHz, 11.3 GHz
Substrate dimensions	70×70×1.6 mm3
No. of radiating elements in CDRA array	9 in a 3×3 Matrix Array Format
Total length of the array	27.82 mm
Total width of the array	45.42 mm
Characteristics impedance of the connecting line	50 Ω
Height of the unit element	9.82 mm
Radius of the unit element	5.96 mm

Horizontal and vertical distance between CDRA unit cells	
Between unit cell CDRA A to B	16.6 mm
Between unit cell CDRA B to C	16.91 mm
Between unit cell CDRA D to G	13.27 mm

5.2.4 Results And Discussion

Fig. 5.4 a,b,c,d illustrates the return loss characteristics of the four designs with one, two, three, and nine CDRA elements. As shown in figure 5.4a, the one element CDRA is resonating at 9.34 GHz having an impedance bandwidth of 7.5% operating from 8.98 GHz to 9.68 GHz for |S11|< -10 dB. As shown in Fig. 5.4b, the two elements CDRA is resonating at 8.12 GHz and 9.66 GHz having an impedance bandwidth of 0.83% and 3.20% from 8.06-8.12 GHz and 9.5-9.81 GHz.

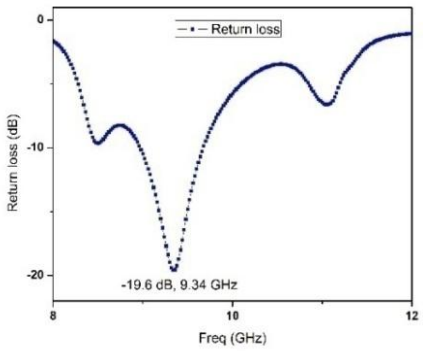

Fig. 5.4a: |S11| Vs Freq (GHz) in single element

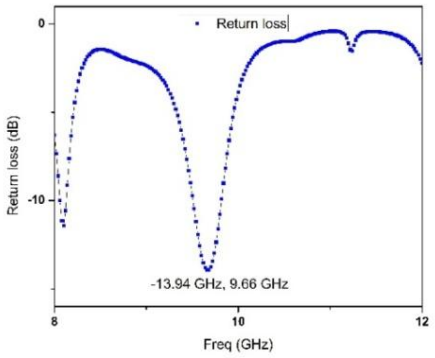

Fig. 5.4b: |S11| Vs Freq (GHz) in double elements

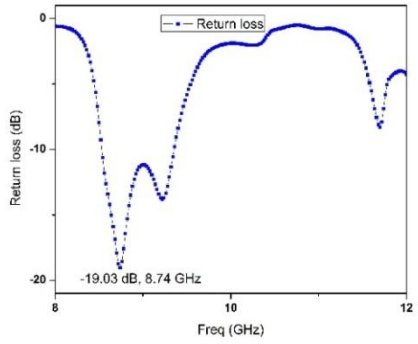

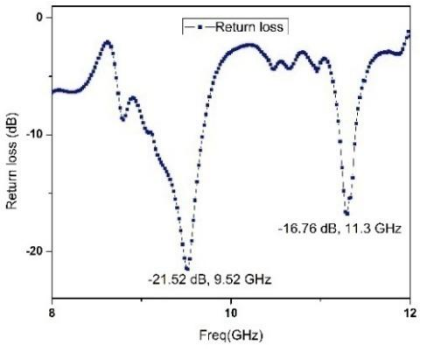

Fig. 5.4c: |S11| Vs Freq (GHz) in three elements

Fig. 5.4d: |S11| Vs Freq (GHz) in nine elements

As shown in Fig. 5.4c, the three elements CDRA is resonating at 8.74 GHz having an impedance bandwidth of 9.17% while operating from 8.53 - 9.35 GHz. As shown in Fig. 5.4d, the nine elements CDRA is resonating at 9.52 GHz and 11.3 GHz while operating from 9.12 - 9.68 GHz and 11.22 - 11.38 GHz respectively. Here proximity direct coupling through the microstrip transmission line is used to couple energy in $TE_{y\delta 11}$ mode from the source to the CDRA. The stub is used for the mitigation of the reactive components and slight altercation of the frequency response for fine-tuning of the antenna.

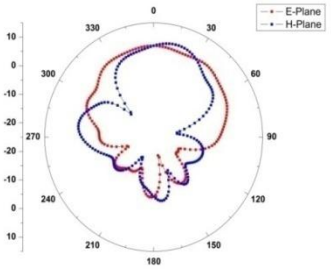

Fig. 5.5a (n = 1) E-H Plane

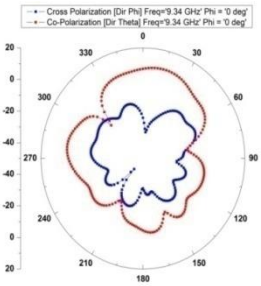

Fig. 5.5b (n = 1): E-Plane Co & Cross Polarization

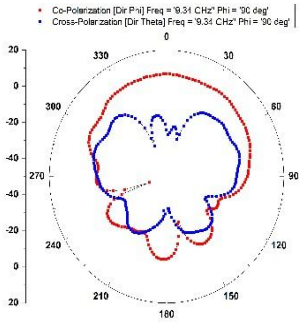

Fig. 5c (n = 1): H-Plane Co & Cross Polarization

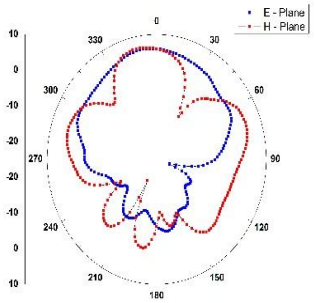

Fig. 5d (n = 2): E-H Plane

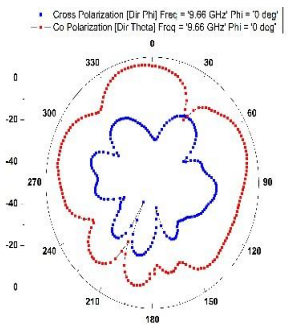

Fig. 5e (n = 2): E-Plane Co & Cross Polarization

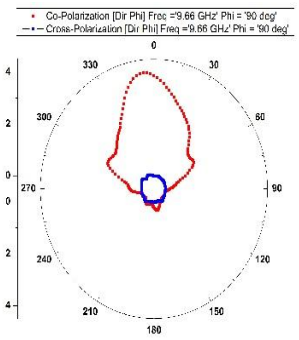

Fig. 5f (n = 2): H-Plane Co & Cross Polarization

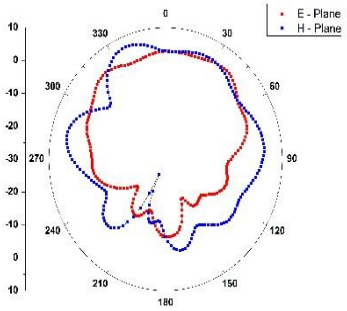

Fig. 5g (n = 3): E-H Plane

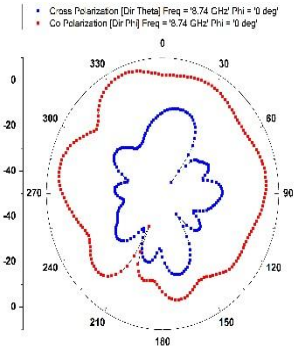

Fig. 5h (n = 3): E-Plane Co & Cross Polarization

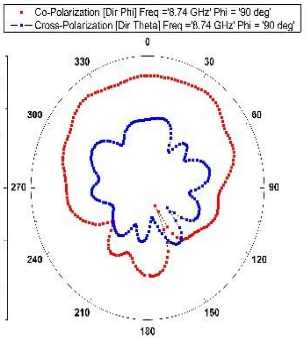

Fig. 5i (n = 3): H-Plane Co & Cross Polarization

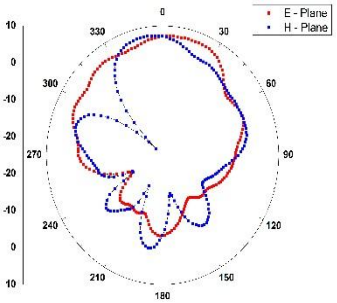

Fig. 5j (n = 9): E-H Plane

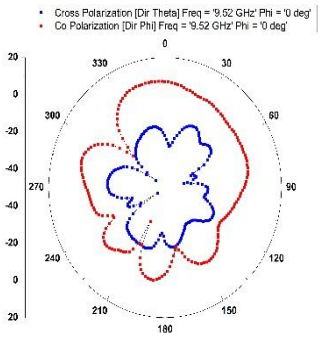

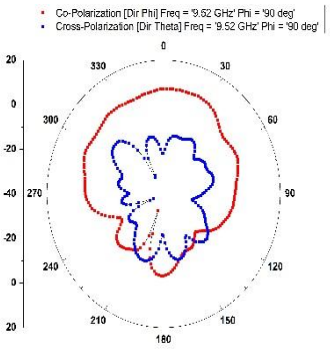

Fig. 5k (n = 9): E-Plane Co & Cross Polarization

Fig. 5l (n = 9): H-Plane Co & Cross Polarization

The radiation characteristics of the antennas are investigated from 8 GHz to 12 GHz. The radiation patterns based on E and H-planes, E and H planes Co and Cross polarization for the single element (n = 1) at 9.34 GHz, double elements (n = 2) at 9.66 GHz, three elements (n = 3) at 8.74 GHz, and nine elements (n = 9) at 9.52 GHz CDRA arrays on an infinite ground plane are shown in Figs 5.5a to 5.6l. H – the plane is considered at ↗ = 0° and E – the plane is considered at ↗ = 90°. H – Plane (x – z plane) and an expanded figure of eight patterns (y-z plane). It implies the inherent characteristics of a conventional monopole antenna shown by the CDRA array. However, H- plane pattern shows beam squint due to the array configuration, mutual coupling, and design of the feeding structure. Sidelobe level is due to discontinuities in the current distribution. The amplitude of the side lobe implies leakage of energy in the undesired direction. Therefore, maximum efficiency can be achieved by reducing the sidelobe level. If we could avoid the sharpness of the current distribution, then the sidelobe level can be reduced. The radiation efficiency for the structure where the number of elements n=1, 2, 3 and 9 is 100.86%, 107.8%, 76%, and 85%. It is observed that E and H plane co and cross-polarization are more than -20 dB except for E plane co and cross-polarization for n = 3 as shown in Fig. 5.5h. This implies co-polarized E and H field between transmitter and receiver is around 100 times more than that of the cross-polarized E and H field. ❑ = 0° to 360° and ↗ = 0° for n= 1, 2, 3, 9 elements architecture at their corresponding resonating frequency. It is observed that there is maximum radiation in the broadside direction at ❑ = 0° and ↗ = 0°. Fig. 5.7 shows the plot of gain versus frequency from 8 to 12 GHz at ❑ = 0° and ↗ = 0°. A comparative analysis of various parameters for single, double, three, and nine elements are depicted in Table 3. Fig. 5.8 shows the distribution of surface current density in Amp/m2 across the nine elements radiating structure which plays a pivotal role in exciting the hybrid mode $HE_{11\delta}$ within the CDRA [200].

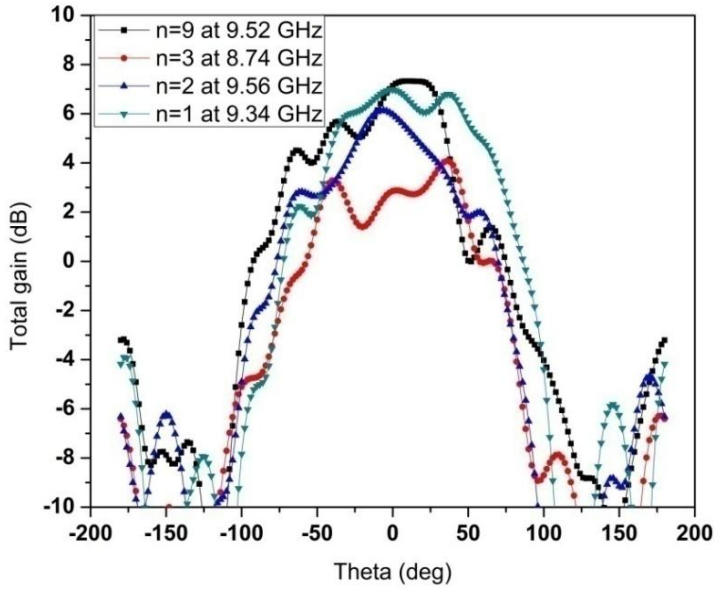

Fig. 5.6: Rectangular plot of total gain versus (dB) Theta (deg) for ❑ = 0°

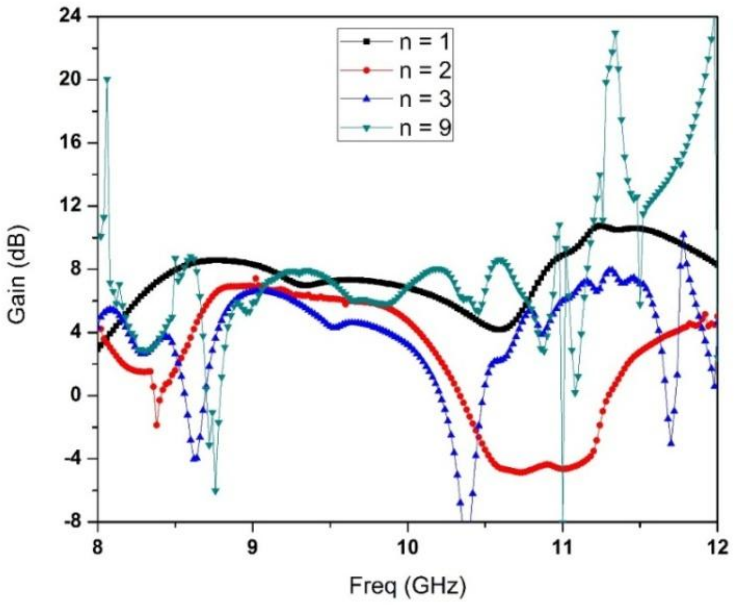

Fig. 5.7: Rectangular plot of Gain versus Frequency at their resonant frequency

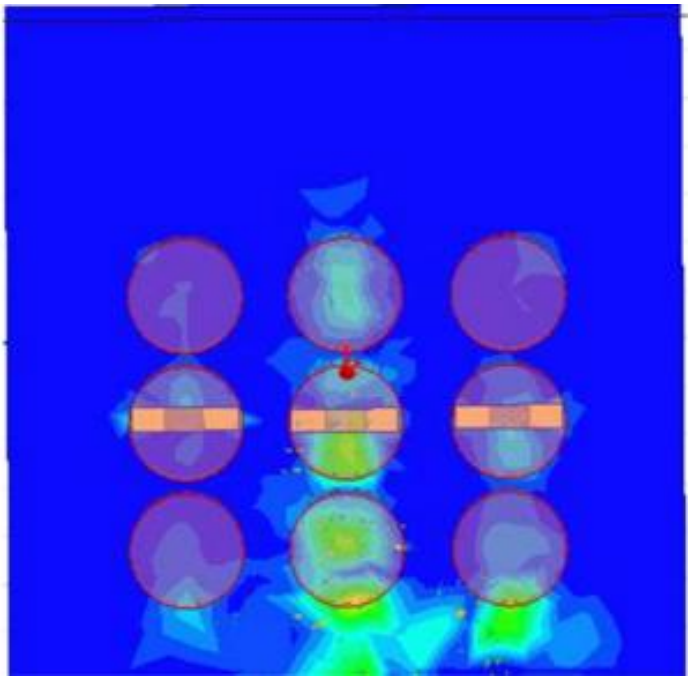

Fig.5.8: Current density in Amp/m^2 in the nine elements array architecture

Table 5.3: A comparative analysis of parameters of all the geometries at 8 GHz

Radiator	**Resonating Frequency (GHz)**	**Impedance Band Width (%)**	**Peak Gain (dB)**	**Peak Directivity**	**Radiation Efficiency (%)**	**Front to Back Ratio (FBR) (dB)**
Single element	9.34	7.5	4.56	4.52	100.86	10.77
Double element	8.12, 9.66	0.8, 3.2	4.67	4.33	107.8	18.62
Three element	8.74	9.17	5.08	6.68	76	13.88
Nine	9.52, 11.3	5.95	11.62	13.67	85	13.01

element						

5.2.5 Conclusion

Above work presents- one, two, three, and nine elements cylindrical dielectric resonator antenna arrays are designed and discussed. At high frequency due to the formation of surface wave and skin effect, losses in the micro-strip line increases rapidly. These architectures are found to be suitable for high resolution, high sensitivity security surveillance sensors as the receiver antenna array, and maximum power output to cover long-range as the transmitter antenna array. The DRA array technology is still in its nascent stage, especially for high-frequency design. The major challenges are due to the effect of surface wave, mutual coupling, and positioning error the array for various operating frequencies. Further improvement can be made by replacing the microstrip line with a dielectric waveguide or image guide and efficient adjustment of the mutual coupling.

5.3 DESIGN OF MULTIFUNCTIONAL INTEGRATED HYBRID RDRA FOR HIGH-SPEED COMMUNICATION

5.3.1 Introduction

Design techniques and problem-solving approaches in microwave and millimeter-wave are distinct from that of long-wave antennas. This article provides a systematic approach to design multifunctional and multi-band based integrated hybrid RDRA. The impedance bandwidth of 22% while operating from 4.63 GHz to 10.84 GHz. It provides ultra-high reliability, low latency, and tenability suitable for modern cellular tunable Internet of Thing based global tracking system and high-speed communication.

The proposed antenna offers maximum impedance bandwidth of 22% while operating from 4.63 GHz to 10.84 GHz. Surface current concentration can be enhanced through inclusions and make it viable for the creation of different mode patterns. Through proper matching, mode degeneracy can be avoided, and there will be no major shift in the output characteristics [201].

5.3.2 Principle of Operation

For the high profile, electrically large antenna current distribution gets severely attenuated as fields are radiated. The fundamental principle to achieve multi-band design is to activate different zones to generate different field patterns under a range of frequency of operation. But all the frequency should be transmitted at the same time. Therefore, the condition of lag and ringing are not acceptable.

The major factors which contribute to the characterization of bandwidth are (i) Impedance bandwidth (ii) radiation efficiency (iii) power gain (iv) beamwidth (v) beam directions (iv) polarization and (v) sidelobe level. The impedance bandwidth determines input impedance, radiation resistance, and antenna efficiency, whereas pattern bandwidth determines gain, sidelobe level, beam direction, and polarization. With suitable structural modifications, the narrowband nature of the linear resonant monopole antenna can be up-converted into a multi-band antenna. The lower operating limit can be decided by defining the longest electrical path of the current, and the upper limit can be decided by the aspect ratio and the architecture of the ground plane. It requires an experiment with different Euclidean shapes such as triangular, square, bow-tie, trapezoidal, circular, and elliptical. Out of these shapes, circular and elliptical provide the highest bandwidth. However, there is always a tradeoff between radiation stability and impedance bandwidth. The current distribution can be altered by adopting the following methods [201-205]:

i. Use of parasitic element: Parasitic elements are those which are not connected directly to the source. These passive elements add the effect of mutual coupling to accomplish partial overlapping between nearby bands. The monopoles placed close to each other should have a different shape to avoid filtration out of the frequency.
ii. Use of short pin: The short circuit pin is to be used in the zone of high current density. It causes the creation of additional modes to enhance the impedance bandwidth.
iii. Asymmetric feed: Through asymmetric feed, the current symmetry within the antenna is lost. It greatly affects the output radiation pattern but bandwidth in the upper limit increases.

iv. Double feed: The two feed points are symmetrically placed w.r.t the center of the antenna. It reduces the horizontal current and there is a reduction in cross-polarization.

v. Broadband matching techniques: The term broadband matching deals with real loads and not for matching arbitrary impedance that varies with frequency. The broadband matching technique comes under the scope of the transmission line model. Effective elimination of reactive components can be achieved by analyzing the current amplitude w.r.t horizontal and vertical components for a particular frequency. It is essential to ensure even distribution of the current. Therefore, the horizontal current contributes less to the overall radiation pattern.

vi. Setting up the lower limit of the frequency band is important. The lower limit can be reduced by enhancing the current path along the perimeter. To achieve high bandwidth graded change is preferable than that of abrupt cut.

5.3.3 Structure Of The Proposed Antenna

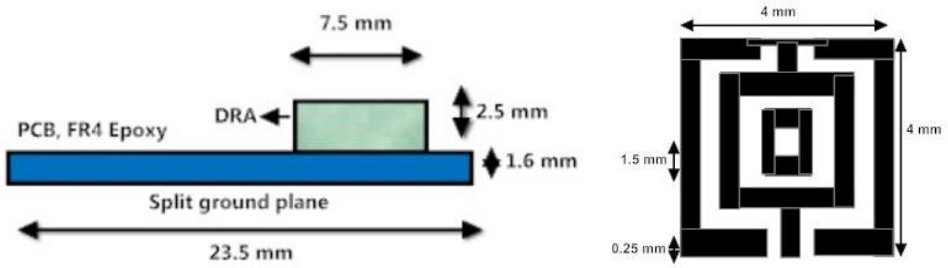

Fig. 5.9: Side view of the proposed antenna and structure of one of its inclusion

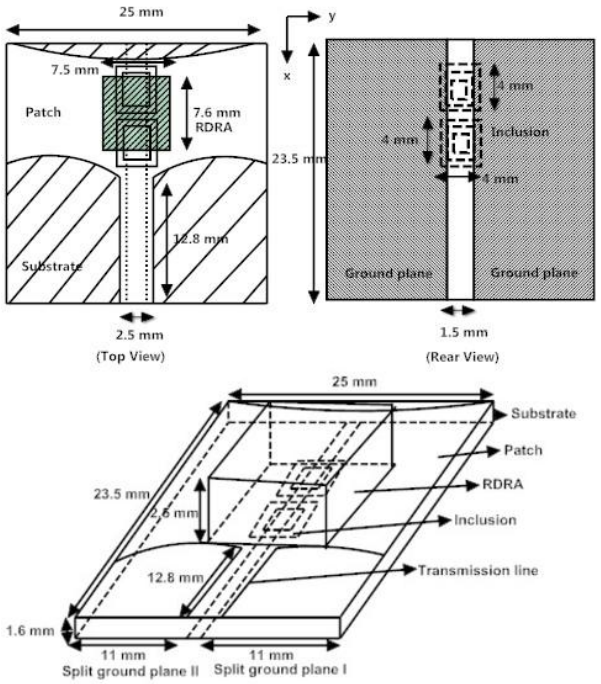

Fig. 5.10: Top view, bottom view, and structure of the total hybrid DRA

Figures 5.9 and 5.10 show the side, top, and rear view of Multifunctional hybrid rectangular dielectric resonator antenna with two inclusions. As shown in Fig. 5.10, two inclusions of external dimensions 4×4 mm^2 each are cut onto the upper portion of the radiator at the upper half of the centerline of the substrate. These inclusions are responsible for reducing the effect of the ground plane on the output characteristics of the radiator. The resonant frequency of the inclusions can be approximated by:

$$\omega_0 = \frac{1}{\sqrt{LC}} \tag{5.9}$$

$$\omega_0 = \frac{\omega}{\sqrt{\tan(\beta l \ short \ ended)\tan(\beta l \ open \ ended)}} \tag{5.10}$$

$$\beta = \frac{\omega}{c}\sqrt{\varepsilon_{eff}} \tag{5.11}$$

If open ended= short ended= 1, then

$$\frac{f_0}{f} = \frac{1}{\tan\left(\frac{\omega}{c}\sqrt{\varepsilon_{eff}}\, l\right)} = \frac{1}{tan\left(\frac{2\pi}{\lambda_g}\right)l} \tag{5.12}$$

The length of the inner stub will be

$$l = \frac{\lambda_g}{8} \tag{5.13}$$

A rectangular DRA (Zirconia, ECCOSTOCK, Emerson & Cuming Microwave Products N.V., ε_r = 4.4, $\tan\delta$ = 0.02) of dimension (d = 7.6 mm, w= 7.5 mm, and

width 2.5 mm) is connected from the source. Two finite ground planes (split ground plane I and split ground plane II) each having a dimension of 23.5×11 mm^2 is etched at the bottom side of the substrate. As shown in the figure, a patch with a top curve shape is placed over the substrate. The introduction of an etched strip on the ground plane improves the matching profile and provides isolation at the lower operating frequency. The bandwidth enhancement of the patch and its impedance tuning can be achieved by loading the antenna on the surface of the patch by a dielectric resonator. The dielectric resonator is pasted by using a thin layer of conducting epoxy. In Fig. 5.14 DR is placed in the middle of the non-radiating edge experimentally to improve the overall matching profile.

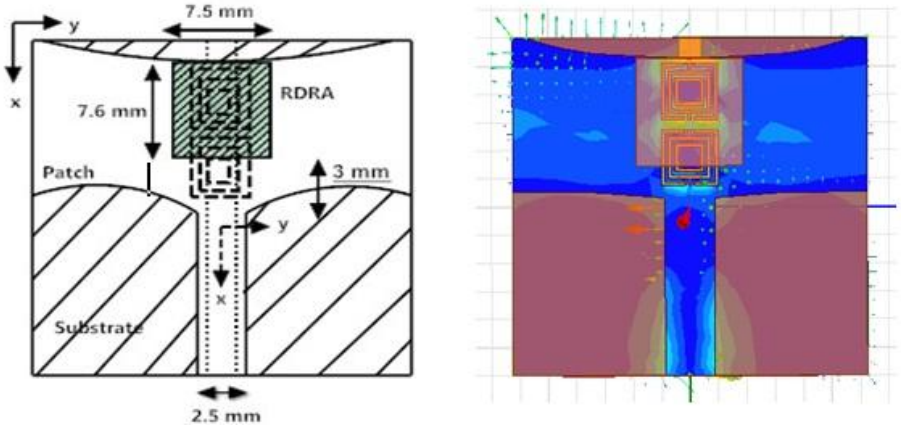

Fig 5.11: RDRA is positioned 3mm away along –x direction and its E (V/m), H (A/m), J (A/m^2)

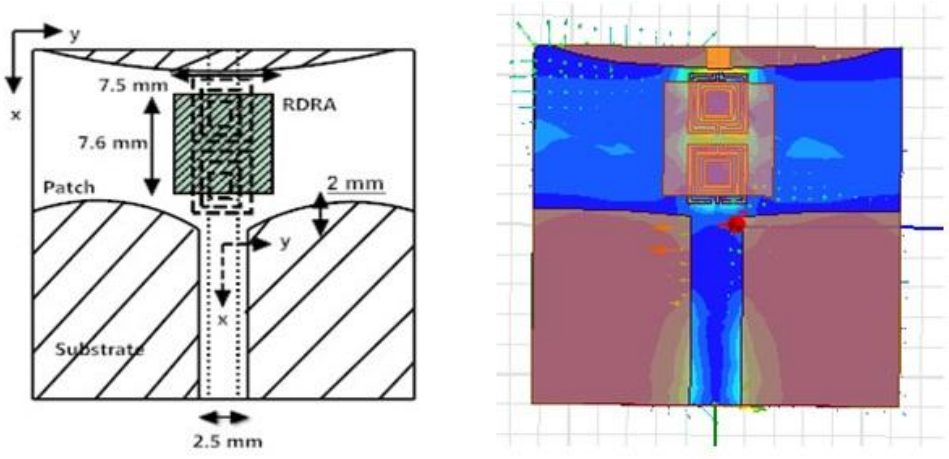

Fig 5.12: RDRA is positioned 2mm away along –x direction and its E (V/m), H (A/m), J (A/m^2)

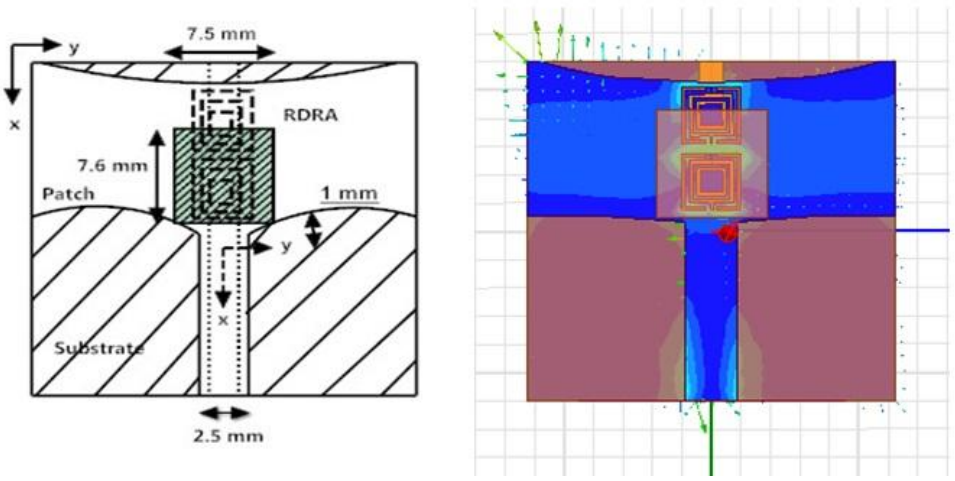

Fig. 5.13: RDRA is positioned 1 mm away along –x direction and its E (V/m), H (A/m), J (A/m^2)

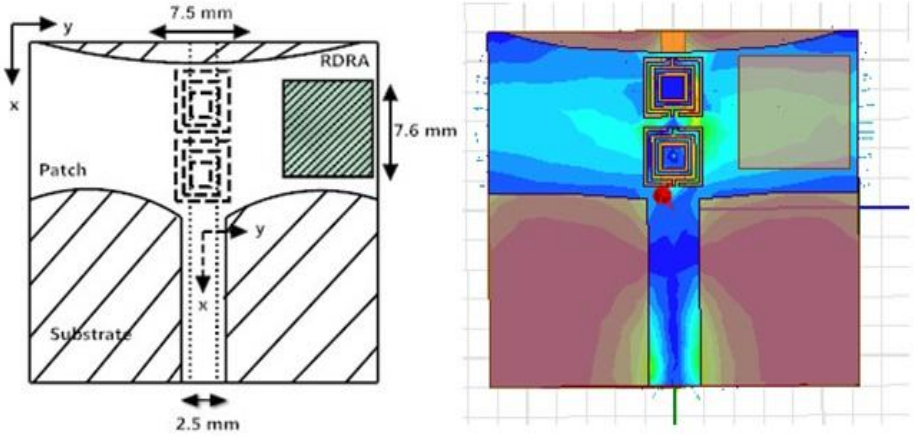

Fig. 5.14: RDRA is positioned at the corner of the patch and its E (V/m), H (A/m), J (A/m^2)

5.3.4 Results And Discussion

For distributed analysis to extract circuit information from a 3 D model like DRA by using Maxwell's equation is too critical. To analyze the performance of the device at any frequencies scattering parameter is used. The S-parameter employs the concept of wave propagation for describing the device. S-parameter is related to the transmission and returns loss relative to a given characteristics impedance. It can be described in terms of VSWR $\leq$2. Fig. 5.15 compares the $|S_{11}|$response against the frequency of the antenna at the various positions of the RDRA with respect to the inclusions and the wideband patch. Table 1 shows the Fig. 5.15, multi-band response of the radiator

in different configurations.

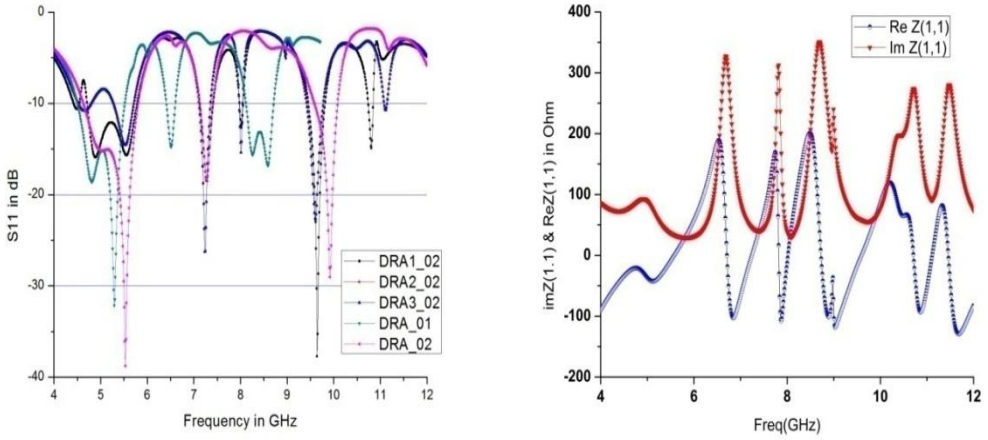

Fig. 5.15: Plot of return loss $|S_{11}|$ vs frequency and Rectangular plot of impedance vs frequency

(DRA1_02 indicates position 1 of the RDRA as shown in the Figure 3, DRA1_02 indicates position 2 of the RDRA as shown in the Fig. 4, DRA1_03 indicates position 3 of the RDRA as shown in the Fig. 5, DRA_01 indicates position 2 of the RDRA with one inclusion, DRA_02 indicates right edge position of the RDRA with two inclusions as given in Fig. 6). The lower and upper portion of the frequency band is almost constant and impedance matching is very sensitive to the position of the RDRA, inclusions, and the finite ground plane. This antenna shows multiband and multi frequency response within this frequency range of operation. Fig. 5.15 shows the rectangular plot of impedance versus frequency of the structure shown in Fig. 5.12. Therefore, output characteristics at the center position as shown in Fig. 5.12 are studied in detail.

Table 5.4: Multiband response of the radiator in different configurations

	Band- I (GHz)	**Band- II (GHz)**	**Band- III (GHz)**	**Band- IV (GHz)**	**Band- V (GHz)**	**Max. f_r (GHz)**	**$\|S_{11}\|_{max}$ in dB**
DRA1_02	4.71-5.78	7.13-7.41	7.97-8.05	9.45-9.81	10.74-10.84	9.64	37.73
DRA2_02	4.52-4.80	5.28-5.71	7.10-7.35	7.96-8.04	9.41-9.77	7.23	26.24
DRA3_02	4.52-4.81	5.28-5.71	7.10-7.35	7.96-8.04	9.41-9.90	7.24	26.18
DRA_01	4.70-6.12	7.37-7.64	9.76-10.59	-	-	5.80	32.16
DRA_02	4.63-5.80	7.12-7.40	9.58-10.09	-	-	5.53	38.71

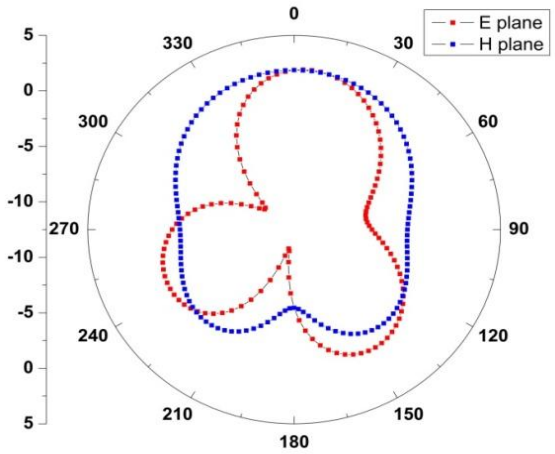

Fig. 5.16: Radiation pattern in E and H plane (10 dB/div)

Gain is the primary design consideration of an antenna. Factors affecting gain are: (i) Back lobe interference effect (ii) Consideration of phase error. Maximum gain can be realized with uniform current distribution. It modifies the phase front to obtain maximum directive. Therefore, at high speed, wideband application phase distribution should be uniform. In addition, to gain, all the side lobes should be suppressed. The subsidiary maxima are called side lobes. The symmetry of the elements is generally

planes of symmetry and referred principal plane of the pattern.

The output field at any point has both E_θ and $E_\emptyset$ components. E_x is the principal polarization component and E_y is the cross-polarization component. Symmetry properties of the antenna w.r.t the principal plane leads to zero cross-polarization in those planes.

Here cross polarization in E-plane pattern is very sensitive to the variation of the RDRA. Therefore, received signal sometimes become noisy as SNR decreases.

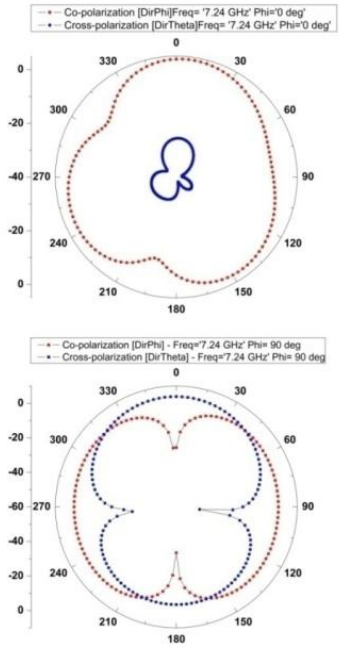

Fig. 5.17: Radiation pattern indicating H & E-plane co- and cross polarization

5.3.5 Conclusion

Narrow bandwidth provides serious limitations on a wider range of applications of the modern wireless system. Multifunctional Integrated Hybrid Rectangular Dielectric Resonator Antenna provides practical innovative extension and coupling of wideband microstrip patch antenna to increase impedance bandwidth while operating over 4.63 GHz to 10.84 GHz covering C, L, and Ku band of operations. This novel compact design provides impeccable phase linearity, high radiation efficiency with exceptional bandwidth response. Apart from this, it radiates an omnidirectional pattern over the operating frequency range. This embedded antenna is suitable to be used in cellular tunable IoT based global tracking module for the operation like tracking, smart metering, a sensor-based smart home which concentrates mainly on 0.5 GHz to 10.4

GHz. With stacked configuration with an appropriate switching mechanism, this antenna can function as a reconfigurable antenna for cellular and cognitive radio platform.

5.4 MICROSTRIP INSET FED RECTANGULAR DRA FOR NEAR FIELD COMMUNICATION

5.4.1 Introduction

Due to the availability of only limited dimensions of dielectric material, frequency tuning is very challenging in a dielectric resonator antenna. The objective is to enhance the tunability range of the DRA by altering the inductive inset feeding techniques. In this paper, novel low-profile rectangular dielectric resonator antennas with three different microstrip inset feeding mechanisms are studied and analyzed. It is observed that by varying the feeding techniques, the operating frequency can be easily altered, without significant variation in the impedance match [206-208]. The dielectric waveguide model is used for approximate calculation of the dimension, and magnetic wall modelling is used for the overall analysis. The reflection coefficient, radiation pattern, co and cross-polarization, and gain are studied. The proposed antenna is resonating in the upper spectrum of the X band, and the lower spectrum of the Ku band with efficiency as high as 99%, a gain of 7 dBi, and the output pattern shows a broadside mode. The influence of the finite ground plane is altered for practical characterization and to test the overall performance of the antenna.

In this paper, a novel RDRA having different microstrip inset feeding mechanisms is being proposed. The matching profile of this antenna is enhanced by concentrating the field underneath the DRA [209, 210]. Here three inset feeds are used to optimize the coupling and to enhance the bandwidth performance. DRA-I is fed by a 50 Ohm horizontal microstrip line, DRA-II is fed by a vertical microstrip feed at the beginning of an aperture, and DRA-III is fed by a vertical microstrip feed at the end of an aperture. DRA-I is considered to be magnetic field coupling whereas DRA-II & III are considered to be electric field coupling. The stub of the transmission line is adjusted to optimize the capacitive and inductive aspects of the matching profile. It is found that DRA-I is operating from 12.22 GHz to 13.84 GHz with a

maximum resonant dip of -38 dB that occurs at 12.48 GHz. DRA-II is operating in two bands. The first band is from 10.54 GHz to 11.06 GHz with a maximum resonant frequency at 10.74 GHz (-23.55 dB). The second band is from 12.22 GHz to 12.96 GHz with resonant frequency at 12.74 GHz (-36.13 dB). DRA-III is operating from 10.86 GHz to 12.1 GHz with the maximum resonant frequency of 11.36 GHz (-58.8 dB). Because of the symmetrical field distribution, the radiation pattern in all these configurations is in a broadside direction. The rectangular DRA is radiating like a short horizontal magnetic dipole. To optimize the proposed design parametric analysis was carried out by employing the finite element method.

5.4.2 Antenna Design

The substrate made up of Roger TMM4 (tm), $\varepsilon_r = 4.5$, loss tangent $\tan\delta = 0.002$ having a dimension of $50 \times 50 \times 1.6\ \text{mm}^3$. The substrate is thin enough to reduce the induction of surface wave but it is mechanically strong enough to provide the required support. RDRA is made up of Rogers RT/Duroid 6010 with $\varepsilon_r = 10.2$, and $\tan\delta = 0.0023$. The dimension of the RDRA is $17.5 \times 4.94 \times 13.7\ \text{mm}^3$. As shown in fig. 5.18 a & b an aperture of dimension $2.5 \times 4.94 \times 9\ \text{mm}^3$ is cut into the RDRA to decrease the quality factor and to improve the effective impedance bandwidth of the RDRA. Silicone sealant is used to join the substrate with the RDRA. An infinite ground plane as a perfect electrical conductor of dimension $50 \times 50 \times 1.6\ \text{mm}^3$ is placed at the backside of the substrate to improve the FBR. The antenna is excited by a microstrip transmission line because it permits easy integration of DRA with the microwave circuits. The dimension of the microstrip transmission line-I from the source side is $4.94 \times 3\ \text{mm}^2$. After that transmission line of various lengths but a width of 2mm is used to optimize the impedance matching. The DRA is placed over the maximum concentrated electric field of the feeding line.

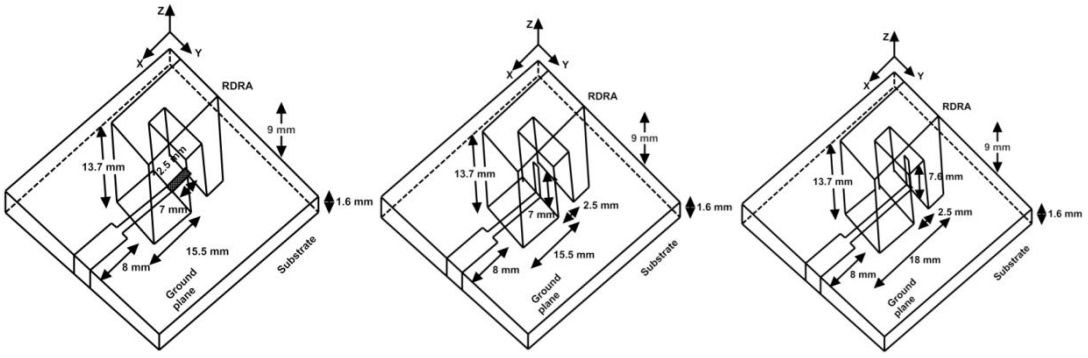

Fig. 5.18a. Showing the side view of DRA-I, DRA-II, DRA-III.

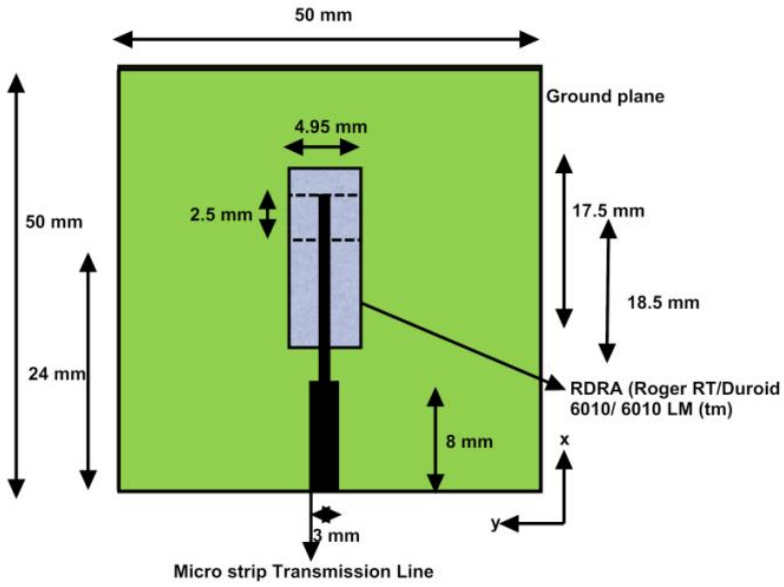

Fig. 5.18b. Showing the top view of DRA-I.

Table 5.5: Antenna dimensions

Structure	Length	Width	Height	Permittivity	Material	tan δ
Substrate	50 mm	50 mm	1.6 mm	4.5	Roger TMM4(tm)	0.002
DRA I,II, & III	17.5 mm	4.94 mm	13.7 mm	10.2	Roger RT/Duroid 6010/6010 LM (tm)	0.0023

5.4.3 Results Analysis

Figure 5.19 shows the return loss $|S_{11}|$ versus frequency for the various dimensions of the ground plane. It shows a comparative analysis of the $|S_{11}|$for the finite ground plane of length 22mm, 23 mm, 24mm, 25 mm, 26 mm, 27 mm, and the infinite ground plane w.r.t 50 mm width. It is observed that -10 dB impedance bandwidth of more than 80% with a peak return loss of 37.5 dB is realized when the dimension of the finite ground plane is 24×50 mm^2.

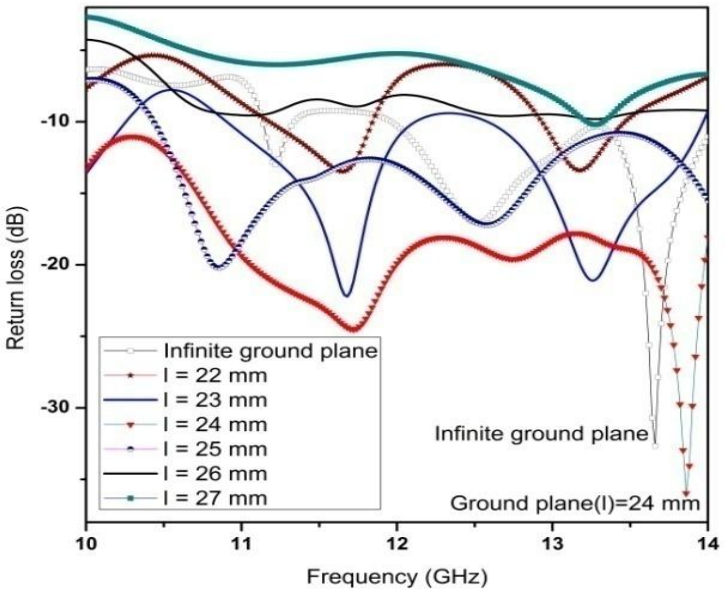

Fig. 5.19: Plot of return loss$|S_{11}|$ versus frequency.

The resonant frequency is one of the significant parameter to decide the characteristics and performance of the antenna. Fig. 5.20 plots the input characteristics of the antenna's S11 Vs frequency parameter. As shown the in the Fig. 5.20, the impedance bandwidth of the DRA-I is found to be 12.43%, DRA-II has two bands. The impedance bandwidth of band-I and band-II are 4.81% and 5.87% respectively, DRA-III provides 10.8% impedance bandwidth. In this band VSWR is found to be less than 2.

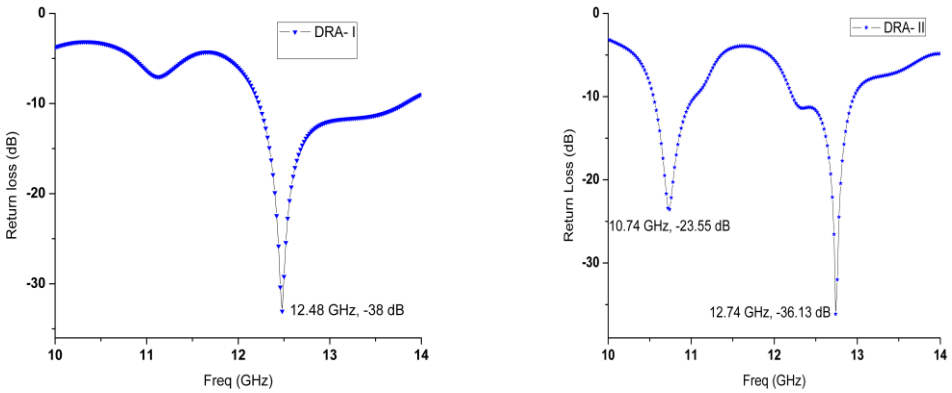

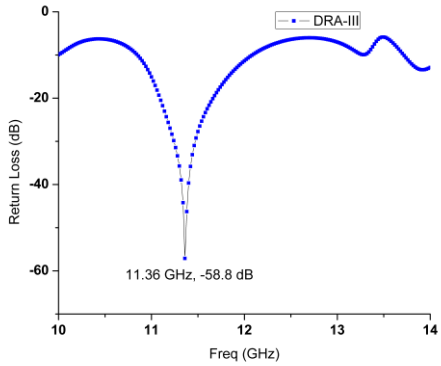

Fig. 5.20. .Plot of Return loss versus frequency in DRA-I, DRA-II and DRA-III

Figure 5.21 shows the resistive and reactive parts of the input impedance for all three designs. The changes along the microstrip line especially when it is within the aperture's initial or final edges. As shown in the figure resistive part of DRA-I increases initially from 10 GHz but after 10.5 GHz it settles down near to 50 Ohms. At near to 12 GHz, DRA-II shows peak input resistance but it also comes down with an increase in the frequency of operation. But DRA-III shows a smooth variation of the input resistance curve. The microstrip position can be used as fundamental parameters for matching and tuning the antenna. It is found that by appropriate matching the real impedance is around 50 ohm.

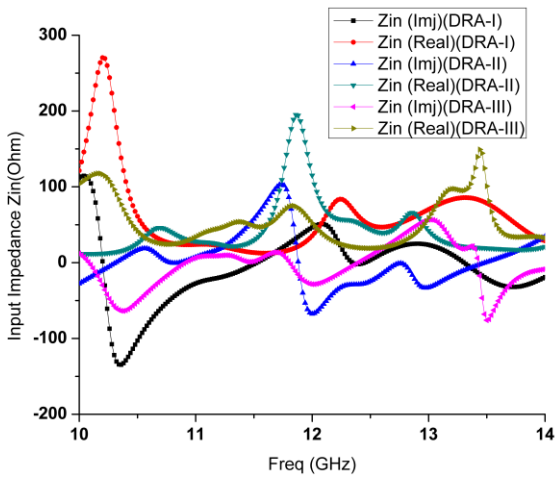

Fig. 5.21 Plot of variation of the real and imj Z_{in}(Ohms) for DRA-I, DRA-II, and DRA-III with frequency.

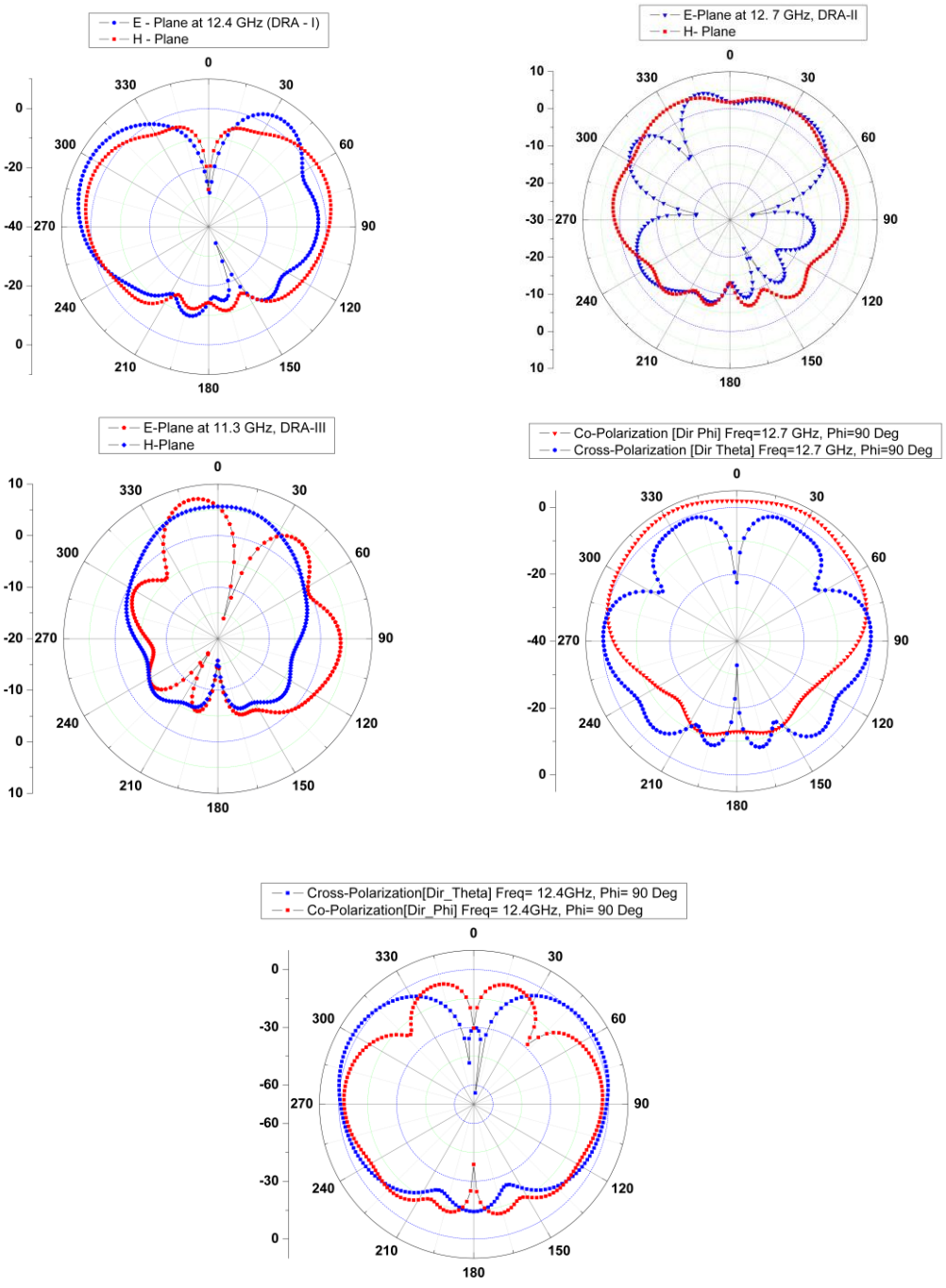

Fig. 5.22 Output pattern in E-plane and H-plane for DRA-I, DRA-II, and DRA-III

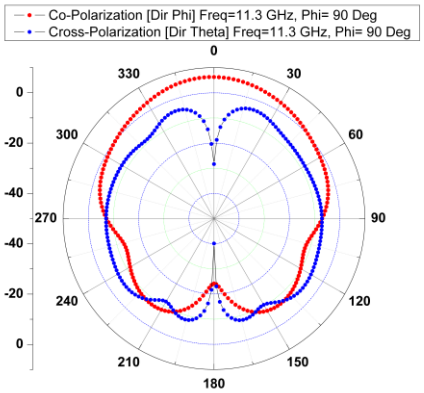

Fig. 5.23. E-plane co and cross polarization of the DRA-I, DRA-II, and DRA-III.

Fig. 5.23 shows the E-plane co and cross-polarization at 12.4 GHz, 12.7 GHz, and 11.3 GHz. The cross-polarization is unavoidable considering the practical aspect of the antenna. It has been observed that the difference between cross and co-polarization is more than 20 dB in the broadside direction for $\theta = 0^0$ for DRA-II and III.

The radiation pattern appears symmetric in H-plane. The difference between co and cross-polarization is seemed to be more than 30 dB

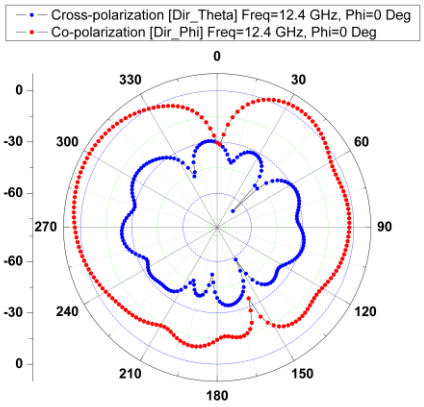

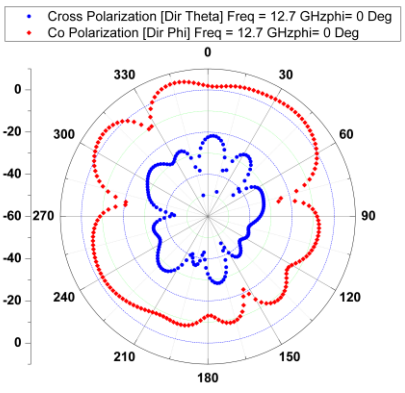

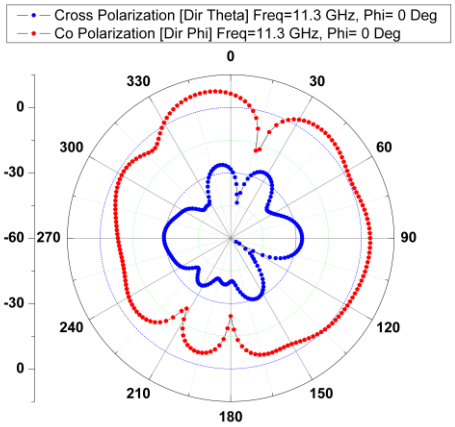

Fig. 5.24. H-plane co and cross-polarization of the DRA-I, DRA-II, and DRA-III.

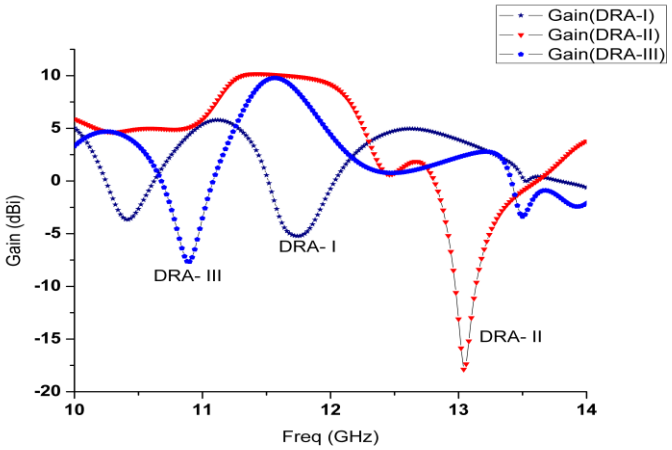

Fig. 5.25 Plot of gain versus frequency for DRA-I, DRA-II, and DRA-III

.

Fig. 5.25 indicates a comparative analysis of gain in dBi for all the three designs at their resonating frequency. DRA-II provides a peak gain of 9.8 dBi with maximum gain stability in its operating band. Fig. 5.26 indicates the three-dimensional gain of DRA-II at 12.74 GHz. It is observed that in DRA-II a front-to-back ratio of 80.51 dB is obtained. Fig. 5.27 shows the formation of surface current density (Amp/m^2), electric field (Volt/m), and magnetic field (Amp/m) in DRA-II while operating at the resonant frequency.

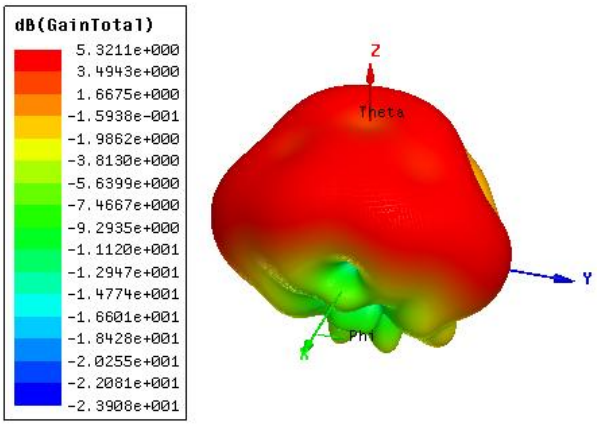

Fig. 5.26 3-D Plot of gain in dB at 12.74 GHz in DRA-II

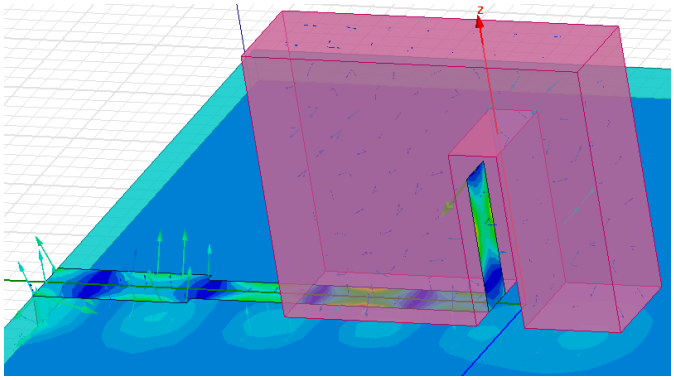

Fig. 5.27 Formation of surface current density, E and H field on DRA-II at 12.74 GHz

Table 5.6 Performance analysis of DRA

	DRA-I	DRA-II	DRA-III
Maximum Resonating Frequency	12.48 GHz (-38 dB)	10.74 GHz (-23.55 dB) 12.74 GHz (-36.13 dB)	11.36 GHz(-58.8 dB)
Operating Band	12.22GHz to 13.84 GHz	Band-I: 10.54 to 11.06 GHz Band-II: 12.22 to 12.96 GHz	10.86 GHz to 12.1 GHz
Impedance Bandwidth (%)	12.43 %	Band-I: 4.81% Band-II: 5.87%	10.8%
Peak Directivity (dB)	7.25	7.28	7.25
Peak Gain (dBi)	7.24	7.32	7.24
Radiation Efficiency (%)	99.85%	100.52%	99.85%

5.4.4 Conclusion

Novel wideband, low-profile, high gain RDRA is proposed. The various microstrip inset feeding configuration shows that proposed antennas provide good impedance matching and stable radiation pattern in the entire frequency of operation. After comparing various parameters it is observed that DRA-II provides excellent input and output characteristics. This proposed antenna is a potentially suitable candidate for the vehicular radar system, imaging, near field communication system, etc.

CHAPTER 6
CONCLUSION AND FUTURE SCOPE

6.1 CONCLUSION

This work uses various theory, modeling, simulation, and optimization of prototype. Fabrication of prototype is carried out, measurement and analysis of the result reveals the true nature and performance of RDRA. In this work different properties of RDRA like fundamental operating principle, feeding and excitation methods, array configuration, miniaturized design are analyzed in details. The common inherent problems and limitations are discussed and suitable solutions are provided to mitigate these problems. Computational techniques like Green functions, MoM, FDTD, FEM along with various design methods such as DWM, MDWM, GTD, and 3-D electromagnetic tools like HFSS, ADS, and CST have been applied, validated, and confirmed by measurements.

The thesis started with the design and analysis of co-planar embedded rectangular DRAs. The embedded DRA offers impedance bandwidth of 26.66% (3.9 to 5.1 GHz) and 15.71% (8.8 to 10.3 GHz). It is potentially a suitable candidate for near-field communication, imaging, biomedical devices, and modern short-range wireless communication system, etc. In the second design, a narrow band rectangular DRA is proposed. The fourth design is based on a dual-band RDRA. It provides impedance bandwidth of 50.6% while operating from 3.1 to 5.2 GHz and 18.18% from 9 to 10.8 GHz. The fifth design proposed a filleted DRA. It provides an impedance bandwidth of 21.92% while operating from 7.32 to 9.12 GHz, and 19.09% from 10.7 to 12.95 GHz. The sixth design proposes a dual-band hybrid DRA. The antenna efficiency is found to be 98.56% with an FBR of 2.48 dB. The seventh design proposes a nine elements CDRA array. The nine-element architecture shows a peak gain of 11.62 dB and directivity of 13.67 dB at 8 GHz. The eighth design proposes a novel multifunctional integrated hybrid RDRA for high-speed communication. It offers a multiband response while operating from 4.63 to 10.84 GHz. Finally, microstrip inset fed RDRA is proposed. The proposed antenna is resonating in the X band and in the Ku band with an efficiency of 98% and gain of 7 dBi.

Analyzing various fundamental resonant lower order mode, higher order mode, radiation patterns, methods of excitation in a dielectric resonator, it is found that DR can act as an efficient and low loss antenna. DRA is in the final stages of wide commercial applications to become the future of modern antenna technologies. Though DRA technology cannot replace matured microstrip antenna technology but it can be used along the side of it.

6.2 FUTURE SCOPE

We are witnessing an era in wireless networking that has ability to give a thrust to a new phase of technologies for human existence. The new era is revolutionized by the digitization and connection of data associated with everything and everyone with an intention of automation and optimization of intelligent decision making. The future is radio frequency based sensing applications for Federal Communication Commission (FCC) recently approved 28/38 GHz bands with at least 1 GHz bandwidth, in addition to the 60 GHz ISM band. Though free space path loss is comparatively high, but still it can be useful for mobile communication by employing technology such as beam forming and beam splitting at mm-wave. The new communication spectral window demands new set of technology such as DRA as a front end device.

Future work:

(i) To design and develop multi antenna system with multi standard and methods for interference suppression.

(ii) On-chip/ on package/ in-package antenna array solution. Desirable parameters in an on-chip array will be:

   a) Wide beam width and high gain.

   b) A miniaturized compact foot prints to reduce the grating lobe.

   c) Low mutual coupling to improve scan blindness.

(iii) Active and flexible integration of DRA with miniaturized active antenna as front and front end modulator. It can be packaged with an active device to form Hybrid

Active DRA. Further DRA can be integrated with low noise amplifier (LNA) to improve impedance matching over broader bandwidth and to improve SINR of the received signal. Active switching elements can be useful for beam forming and beam splitting techniques.

(iv) Proper testing and characterization of on package arrays, embedded antenna solution.

(v) Enhancement in modeling tools.

(vi) Proper integration of antenna, electronics, and algorithm.

(vii) To enhance the energy efficiency requirements.

(viii) DRA technology is still in its early stages of development, and more research is required to overcome some of the challenges associated with fabricating a large number of DRA elements and assembling them into an array.

(ix) DRA uses an insufficient and un-matured numerical technique for its performance analysis (especially Rectangular DRA). It is required to improve RDRA's mathematical modeling to analyze its design characteristics.

(x) DRA is proved to be one of the best candidates at microwave and mm-wave frequency. DRA is suitable in those applications where there is a requirement of continuous change in frequency such as software-defined radio, military communication, etc. It has huge potential to become the next generation of antenna technology.

(xi) The amalgamation of digital and analog technology leads to multiple RF front ends, antenna arrays in massive MIMO, and multi-user MIMO, which supports high user capacities in the 5G radio standard. Due to the complexities of the modern system, sensible prioritization of the allocated resource, the modern antenna is strongly influenced by the presence of components and materials in its direct vicinity. The radiation pattern and the frequency tuning can alter significantly due to the impact of the near field of the antenna. Matching of the

antenna to the test equipment may be different from the matching of the antenna to the integrated components of the system. Therefore efficiency can be changed in the highly integrated system. As complex simulation may take a long time, measurement is still the best way to determine real-life performance.

(xii) Beam steering provides enhancement in gain and directivity. It can be achieved by changing the magnitude of different elements in a complex phase linear and planar array

(xiii) Microwave and millimeter waves are the backbones of wireless communication and data networks. For computers, higher frequency translates to faster performance, and for a communication system, higher frequency translates to higher bandwidth. Milli-meter wave computing is suitable for parallel processing and fast speed of operation. At such frequency of operation radiation analysis for digital design, the rise and fall time are crucial parameters.

REFERENCES

[1] R. C. Johnson, “Antenna Engineering Handbook,” 3rd edition, Mc-Graw-Hill, 1993.

[2] Simon Haykin, "Communication System," John Wiley and Sons Ltd, United Kingdom, 5th edition 2009.

[3] D. Valderas, J. I. Sancho, D. Pente, C. Ling, X. Chen, “Ultra Wide Band Antenna Design and Application,” Imperial College Press, 2011.

[4] D. M. Pozar, "Microstrip Patch Antenna," IEEE Press, 1st edition,1992, pp. 203-259.

[5] L. V. Blake, “Antennas,” Artech House, John Wiley & Sons, 1966.

[6] D. Guha, Y. M. M. Antar, "Microstrip and Printed Antennas New Trends, Techniques and Applications,"1st edition, John Wiley and Sons Ltd, United Kingdom, 2011, pp.305-340.

[7] S. Ramo, J. R. Whinnery, T. V. Duzer, “Fields and Waves in Communication Electronics,”3rd edition, Wiley.

[8] K. L. Wong, “Compact and Broadband Micro-Strip Antenna,” John Wiley and Sons Ltd, New York, 2002.

[9] K. M. Luk, K. W. Leung, "Dielectric Resonator Antennas," Research Studies Press, Baldock, Herfordshire, U.K, 2003.

[10] A. Petosa, A. Ittipiboon, Y. M. M. Anter, D. Roscoe, and M. Cuhahi, “Recent advances in Dielectric Resonator Antenna Technology,” IEEE Antenna and Propagation Magazine, Vol. 40, No. 3, June 1998.

[11] D. Soren, R. Ghatak, R. K. Mishra, and D. R. Podar, “Dielectric Resonator Antennas: Designs and Advances,” Progress in Electromagnetics Research B, Vol. 60, 195-213, 2014.

[12] Q. Rao, T. A. Denidni, and A. R. Sebak, “Study of Broadband Dielectric Resonator Antennas, “Progress in Electromagnetics Research Symposium, Hanzhou, China, August 22-26, 2005.

[13] G. Matthaei, L. Young, and E. M. T. Jones,”Microwave Filters, Impedance Matching Networks, and Coupling Structure,”Artech House, 685 Cannon Street, Norwood, 1980.

[14] R. S. Yaduvanshi, H. Parthasarathy, “Rectangular Dielectric Resonator Antennas, Theory and Design,” Springer, 2016.

[15] A. Petosa, A. Ittipiboon, Y. M. M. Anter, D. Roscoe, and M. Cuhahi, “Recent advances in Dielectric Resonator Antenna Technology,” IEEE Antenna and Propagation Magazine, Vol. 40, No. 3, June 1998.

[16] R. B. Waterhouse, “Microstrip Patch Antennas: A Designer’s Guide,” Khuwer Academic Publishers, Massachusettes, USA,2003.

[17] Y. Huang, K. Boyle, “Antenna from Theory to Practice,” John Wiley and Sons Ltd, 2008.

[18] R. K. Mongia, P. Bhartia, “Dielectric Resonator Antennas- A Review and General Design Relations for Resonant Frequency and Bandwidth,” International Journal of Microwave and Millimeter-Wave Computer-Aided Engineering, Vol.4, No.3, 1994, pp.230-247.

[19] F. Wang, C. Zhang, H. Sun, Y. Xiao, “Ultra-Wideband Dielectric Resonator Antenna Design Based on Multilayer Form,” Hindawi International Journal of Antennas and Propagation, Volume 2019, Article ID 4391474.

[20] Roger F. Harrington, “Time Harmonic Electromagnetic Fields,” IEEE Press Series on Electromagnetic Wave Theory, 2001.

[21] Li. B, K. W. Leung,”Strip-Fed Rectangular Dielectric Resonator Antennas with/without a Parsitic Patch,” IEEE Trans.Antennas Propag., vo1.53, no. 7, pp. 2200-2207, Jul. 2005.

[22] Y. Coulibaly, T. A. Denidni, "Broadband microstrip fed dielectric resonator antenna for X-band applications" IEEE antenna and wireless propagation letters, Vol. 7, 2008.

[23] P. V. Bijumon, “Broadband Cylindrical Dielectric Resonator Antenna Excited by Cavity Backed Circular Aperture with Modified Microstrip Line,” IEEE Electronics Letters, Vol.41, No.7, March 2005, pp.385-387.

[24] Leung. K. W., “Annular Slot Coupled Dielectric Resonator Antenna,’ IEE Electronics Letter, Vol. 34, No. 13, Jun 1998, pp.1,275-1,277.

[25] S. Mohanty, B. Mohapatra, “Printed SlotWideband Rectangular Dielectric Resonator Antenna,” Innovations in Electrical and Electronic Engineering, Lecture Notes in Electrical Engineering 661, https://doi.org/10.1007/978-981-15-4692-1_44, pp. 575-583, 2021.

[26] S. Mohanty, B. Mohapatra, "Leaky Wave-Guide Based Dielectric Resonator Antenna for Millimeter-Wave Applications," Trans. Electr. Electron. Mater., https://doi.org/10.1007/s42341-020-00240-w, 2020.
[27] X. Li, Y. Yang, F. Gao, H. Ma, X. Shi, "A Compact Dielectric Resonator Antenna Excited by a Planar Monopole Patch for Wideband Applications," Hindawi International Journal of Antennas and Propagation, Volume 2019, Article ID 97344781.
[28] Y. X. Guo, K. M. Luk, and K. W. Leung, "Mutual Coupling Between Rectangular Dielectric Resonators," IEE Proceeding on Microwave Antennas and Propagation, Vol. 146, No. 4, Aug 1999, pp. 2164-2166.
[29] N. A. Shalaby, S. E. Sherbiny, "Mutual Coupling Reduction of DRA for MIMO Applications," Advanced Electromagnetics, Vol.8, No.1, May 2019.
[30] A. Ittipiboon, A. Petosa, and S. Thirakoune, " Bandwidth Enhancement of a Monopole Using Dielectric Resonator Antenna Loading,' Symposium on Antenna Technology and Applied Electromagnetics ANTEM 2002, Montreal, Canada, Aug. 2002, pp. 387-390.
[31] R. K. Mongia, A. Ittipiboon, "Theoretical and experimental investigations on Rectangular Dielectric Resonator Antennas" IEEE transaction on antennas and propagation, Vol. 45. No.9 September 1997.
[32] R. B. Waterhouse, "Microstrip Patch Antennas: A Designer's Guide," Khuwer Academic Publishers, Massachusettes, USA,2003.
[33] C. Trueaman, "Computation and Measurement of the Resonant Frequencies and Q- factors of High Permittivity Dielectric Resonators," Symposium of Antenna Technology and Applied Electromagnetics ANTEM 94 Digest, Ottawa, Canada, Aug. 1994, pp. 395-402.
[34] A. Petosa, "Dielectric Resonator Antenna Handbook", Artech House, 685 Canton Street, Norwood, 2007.
[35] M. Abioghli, A. Keshtkar, M. N. Moghadasi, and B. Ghalamkari, "UWB Rectagular DRA Integrated with Reconfigurable Narrowband Antenna for Cognitive Radio Applications, IETE Journal of Research, ISSN:0377-2063, 08 Oct 2018.
[36] A Khan and S Mohanty, "Investigations of Rectangular Dielectric Resonator Antenna Excited by CPW Feed", Lecture Notes in Network and Systems, SCOPUS LNE series, Vol. 106, DOI: https://doi.org/10.1007/978-981-15-2329-8_52, April 2020. [SPRINGER NATURE]
[37] A Khan and S Mohanty, "Analysis of Cylindrical Dielectric Resonator Antenna with Modified Micro-Strip", 2020 ICCCA Conference Proceedings of IEEE, 978-1-7281-5432-9/20/$31.00 ©2020 IEEE, DOI: 10.1109/IC3A48958.2020.233271 [IEEE Explore Digital Library]
[38] A Khan, S Mohanty and B Mohapatra, "Analysis of Micro Strip fed Cylindrical Dielectric Resonator Antenna" Vigyan Garima Sindhu Journal, Vol. 112, ISSN: 2320-7736, Jan-March 2020. [UGC CARE Journal]
[39] S. Mohanty, A. Khan, B. Mohapatra, "Embedded Rectangular Dielectric Resonator Antenna for Ku-Band Applications", DOI: http://dx.doi.org/10.2139/ssrn.3549250, 21 Feb 2020. [SSRN: ELSEVIER].
[40] S. Mohanty, A. Khan, B. Mohapatra, "Comparative Analysis of Stacked Rectangular Dielectric Resonator Antennas Based on Finite Defected Ground Plane", DOI: http://dx.doi.org/10.2139/ssrn.3551000, 21 Feb 2020 [SSRN: ELSEVIER].
[41] S Mohanty, A Khan, and B Mohapatra, "Stacked Rectangular Dielectric Resonator Antenna for Biomedical Electromagnetic Applications", National Conference on Biomedical Engineering 2020 held at NITTTR Chandigarh, DSIR, Jan 2020 [UNDER REVIEW]
[42] A Khan, S Chaturvedi and S Mohanty, "Slot Coupled Dual Band Etched Rectangular DRA", Emerging Issues on Contemporary Business Practices Conference Proceedings, Nov. 2019. [Research Paper presentation in EICBI 19 Conference held at SRMS CET]
[43] A Khan, S Mohanty and B Mohapatra, "Analysis of Aperture Coupled Dual Band Rectangular Dielectric Resonator Antenna", Vigyan Prakash Journal, ISSN Num: 1549-523X. [Accepted and is UNDER REVIEW in UGC CARE listed mentioned journal]
[44] R. D. Richtmeyer, "Dielectric Resonators", Journal of Applied Physics, DOI: http://dx.doi.org/10.1063/1.1707320, Volume 10, June 1939.
[45] A Okaya and L F Barash, 'The dielectric microwave resonator', Proc. IRE, vol. 50, pp. 2081-2092, 1962.
[46] S. A. Long, M. W. McAllister, and L. C. Shen, "The resonant cylindrical dielectric cavity antenna", IEEE Trans. Antennas Propagat ., Vol. 31, pp.406–412, May 1983.

[47] Petosa, A. Ittipiboon, YM M Antar 1 , D. Roscoe, and M. Cuhaci, "Recent advances in Dielectric-Resonator Antenna technology", IEEE Antennas and Propagation Magazine, vol. 40, no. 3, June 1998.
[48] Agouzoul 1 , M. Nedil 1 , Y. Coulibaly 1 , TA Denidni 1,2 , I Ben Mabrouk 3 and L. Talbi 3 , "Design of a high gain hybrid dielectric resonator antenna for millimeter-waves underground applications ". , 978-1-4244-9561-0/11/$ 26.00 © 2011 IEEE.
[49] K. M. Luk, K. W. Leung, "Dielectric Resonator Antennas " Baldock, Herfordshire, UK: Research Studies, 2002.
[50] Aldo Petosa, A. Ittipiboon, "Dielectric Resonator Antennas: A Historical Review and the Current State of the Art" IEEE Antennas and Propagation Magazine , vol. 52, No.5, October 2010.
[51] Ittipiboon, R. Mongia, Y. M. M. Antar, P. Bhartia, and M. Cuhaci, "Aperture fed rectangular and triangular dielectric resonators for use as magnetic dipole antennas," Electron. Lett., vol. 29, no. 23, pp. 2001–2002, Nov. 1993.
[52] R. K. Hoffmann, Handbook of Microwave Integrated Circuits. Norwood, MA: Artech House, 1987.
[53] R K Mongia, "Theoretical and experimental resonant frequencies of rectangular dielectric resonators". IEEE Proceedings-H, Vol. 139, No. 1, February 1992.
[54] C Chang, and T Itoh, 'Resonant characteristics of dielectric resonators for millimeter wave integrated circuits', Arch. Elektron. Obertrag. tech., AEU-33, pp. 141-144, 1979.
[55] R. S. Yaduvanshi and H. Parthasarathy, "Rectangular Dielectric Resonator Antennas Theory and Design" Springer ISBN 978-81-322-2499-0 ISBN 978-81-322-2500-3 (eBook) DOI 10.1007/978-81-322-2500-3 Springer New Delhi Heidelberg New York Dordrecht London © Springer India 2016.
[56] M. Ben Omar and A. Matoussi, "Dielectric and conductivity investigations of Rutile Titanium dioxide single crystals", 978-1-4673-1252-3/12/$31.00 ©2012 IEEE
[57] Okaya, et at., Columbia Radiation Lab. Quart. Rept., Columbia University, New York, March 16-JuInie 15, 1959(unpublished), June 16-September 15, 1959 (unpublished), September 16-December 15, 1959 (unpublished).
[58] S. Keyrouz, D. Caratelli, "Dielectric Resonator Antennas: Basic Concepts, Design Guidelines, and Recent Developments at Millimeter-Wave Frequencies", International Journal of Antennas and Propagation© 2016.
[59] R. Chaudhary, N. Mishra, M. S. Sani and R. N. Chaudhary "Analysis of a Wideband Circularly Polarized Cylindrical Dielectric Resonator Antenna with Broadside Radiation Coupled with Simple Micro strip Feeding", **Electronic ISSN:** 2169-3536 **Published in:** IEEE Access (Volume 5) 2169-3536 © 2017 IEEE.
[60] R Chowdhury, R. K Chaudhary. Circularly polarized rectangular dielectric resonator antenna fed with unequal parallel microstrip lines for Wi-MAX applications. Microwave and Optical Technology Letters, 2017, vol. 59, no. 5, p. 1182–1188. DOI: 10.1002/mop.30492.
[61] S. K. K. Dash, T. Khan & A. De "Modelling of Dielectric Resonator Antennas using Numerical Methods: A Review", ISSN: 0832-7823, Journal of Microwave Power and Electromagnetic Energy, 2016 VOL. 50, NO. 4, 269–293 http://dx.doi.org/10.1080/08327823.2016.1260677.
[62] S. K. K. Dash, S. Sahu, D. Behera and N. D. Manish, "Concentric Three-Layer Cylindrical DRA For UWB Applications", 978-1-4 799-8081-9/15/$3l.00 © 2015 IEEE.
[63] Sharma, G. Das, P. Ranjan, N. K. Sahu and R. K. Gangwar, "Novel Feeding Mechanism to Stimulate Triple Radiating Modes in Cylindrical Dielectric Resonator Antenna", DOI 10.1109/ACCESS.2016.2633361, 2169-3536 © 2016 IEEE.
[64] Kao-Cheng Huang and David J. Edwards, "Millimetre Wave Antennas for Gigabit Wireless Communications", JohnWiley & Sons Ltd. © 2008
[65] Simon Haykin, "Communication System" 3e Wiley.
[66] Roger F. Harrington, "Time Harmonic Electromagnetic Fields," New York: Mc Graw-Hill IEEE Press, 1961.
[67] Y. Coulibaly, T. A. Denidni, "Broadband micro-strip fed dielectric resonator antenna for X-band applications" IEEE antenna and wireless propagation letters, Vol. 7, 2008.
[68] T. A. Denidni and Z Weng, "Rectangular dielectric resonator antenna for ultra wideband applications" Electronics letters 19, vol. 45 No. 24. Nov 2009.
[69] Ahemed A Kishk, A. Ittipiboon, Y. M. M. Anter and M. Cuhehi "Slot excitation of the dielectric disk radiator," IEEE transaction on antennas and propagation, Vol. 43. No.2 February 1995

[70] Richard C. Johnson. Antenna Engineering Handbook, 3e, McGraw-Hill.
[71] R. Garg, P. Bhartia, I. Bahl, and A. Ittipiboon. (2001).Micro-strip Antenna Design Handbook, Artech House, Canton, MA, 2001.
[72] J. D. Kraus, D. A. Fleisch. (2010). Electromagnetics with Applications, 5e, Tata Mc-Graw Hill.
[73] M. Amin, J. S. Hong, C. M. Luo, X. Ming, M. Abdullah, "A High Gain and Broadband Rectangular Dielectric Resonator Antenna with Modified Slot" 2016.
[74] Y. Diao, M. Su, Y. Liu, S. Li, W. Wang (2015). Compact and Multiband Dielectric Resonator Antenna for Mobile Terminals, IEEE transaction on antennas and propagation.
[75] Jean Van Bladel.(1975). On the Resonance of a Dielectric Resonator of Very High Permittivity, IEEE MTT, Vol-23, No.2.
[76] Petosa, M. Cuhahi, N. R. S. Simons, A. Ittipiboon, R. Larose. (1996), A Novel Microstrip Fed Multi-Segment Dielectric Resonator Antenna, ANTEM.
[77] R. P. Feynman, R. B. Leighton, M. Sands. "Lectures on Physics," Addison-Wesley Publishing Company, 1964.
[78] F. Wang, C. Zhang, H. Sun, Y. Xiao, "Ultra-Wideband Dielectric Resonator Antenna Design Based on Multilayer Form", Hindawi International Journal of Antennas and Propagation, Article ID 4391474. 2019.
[79] X. Li, Y. Yang, F. Gao, H. Ma, X. Shi, "A Compact Dielectric Resonator Antenna Excited by a Planar Monopole Patch for Wideband Applications" Hindawi International Journal of Antennas and Propagation, Article ID 97344781, 2019.
[80] Harrington RF, "Origin and development of the method moments for field computation", IEEE Antennas and Propagation Magazine, Volume 32 , Issue: 3 , June 1990.
[81] Capolino F., "Theory and phenomena of metamaterials", Boca Raton, FL: CRC Press. 2009
[82] K. W. Leung and H. K. Ng, "Rigorous analysis of the hemispherical dielectric resonator antenna with a parasitic patch", IEEE Transactions on Antennas and Propagation, doi: https://doi.org/10.1109/TAP.2003.809844, vol. 51, number: 3, March 2003.
[83] J M Jin, "The finite element method in electromagnetic". New York: Wiley, 1993
[84] P P Silvester,R L Ferrari, "Finite elements for electrical engineering" Cambridge: Cambridge University Press, 1983
[85] J L Volakis, A Chattejee, L C Kempel, "Finite element method for electromagnetics: antennas, microwave circuits, and scattering applications". Piscataway, NJ: Wiley IEEE Press Series on Electromagnetic Wave Theory. 1998.
[86] C Zienkiewicz, R L Taylor, J Z Zhu, "The finite element method: its basis and fundamentals", Burlington, MA: Elsevier Butterworth-Heinemann, 2005.
[87] S K K Dash, T Khan & A De, "Modelling of dielectric resonator antennas using numerical methods: a review". Journal of Microwave Power and Electromagnetic Energy, ISSN: 0832-7823 (Print) (Online) Journal homepage: http://www.tandfonline.com/loi/tpee20.
[88] P. Rezaei, M. Hakkak, and K. Forooraghi, "design of wide-band dielectric resonator antenna with a two-segment structure" Progress In Electromagnetics Research, PIER 66, 111–124, 2006.
[89] K. M. Luk, K. W. Leung, Dielectric Resonator Antennas (Electronics and Electrical Engineering Research Studies Press, Baldock, Hertfordshire, England, 2003), pp. 355-385.
[90] R. Garg, P. Bhartia, I. Bahl, A. Ittipiboon, Microstrip Antenna Design Handbook (Artech House, Canton, MA, 2001)
[91] A. Petosa, Dielectric Resonator Antenna Handbook (Norwood, MA: Artech House, 2007), pp. 29-42.
[92] S. A. Kumar, T. Shanmuganantham, Design of CPW-fed inverted six shaped antenna for IOT applications. Springer Transactions on Electrical and Electronic Materials, (2020).https://doi.org/10.1007/s42341-020-00213-z
[93] A. Razzaq, A. A. Khan, U. Shakir, A. Arshad, Next generation flexible antennas for radio frequency applications. Springer Transactions on Electrical and Electronic Materials, (2018). https://doi.org/10.1007/s42341-018-0051-7
[94] Harold A. Wheeler, Fundamental limitations of small antennas. Proceedings of the I.R.E, 35(12),1479-1484 (1947)
[95] R. K. Mongia, P. Bhartia, Dielectric resonator antennas – A review and general design relations for resonant frequency and bandwidth, International J. of Microwave and Millimeter-Wave Computer-Aided Engg., 4, 960-966 (1994)

[96] A. Petosa, M. Cuhahi, N. R. S. Simons, A. Ittipiboon, R. Larose, A Novel Microstrip Fed Multi-Segment Dielectric Resonator Antenna, Symposium on Antenna Technology and Applied Electromagnetic, 6-9 Aug. 1996
[97] A. Petosa, A Ittipiboon, Y. M. M. Antar, D. Roscoe, and M. Cuhahi, Recent Advances in Dielectric Resonator Antenna Technology. IEEE Antenna and Propagation Magazine, 40(3), 35-48 (1998)
[98] F. Schwering, A. A. Oliner, Antenna Handbook Theory, Applications, and Design (Springer, Boston, MA, 1988), pp. 1135-1282
[99] A. A. Oliner, Leaky Wave Antennas in Antenna Engineering Handbook, 3rd edn.(R. C. Johnson, McGraw-Hill, New York, 1993) Ch. 10.
[100] R. F. Harrington, Time Harmonic Electromagnetic Fields (IEEE Press Series on Electromagnetic Wave Theory, 2001)
[101] S. T. Peng, A. A. Oliner, Guidance and leakage properties of a class of open dielectric waveguides: part I- mathematical formulations. IEEE Trans. Microwave Theory Tech., 29, 855-869 (1981)
[102] A. A. Oliner, S. T.Peng, T. Hsu, Guidance and leakage properties of a class of open dielectric waveguides, part II: new physical effects.IEEE Trans. Microwave Theory Tech.,29, 843-855 (1981)
[103] A. Sanchez, A.A. Oliner, Accurate theory for a new leaky wave antenna for millimeter waves using nonradiative dielectric waveguide. Radio Science, Vol.19(5), 1225-1228,(1984)
[104] M. T. Lee, K. M. Luk, S. J. Xu, E. K. N. Yun, Leaky wave antenna based on image NRD guide with staircase-shaped dielectric slab. Electronics Letters, 36(13), 1102-1103 (2000)
[105] C. Balanis, An Antenna Theory Analysis and Design (New York, John Wiley, 1997)
[106] A.A. Oliner, S.T. Peng and K.M. Sheng, Leakage from the gap in NRD guide. IEEE MTT-S International Microwave Symposium Digest, 4-6 June 1985
[107] T. Yoneyama, N. Tozawa, S. Nishida, Lossmeasurement of nonradiative dielectric waveguide. IEEE Transactions on Microwave Theory and Techniques, 32(8) ,943-946 (1984)
[108] Z. Ma, E. Yamashita, Wave leakage from groove NRD structures. IEEE Microwave and Guided Wave Letters, 3(6),170-172 (1993)
[109] A. Ittipiboon, R. K. Mongia, Y. M. M. Antar, P Bhartia and M. Cuhahi, Aperture Fed Rectangular and Triangular Dielectric Resonators for Use as Magnetic Dipole Antennas. Electronics letters 11, 29(23), 2001-2002 (1993)
[110] Ahmed A Kishk, A. Ittipiboon, Y. M. M. Anter and M. Cuhehi, Slot excitation of the dielectric disk radiator. IEEE transaction on antennas and propagation, 43(2), 198-201 (1995)
[111] Jean Van Bladel, On the Resonance of a Dielectric Resonator of Very High Permittivity. IEEE Trans. Microwave Theory Tech., 23(2), 199-208 (1975)
[112] R. K. Mongia, A. Ittipiboon and M. Cuhehi, "Low profile dielectric resonator antennas using a very high permittivity material," Electronics Letters, 30(17), 1362-1363 (1994)
[113] M. Yamamoto, K. Itoh, Resonant type leaky wave antenna using image NRD guide. Electronics Letters , 35(11) ,857-858, (1999)
[114] Jean Van Bladel, The Excitation of Dielectric Resonators of Very High Permittivity, IEEE Trans. Microwave Theory Tech., 23(2), 208-217 (1975)
[115] J. Zhang, and J. Fu, Comments on TE and TM modes of some triangular cross-section waveguides using superposition of plane waves, IEEE Trans. Microwave Theory Tech., 39, 612-613 (1991)